DIPLOMARBEIT

Titel der Diplomarbeit

Establishment and analysis of bronchus carcinoma xenograft models in mice

Verfasser

Patrick Reichl

angestrebter akademischer Grad

Magister der Naturwissenschaften (Mag.rer.nat.)

Wien, 2011

Diese Arbeit ist meiner Familie gewidmet.

Contents

Introduction

1. Cancer

Even though cancer research has led to many rapid advances in the last quarter century, malignant neoplasms are still one of the major causes of death worldwide[1]. Currently, one in 4 deaths in the United States and Europe is due to cancer. Every year, more than 550000 people die of cancer in the United States alone, corresponding to over 1500 per day. Almost half of all men and more than a third of all women will develop cancer during their lifetimes[2].

It has been established that cancer, the transformation of a normal somatic tissue into a malignant tumor, is the result of a multi-step process of consecutive genetic alterations which confer specific properties to the *a priori* normal cell. This process originates in the mutation of a single gene in a single cell which then gives rise to clonal waves of abnormal daughter cells[3]. Since there are many obstacles in the mammalian organism for such a cell to multiply endlessly, the descending premalign cells undergo a constant process of Darwinian selection as they face different selection barriers. Since the endogenous mutation rate would not suffice to generate enough genetic alterations within the human life-span, these cells must possess a certain genetic instability in order to overcome the selection obstacles (Figure 1).
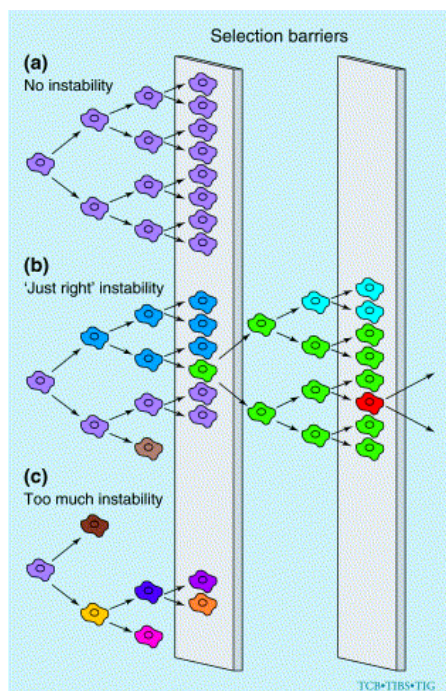
Figure 1: Selection barriers and genetic instability in tumorigenesis
Normal, non-malignant cells harbor a low intrinsic genetic instability rate and thus succumb easily to selection barriers, which inhibit tumor formation (a). Tumor cells or pre-malignant cells show a certain instability, which results in a more and more heterogeneous cell-mass and increases the chance for at least one of these cells to overcome the selection barriers (b). If genetic instability is too high, DNA damage quickly accumulates and leads to unviability of the cells (c)[4].

The degree of this instability is crucial for the further progression of the altered tissue. If the instability rate is too high, accumulation of DNA damage rapidly leads to unviability of the cell and if the rate of genetic instability is too low, it cannot overcome the selection barriers it faces[4]. Many different sources of genetic instability have been identified. One of them is the alteration or inactivation of DNA mismatch repair[5]. This leads to microsatellite instability which in turn produces nucleotide mutation rates two to three orders of magnitude higher than normal[6]. Another form of instability occurs at the chromosomal level. This chromosomal instability, accompanied by changes in chromosome size and number, can be due to alterations in different tumor suppressor genes involved in DNA maintenance[7]. This leads to destabilization of the segregation machinery during mitosis and provokes further aneuploidy[8].

1.1. Physiological alterations in cancer cells

Regardless of the mechanism of genetic instability acting in a tumor cell, the types of mutations which are necessary to acquire the properties needed for cancer progression are always the same, either dominant gain of function mutations of oncogenes or recessive loss of function mutations of tumor suppressor genes. Altogether, there are six major selection barriers that must be overcome and accordingly six necessary alterations in cell physiology which must be acquired (Figure 2)[9].
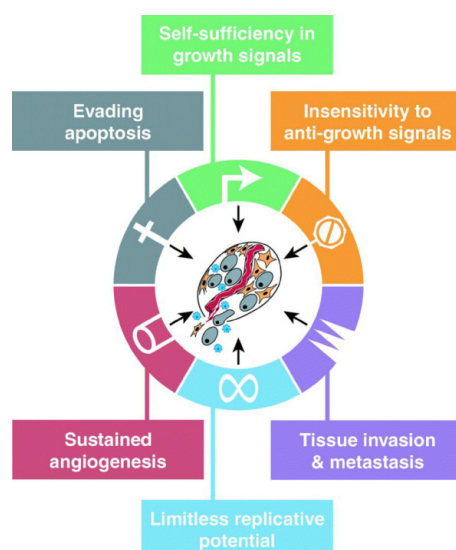
Figure 2: Acquired capabilities of cancer cells
Cancer cells need to establish six major characteristics to allow tumor initiation and progression: Self-sufficiency in growth signals, insensitivity to anti-growth signals, evasion of apoptosis, limitless replication, sustained angiogenesis and tissue invasion and metastasis[9].

Somatic cells need mitogenic growth signals in order allow their proliferation. These signals are transmitted in a paracrine manner, from one cell type to another, via the secretion of soluble signaling molecules that bind specific transmembrane receptors on the target cell. Thus, in order to be able to proliferate, tumor cells must acquire self-sufficiency in growth factors, either by secreting their own or by up-regulating the expression of the respective cell surface receptors, thereby becoming hyper-responsive to ambient levels of growth factors that would not trigger proliferation in normal cells. Also, alterations in the signaling cascade downstream of the ligand-receptor binding are possible, such as constitutively active receptors or downstream signal transduction molecules[11].

In addition to the limited presence of growth factors, another signaling mechanism restricts uncontrolled proliferation in normal tissue, namely antigrowth signals. These restrictive signals act in the same way as the mitogenic signals, via membrane bound receptors. Antigrowth signals block proliferation either by temporarily forcing the target cells into a quiescent cell cycle state (G0) or through the induction of terminal postmitotic differentiation, which is permanent[9]. In cancer cells, the responsiveness to these antigrowth signals must be disrupted to allow proliferation.

Another hurdle for cancer progression is the apoptotic machinery, present in most cell types throughout the body. It initiates a programmed cell-death through the release of cytochrome C from the mitochondria and subsequent activation of caspases which lead to chromosome degradation and cell membrane disruption. This program can be triggered by many physiological signals such as soluble death factors which again bind to cell surface receptors or the abrogation of cell-matrix and cell-cell adherence molecules which normally inhibit the induction of apoptosis. In addition, intracellular sensor proteins are capable of detecting DNA damage. They can either induce cell cycle arrest, which gives the cell more time to repair the damage or apoptosis, if the damage is too severe[10]. There is a constant balance between pro- and antiapoptotic signals which can lead the cell in either direction. In cancer cells, all of these signaling pathways can be altered. Death factor receptors, intracellular proapoptotic regulators that sense DNA damage as well as transmitters of antiapoptotic survival signals can be mutated, rendering the cancer cell resistant to apoptosis[9].

Except its dependency on environmental signals, proliferation of somatic cells is further restricted by an inherent, cell-autonomous program. Most normal human cells

have the capacity for 60-70 doublings (the Hayflick limit) after which they fall into a state of senescence[12]. Even if this limit is circumvented in the mutated cancer cell, another problem persists. Due to the shortening of telomeres (repetitive, noncoding sequences at the end of each chromosome) the DNA becomes increasingly unstable with every supplemental round of replication which ultimately leads to cell death. The enzyme telomerase contains the template for telomeres in the form of a short RNA molecule. Even though it is normally inactive in somatic cells, it can be reactivated in cancer cells[13].

In order to allow cell function and survival, oxygen and nutrients have to be supplied by the vasculature. Therefore, a tumor exceeding a certain size must develop the ability to recruit new vessels. Analogously to the self-sufficiency in growth factors, this can be achieved by upregulation of proangiogenic growth signals, the downregulation of angiogenic inhibitors or alterations of the intracellular signaling pathways involved[14].

The last step in cancer progression is the colonization of distant organs through the formation of metastases.

1.2. Lung cancer

Despite the continuous reduction of smoking prevalence since the late 1960s and numerous therapeutic advances, lung cancer is still by far the most common cause of cancer-related deaths in Europe and the United States, accounting for one fifth of all cancer deaths[2,15]. Close to 70 % of lung cancer patients show locally advanced or metastatic disease at the time of diagnosis[16]. The overall 5 year survival rate is 15 to 17 %[17].

Malignant lung cancer is histologically classified into two major groups which account for over 95 % of all lung cancers, the small cell bronchus carcinoma (SCLC) and the non-small cell bronchus carcinoma (NSCLC). The latter one is further divided into three subtypes, the large cell carcinoma, the squamous cell carcinoma and the adenocarcinoma.

Adenocarcinomas are the most commonly observed lung cancer subtype in Europe (40 % of all lung cancers) and their incidence has increased over the past years. It has its origin in glandular tissue. Squamous cell carcinomas are a little less frequent (25 % of all lung cancers). Large cell bronchus carcinomas account for 5 to 10 % of

lung cancers[18, 19]. The small cell bronchus carcinoma is less frequent than the NSCLC (about 17 % of all lung cancers) and has the worst prognosis among lung cancers[19, 20, 21].

2. Metastasis

Metastasis, the foundation of distant colonies by cancer cells, moving out of the primary tumor mass, travelling through the vascular system of the body and finally reaching a new soil allowing them to grow again, is the cause for 90% of cancer deaths[22].

In addition to the abilities necessary for primary tumor initiation, the establishment of metastases from a well vascularized malignant tumor requires several new ones. As for the primary tumor, this can be attributed to a number of alterations in the genome, whose chronological order coincides with the overcoming of several selection barriers.

The first step in this process is the destruction of the basement membrane, a non-cellular network of collagen fibers, anchoring the epithelium to the tissue underneath through cell-matrix adhesion. In cancer, the basement membrane is a mechanical barrier to uncontrolled invasive growth of malignant cells. In order for the tumor to grow beyond this boundary and enter the bloodstream, the basement membrane needs to be broken down[23]. This is achieved by the secretion of extracellular proteases which have the ability to degrade the adjacent extracellular matrix[24]. They do not necessarily originate from the tumor itself, but can be secreted by cancer promoting tumor associated macrophages (TAMs)[25].

Concomitantly to the clearance of this physical obstacle, cancer cells which are in most cases epithelial in nature must acquire a mesenchymal phenotype with the ability to migrate and thus leave their primary growth site, either directly into the surrounding tissue or into a nearby vessel which carries them across the entire body. The latter process is called intravasation. Epithelial and mesenchymal cells differ in various functional and phenotypic characteristics. Epithelial cells grow as layers of cells that show complete cell-cell adhesion with their neighbors through a multitude of specialized membrane structures such as gap junctions, tight junctions, adherens junctions and desmosomes. Furthermore, they exhibit an apical-basolateral polarity

which manifests itself through the distribution of cell adhesion molecules, cell-cell junctions and the organization of the actin cytoskeleton. In contrast, mesenchymal cells have a fibroblastoid spindle-like morphology and do not form tight cell layers, touching their neighbors only focally, nor do they show the same apical-basolateral polarity. They are highly motile in culture. The process by which epithelial cells turn into mesenchymal cells is called epithelial to mesenchymal transition (EMT). It is triggered by a variety of growth factors and requires several mutations[26].

The question whether cancer cells which have managed to enter the circulation home for specific organs in order to establish metastases or are merely retained by physical barriers is not completely solved. It seems however that both mechanisms are significant. Capillaries are small (3 to 8 µm in diameter) compared to most cancer cells (50 µm in diameter)[27]. It has been shown that lung and liver capillaries can arrest circulating cancer cells very efficiently, purely by size restriction[28].There is also evidence for specific adhesion of cancer cells to certain endothelia, depending on their activation state[29]. Nevertheless, it seems that the preference of certain cancers to colonize specific organs does depend on their ability to proliferate inside the respective tissue rather than a homing mechanism. Multiple molecular factors have been identified, which give the tumor cells specific growth advantages inside specific tissues[30, 31].

3. Vessel development

3.1. Blood vessels

Mammalian cells require oxygen and nutrients for their survival. Since oxygen has a diffusion limit of 100 to 200 µm, every organism which grows beyond this size must assure the supply of its tissues through a widely ramified system of blood vessels. In order to generate such a system, mammals have to form new vessels constantly during development by processes called vasculogenesis, the recruitment of endothelial progenitors which spontaneously form new blood vessels and angiogenesis, the sprouting of new vessels from preexisting ones and subsequent stabilization of these sprouts by mural cells[32]. Many of the mechanisms involved in the vascular development of the embryo can be recapitulated in the adult organism.

This process, called neoangiogenesis, occurs for example during repair and healing following tissue damage. In general, angiogenesis is regulated by a balance of pro- and antiangiogenic factors[33]. The disturbance of this balance in either direction is the cause for a wide variety of diseases, including among others cancer progression, psoriasis, arthritis, blindness, neurodegeneration, hypertension, pre-eclampsia, respiratory distress and osteoporosis[14, 34]. In the case of cancer, neoangiogenesis allows the tumor to grow beyond a critical size, where the limited availability of nutrients and oxygen would restrict its growth. In addition, blood vessels serve as a gateway into the body, permitting the entrance of tumor cells into the circulation and the subsequent colonization of distant organs and thus the formation of metastases. The hypothesis that tumors produce proangiogenic substances was proposed in 1968[35]. It has become clear since then, that during cancer progression, an "angiogenic switch" is turned on, as the balance between pro- and antiangiogenic factors is moved towards angiogenesis[9, 14]. Several physiological changes which occur during tumor growth can trigger this angoigenic switch. Among them are hypoxia, low pH, hypoglycemia, mechanical stress from proliferating cells, inflammatory response following invasion by immune cells and mutation of genes that control angiogenesis regulators[36, 37]. The molecular players involved are numerous but present research indicates that the most important ones are members of the vascular endothelial growth factor (VEGF) and angiopoietin (Ang) families[38].

3.2. Lymphatic vessels

In addition to the supply of nutrients and oxygen, several other biological maintenance functions are necessary in mammalian tissues, which cannot be fully accomplished by a closed cardiovascular system. The open lymphatic system assures the control of intercellular fluid transport through the absorption of extravasated water from the venous system and thus maintains an appropriate plasma volume and prevents pressure build-up inside the tissue. Furthermore, it plays a crucial role for the immune system of the body by serving as a route of transportation for leukocytes[39]. It is established during embryogenesis by the formation of primordial lymphatic vesicles through the budding off from venous endothelial cells[40]. Even though their origin is the same, lymphatic endothelial cells (LEC) are distinct from blood vascular endothelial cells[41, 42]. Lymphatic vessels show

differences in structural and functional properties from those of blood vessels. They are thin walled, have little or no basement membrane and their inter-endothelial cell-junctions are discontinuous, which increases their permeability. Furthermore, they have a higher lumen diameter, are less regular and can frequently be collapsed. In the absence of a pressure source such as the heart, they have to maintain the lymph flow by contractions of the smooth muscles around them and direct it through a system of valves[43]. As is the case with angiogenesis, lymphatic vessels can develop in response to damage and inflammatory signals in somatic tissues, after embryogenesis is accomplished. Lymphatic vessel development is also dependent on a specific growth factor environment, which encourages or inhibits lymphatic endothelial cell migration and vessel formation[44]. Again, the disturbance of this balance results in many diseases such as chronic inflammations (e.g.: psoriasis or rheumatoid arthritis), lymph edema and hypertension[45, 46, 47, 48, 49]. In many human cancers, it is well established that regional lymph node metastasis is the first step of tumor dissemination[50, 51]. It is currently unclear whether lymphatics can really promote further metastases formation in distant organs in analogy to blood vessels, by serving as a "launch pad", but it is known that tumor cells can enter the lymphatic vasculature, either by invading preexisting lymph vessels or by inducing lymphangiogenesis through the secretion of lymphangiogenic factors[45, 50, 52, 53]. Compared to angiogenesis, the physiological causes for lymphangiogenesis in the lung cancer cancer context, as well as the underlying molecular networks are poorly studied but similar signaling pathways are involved, such as specific members of the VEGF and Ang/Tie systems[54, 55].

3.3. The VEGF system

The vascular endothelial growth factor family is a group of multifunctional signaling molecules with several important biological activities during embryonic development as well as in somatic tissue homeostasis of specific organs[56]. The VEGF family consists of seven secreted glycoproteins, VEGF-A, VEGF-B, VEGF-C, VEGF-D, VEGF-E, VEGF-F and placental growth factor (PlGF)[57, 58, 59].VEGF-E and VEGF-F differ from the other, endogenous VEGFs in their origin. VEGF-E is virally encoded and VEGF-F is a component of snake venom[60]. VEGFs convey their biological function through the binding to their respective receptors VEGFR-1 (Flt-1), VEGFR-2

(KDR), VEGFR-3 (Flt4) and lastly the coreceptors Neuropilin NP-1 and NP-2. Binding of these receptors leads to modification of multitude of downstream targets and alteration of cell behavior in many ways (Figure 3).
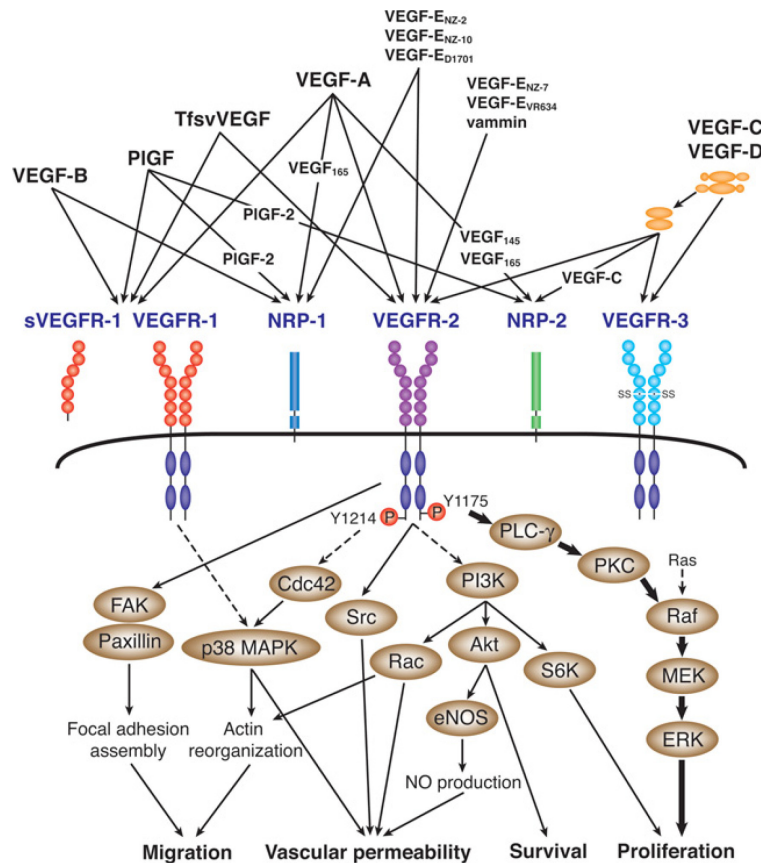
Figure 3: The VEGF-family

Receptors, ligands and downstream pathways.[85]

Structure and function of VEGF-A

VEGF-A (also called VEGF) was first identified as a permeability factor secreted by tumor cell lines[61]. Soon after, it became evident that VEGF also displays the ability to stimulate endothelial cell proliferation and migration, acting as an angiogenic factor[62]. VEGF-A is a homodimeric 46 kDa glycoprotein. Its gene is located on chromosome 6p21.3, spans approximately 14 kb and consists of eight exons. Alternative splicing yields seven isoforms (VEGF-A$_{206, 189, 183, 165, 148, 145, 121}$), where the numeric value denotes the number of amino acids in the protein (Figure 4).
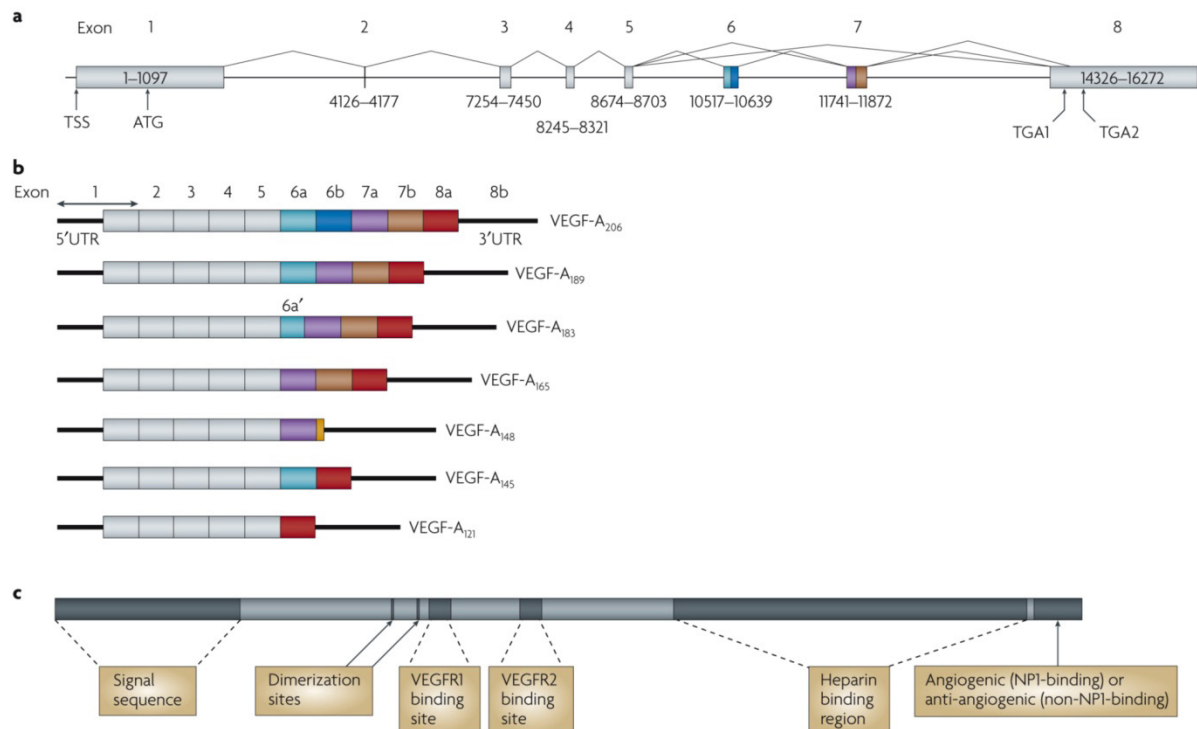
Figure 4: VEGF-A

Gene structure of human VEGF-A (a). Known splice variants of VEGF-A (b). Protein structure of VEGF-A (c) adapted from [63].

All isoforms possess the N-terminal signal sequence, the dimerization domain and the VEGFR-binding domain, which are encoded in exons 1-5. They do however differ in their ability to bind to the highly negatively charged glycosaminoglycan carbohydrate heparin and similar molecules, which is encoded in exon 6 and 7. Furthermore, they can be divided into two families which differ by their six C-terminal amino acids, due to the existence of two alternative splice sites in exon 8, a proximal and a distal one (PSS and DSS). If the PSS is chosen, the resulting protein has pro-angiogenic properties (VEGF$_{xxx}$), if the DSS is selected, the protein exhibits anti-angiogenic properties (VEGF$_{xxxb}$)[63].

VEGF-A acts through the binding to its receptors VEGFR-1 (Flt-1) and VEGFR-2 (Flk-1). These are transmembrane tyrosine kinases, specifically expressed on vascular endothelial cells. Upon binding, they dimerize and autophosphorylate their intracellular kinase portion, leading to the activation of multiple downstream effectors[64]. In addition, VEGF-A also interacts with the neuropilin receptors (NP-1 and NP-2), which are expressed on vascular endothelial cells and neurons.

In embryonic development, VEGF-A expression coincides with blood vessel formation[65]. Its mRNA can be identified in the primary vasculature, the primordial

18

heart, kidney and brain[66]. The ablation of even a single allele results in embryonic lethality due to abnormal vascular development[67].After birth, as the endothelial development slows down, VEGF-A expression declines accordingly to low levels. Nevertheless, VEGF-A expression is persistent in some specific somatic tissues such as kidney, brain, placental, lung and cardiac endothelia in order to maintain a specialized, fenestrated endothelium[68, 69, 70, 71, 72]. The effects of specific over-expression of VEGF-A in defined tissues further underline its importance as a major regulator of blood vessel development and maintenance in embryogenesis and in the adult organism[73].

Also, VEGF-A plays a significant role in wound healing which is impaired in mice carrying a VEGF-A mutation[74].Eventhough VEGF-A$_{165}$ is the predominant isoform in most tissues, VEGF-A$_{189}$ is highly expressed in the rat heart and lung and VEGF-A$_{121}$ is the most abundant isoform in the placenta[58, 75, 76].

In addition to its ability to induce proliferation, migration and tube formation of endothelial cells, VEGF-A can also provoke the attraction of hematopoietic stem cells and monocytes as well as osteoblast-mediated bone formation[57, 77].

Apart from its important physiological roles in organogenesis, vessel maintenance and tissue repair, aberrant VEGF-A expression has a strong influence on tumor growth and progression. The over-expression of VEGF-A$_{165}$ and VEGF-A$_{189}$ has been shown to be involved in the vascularization of various cancers, including bronchus carcinoma[75, 78].

VEGF-A expression can be induced in vitro by a multitude of other growth factors such as platelet-derived growth factor (PDGF), basic fibroblast growth factor (bFGF), epidermal growth factor (EGF) and transforming growth factor beta (TGF-β).

Another prominent feature of VEGF-A regulation is its inducibility by hypoxia through the HIF-1 alpha pathway. So far, it is the only angiogenic factor for which this has been shown both in vivo and in vitro[79].

In conformity with this, VEGF-A expression in the tumoral context can originate from the tumor itself as a response to hypoxia. Nevertheless, VEGF-A production can also occur as a consequence of inducing factors secreted by stromal cells. Most leukocyte subtypes produce PDGF, bFGF, EGF and TGF-β, as well as VEGF-A itself, therefore stimulating VEGF-A expression and angiogenesis inside the tumor and the adjacent

tissue[80, 81]. Especially important in this respect are tumor associated macrophages, which are attracted by tumor secreted colony stimulating factor 1 (CSF-1)[82].

VEGF-A promotes cancer not only by its ability to stimulate angiogenesis, but also by the inhibition of the functional maturation of dendritic cells, thereby attenuating the anti-tumoral immune response[83, 84].

Structure and function of VEGF-C and VEGF-D

VEGF-C was first discovered in 1996, when it was cloned from a cDNA library of human prostate cancer cells. It was found during the search for a ligand for VEGFR-3 (Flt4). Since it was known that Flt4 is specifically expressed on lymphatic endothelia, it was soon clear that VEGF-C plays a role in the regulation of lymphangiogenesis[86].

The active form of VEGF-C is a 21 kDa glycoprotein. Its gene is located on chromosome 4q34, spans over 40 kb and comprises 7 exons. In contrast to VEGF-A, where different isoforms are the result of alternative splicing, VEGF-C is produced as a single precursor protein, which is proteolytically processed by the intracellular secretory proprotein convertases furin, PC5 and PC7[87, 88]. VEGF-C is then secreted as a VEGFR-3 binding form, containing two 31 and 29 kD subunits, linked together by disilfude bonds. The factor is further proteolyzed in the extracellular environment, leading to the final 21 kD homodimeric protein, with high affinity for both VEGFR-2 and VEGFR-3[89]. VEGF-C possesses a VEGF homology domain, which shows 31 and 61 % protein sequence identity to VEGF-A and VEGF-D respectively.

As VEGFR-2, mentioned earlier already, VEGFR-3 is a receptor tyrosine kinase which gets activated upon binding, leading to the subsequent phosphorylation of a multitude of downstream effectors[90]. In contrast to VEGFR-2, VEGFR-3 expression in the adult organism is mostly confined to lymphatic endothelia[91, 92]. Furthermore, VEGF-C has the ability to bind the neuropilin-2 receptor, which is internalized with VEGFR-3 upon stimulation and may increase affinity of VEGFR-3 for VEGF-C[93].

In embryogenesis, VEGF-C expression is found predominantly at sites of lymphatic development[51, 94]. In mice, where VEGF-C has been deactivated, lymphatic endothelial cells begin differentiation but fail to migrate from the veins to form primary lymph sacs[94, 95, 96]. In addition, homozygous deletion of VEGF-C in mice causes lethality through a complete absence of the lymphatic system. Even heterozygous

deletion leads to severe lymphatic hypoplasia[94]. This suggests that VEGF-C has a predominant role in lymphangiogenesis and the establishment of a lymphatic system. VEGF-C also plays a role in angiogenesis, since it binds VEGFR-2 and has the ability to induce mitogenesis, migration and survival of endothelial cells[41]. Its angiogenic function is however not essential for blood vessel development.

VEGF-C has been shown not only to be involved in lymph vessel development during embryogenesis, but also in the context of inflammation and tissue repair, which was proven in a rabbit cornea model of inflammatory lymphangiogenesis. Marcophages have been found to abundantly express VEGF-C and lymphangiogenic responses are inhibited upon macrophage depletion[97]. In addition, VEGF-C mRNA expression is induced in ECs in reponse to proinflammatory cytokines suggesting that these can play a role in VEGF-C mediated lymphangiogenesis[97, 98].

VEGF-C is linked to a number of diseases. It has been shown that abundant VEGF-C expression leads to excessive lymphangiogenesis and rejection in human kidney transplants[99]. In addition, high VEGF-C expression is found in arthritic joint synovium of patients suffering from rheumatoid arthritis, indicating that lymphangiogenic response is insufficient in this disorder[100].

Importantly, VEGF-C shows a possible influence on cancer progression, including lung cancer. It was found to promote lymphangiogenesis in human lung adenocarcinoma as well as increased lymph node metastasis in lung adenocarcinoma and non-small cell lung cancer[90, 101]. Although enlarged extra-tumoral lymphatic vessels have been found, functional intra-tumoral lymphatic vessels have not[102].

Similarly to VEGF-A, VEGF-C is upregulated by a variety of inflammatory cytokines, such as insulin-like growth factor-1 (IGF-1), platelet derived growth factor (PDGF), epidermal growth factor (EGF), transforming growth factor beta (TGF-β) and basic fibroblast growth factor (bFGF).

In contrast to VEGF-A, VEGF-C is not upregulated by hypoxia[103, 104].

Murine VEGF-D was found by differential mRNA screening of mouse fibroblasts, whereas in humans, it was identified by computer-based homology searching for VEGF-related sequences[105, 106].

The VEGF-D gene is located on chromosome Xp22 and spans about 50 kb. It shows similar organization to VEGF-C, with 7 exons and 6 introns[90]. The active form of

VEGF-D is also a 21 kDa glycoprotein and its origin is very similar to VEGF-C. It gets translated as a 50 kDa preprotein, which is further proteolytically processed by the same proprotein convertases, as VEGF-C (PC5 and PC7)[107]. This results in the active, homodimeric 21 kDa form. It also possesses the VEGF homology domain, which shows 30 % sequence identity to VEGF-A and 61 % identity to VEGF-C[90]. Overall, it is 48 % identical to VEGF-C. As VEGF-C, human VEGF-D has the ability to bind and activate VEGFR-2 and VEGFR-3, as well as NP-2, although with different binding affinities. Interestingly, murine VEGF-D only binds VEGFR-3, suggesting a different role in mice[108].

During embryogenesis, VEGF-D expression can be detected in many tissues, most abundantly in the lung and skin[109]. In contrast to VEGF-C, deletion of VEGF-D does not affect the development of lymphatic vasculature[94, 110].

Nevertheless, VEGF-D has the same mitogenic, migration and survival effect on ECs as does VEGF-C[89]. In addition, it presents prolymphangiogenic features in the same context as VEGF-C, namely during inflammatory response and wound healing, where it is also expressed by macrophages[97].

Concerning cancer, VEGF-D shows similar tendencies as VEGF-C, although it is far less intensively studied. It has been shown to increase lymphangiogenesis and metastasis to the lymph nodes in experimental tumor models and it seems to enhance angiogenesis as well[111, 112]. In the case of lung cancer, very few investigations have been conducted to this date, but it has recently been suggested that VEGF-D, along with VEGF-C may be involved in lymphatic metastasis in experimental intrathoracic lung cancer[113]. Also, it has a prognostic value in general for lymphatic vessel invasion and survival in certain human cancers[114].

Regulation of VEGF-D is quite different from VEGF-C since it is not upregulated in the presence of inflammatory cytokines. There are indications that VEGF-D may be inducible by hypoxia, as its genomic sequence reveals a hypoxia response element and VEGF-D has been shown to be upregulated by hypoxia in rat lung smooth muscle cells[115]. Also, it is induced by the activation of the proto-oncogene c-fos and by cell-cell contact, mediated by cadherin-11[116, 117].

3.4. Tumor associated macrophages and CSF-1

Since the nineteenth century, it has been known that macrophages are present within and around tumors[118]. For a long time, it has been widely accepted that these tumor-associated macrophages (TAMs) exert a tumor suppressive role, by performing their usual immunological and repair functions, such as the recruitment and activation of other immune cells or the production of proteases in order to eradicate the tumor[119]. Nevertheless, evidence has grown recently that TAMs may play a less appreciated role during tumor progression. Instead of activating other immune cells, TAMs may even inhibit their action by secretion of TGF-β, a cytokine which attenuates immune response[120]. In addition, they are also capable of secreting several matrix metalloproteinases, which can degrade extracellular matrix and the basement membrane which serves as a barrier against invasive tumor growth[121]. Most importantly, TAMs can strongly promote angiogenesis and lymphangiogenesis through the secretion of bFGF, angiopoietins, tumor necrosis factor-α (TNF-α), interleukin 1 and 8, thymidine phosphorylase and also VEGF-A, VEGF-C and VEGF-D[33, 121]. In addition, VEGF-A serves as a chemoattractant for macrophages and further increases the invasion by TAMs (Figure 4).

Colony stimulating factor-1 (CSF-1) is the most potent attractant for macrophages[119]. Its gene was discovered in 1985 in a genomic library[122]. The gene is located on chromosome 1p21, consists of 10 exons and spans about 20 kb.

There are two forms of alternative splicing of the CSF-1 mRNA. One implies the alternative use of exon 9 or 10, which encode the 3' untranslated region. The other leads to alternative splicing in exon 6 of which a large part can be left out, resulting in two different forms of the CSF-1 precursor. The form containing full-length exon 6 encodes a protein which is then glycosylated and cleaved either at the N or C-terminal end. It is secreted respectively either as a glycoprotein or a proteoglycan of 86 kDa. The shorter precursor which lacks part of exon 6 is expressed as a membrane-spanning glycoprotein, which is only released by slow proteolysis. The existence of a membrane-bound as well as a secreted form of CSF-1 suggests two mechanisms of action, one of which is mediated by direct cell-cell contact, the other one is a response to the environmental concentration of secreted CSF-1.

CSF-1 exerts its biological functions by binding to its receptor CSF-1R, strongly expressed on the surface of macrophages. It is a membrane-bound tyrosine kinase and, upon binding, phosphorylates a multitude of target molecules[123].

CSF-1 has the ability to promote macrophage survival, proliferation, differentiation and chemotaxis. It has been shown to be overexpressed in many human cancers, including ovarian, uterine, breast and prostate tumors. Importantly, CSF-1 has the ability to induce VEGF-A expression[124, 125, 126, 127].
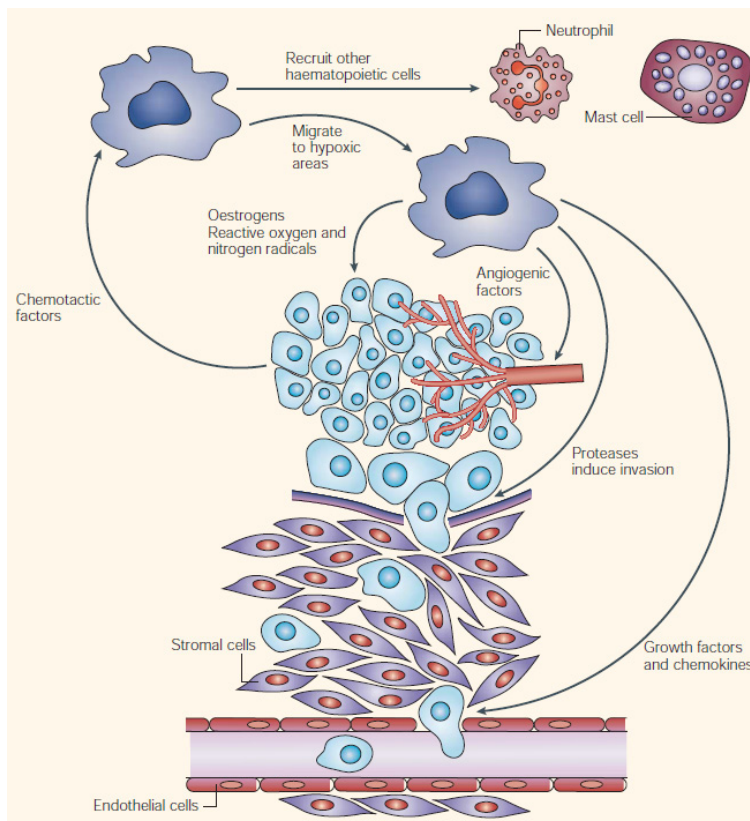
Figure 4: Pro-tumorigenic functions of TAMs
Tumor associated macrophages (TAMs) can be attracted to tumors by hypoxia or recruited by tumor-released factors such as CSF-1. They secrete angiogenic factors, as well as proteases which facilitate tumor invasion[119].

4. ANGPTL4

Angiopoietin like-4 (ANGPTL4) was discovered in 2000 by multiple groups independently, during a search for additional angiopoietin-related proteins from embryonic cDNA, as a fasting-induced gene or as a factor expressed during preadipocyte differentiation[128, 129, 130].

ANGPTL4 is a 43 kDa glycoprotein. Its gene is located on chromosome 19p13, spans approximately 7 kb and consists of seven exons[129]. Two isoforms are produced via alternative splicing, the shorter one lacking exon 4 and it is unknown in

what respect this alters its function. The ANGPTL4 protein possesses two structural domains, an N-Terminal coiled-coil domain and a C-terminal fibrinogen-like domain. It shows oligomerization, mediated by disulfide bonds, prior to secretion and can be proteolytically processed by a membrane-associated protease, leading to the release of the full length form, and a truncated form, consisting of the N-terminal coiled-coil domain[131]. The latter can form higher oligomers after secretion[132].

The ANGPTL family of proteins is named for its structural resemblance to angiopoietins. These are pro-angiogenic proteins which bind the receptor tyrosine kinases Tie 1 or Tie 2 but unlike angiopoietins, ANGPTLs do not bind either of these receptors and are considered orphan ligands[133].

ANGPTL4 is expressed predominantly in adipose tissue, liver and placenta, but also keratinocytes, intestine and pituitary gland[134].

In general, ANGPTL4 is best known for its ability to inhibit lipoprotein lipase (LPL), a membrane-associated enzyme found on endothelial cells and responsible for the hydrolysis of triglycerides in plasma lipoproteins, thereby generating fatty acids for storage or energy production. This inhibition is accomplished by the selective binding of LPL and its subsequent conversion from active dimers to inactive monomers[132].

It has been suggested that, in conformity with its name giver, ANGPTL4 may have pro-angiogenic effects, since its expression is strongly increased in human fetal cardiac cells and neonatal rat cardiomyocytes, when cultured under hypoxia[135]. However, ANGPTL4 expression has been shown to be activated by hypoxia inducible factor-1α in many tissues, not only cardiac cells and in other studies, ANGPTL4 has even been shown to inhibit angiogenesis[134, 136]. Also, ANGPTL4 seems to enhance cell survival and modulate cell-cell adhesion of endothelial cells[128, 137].

Concerning cancer, systemic ANGPTL4 overexpression in transgenic mice has been shown to inhibit metastasis by xenografted melanoma cells[138].

Most interestingly and in contrast to previous findings, xenografted breast carcinoma cells overexpressing ANGPTL4 seem to have strongly increased metastatic potential, specifically to the lungs[139]. This ability is attributed to an endothelium-disruptive effect of ANGPTL4, which is in conformity with other recent publications, where ANGPTL4 has been shown to loosen endothelial cell-cell adhesion[137].

The pathways of ANGPTL4 regulation are still largely unknown. It seems to be upregulated by fasting, hypoxia and by TGF-β[134, 139].

Rationale

The cell lines used in this thesis included NSCLC (H460 large bronchus carcinoma, H520 squamous bronchus carcinoma, Calu-3 bronchus adenocarcinoma) as well as SCLC cells (DMS 53 small cell bronchus carcinoma).

The main aim was to develop murine xenograft models of all four major bronchus carcinoma subtypes and to assess differences in their growth, neoangiogenesis, lymphangiogenesis and metastases formation.

In addition, the question was addressed whether these phenotypic differences correlate with the mRNA or protein expression levels of certain known angiogenic and lymphangiogenic factors *in vitro* as well as *in vivo*, namely members of the vascular endothelial growth factor family (VEGF-A, VEGF-C and VEGF-D), the colony stimulating factor-1 (CSF-1) and the novel angiopoietin-related molecule angiopoietin like-4 (ANGPTL4).

This may allow the analysis of advantages and disadvantages of antiangiogenic therapies, as well as the development of new experimental approaches in different forms of lung cancer.

Materials and Methods

1. Cells

1.1. Cell lines

H460 (ATCC number HTB-177)

H460 is an epithelial-like metastatic human large cell bronchus carcinoma cell line, isolated in 1982 from the pleural fluid of a male patient. The cell line does form tumors in nude mice and grows in culture in adherent monolayers with an average doubling time of 23 hours in medium supplemented with 10% fetal bovine serum (FBS). It is hypotriploid with a modal chromosome number of 57 and several structural abnormalities, such as the absence of several normal chromosomes. The cells show p53 expression comparable to normal lung tissue.

H520 (ATCC number HTB-182)

H520 is an epithelial-like human squamous cell bronchus carcinoma cell line, isolated in 1982 from a sample of the lung mass taken from a male patient. It forms tumors in nude mice and grows in culture in adherent monolayers with an average doubling time of 61 hours in medium supplemented with 10% FBS. It is hypotriploid, with an average chromosome number of 58 and many structural abnormalities, such as the absence of several normal chromosomes. The y chromosome can no longer be detected and the X is single. The cells show greatly reduced p53 expression in comparison with normal lung tissue.

Calu-3 (ATCC number HTB-55)

Calu-3 is an epithelial-like metastatic human bronchus adenocarcinoma cell line, isolated from the pleural fluid of a male patient. It forms well differentiated adenocarcinomas in nude mice and grows in culture in adherent monolayers. It is hypotriploid with some structural abnormalities, including the absence of several normal chromosomes. The Y chromosome can no longer be detected.

DMS53 (ATCC number CRL-2062)

DMS53 is an epithelial-like human small bronchus carcinoma cell line, isolated in 1975 from a mediastinal biopsy of a male patient. It is tumorigenic in nude mice and grows in culture in adherent monolayers. It secretes a large variety of hormones.

1.2. Cell culture

The aim of cell culture is to sustain cell proliferation in an artificial environment by the adjustment of several factors, such as growth media composition, pH and temperature, mimicking their original environment.

H460 cells were cultured on 10 cm tissue culture dishes (Iwaki) in 15 mL RPMI medium, supplemented with 10% FBS and penicillin/streptomycin (pen/strep, PAA) in order to suppress the growth of unwanted microorganisms. The medium was changed twice a week and incubation took place in an incubator (Binder) at 37°C and 5% CO_2. Subcultivation was conducted at 80% confluency and the cells were split at a 1:8 ratio.

H520 cells were cultured under the same conditions.

Calu-3 cells were cultured in MEM medium, supplemented with 10% FBS and pen/strep. Sodium pyruvate and non-essential amino acids (NEAA) were added as a supplement. Medium changes and subcultivation were conducted in the same way as for the other cell lines, but the cells were split at a ratio of 1:6.

DMS53 cells were cultured in Waymouth's medium, supplemented with 10% FBS and pen/strep. Medium changes were also conducted twice a week but the cells were split at a lower confluency of 60% and at a lower ratio of 1:3.

Subculturing of the cells

Since many cells show growth inhibition and can become necrotic when in close contact, they must be split at a defined confluency. This is achieved by digestion of cell-cell junctions by trypsin, a protease found in the digestive tract of many vertebrates.

Cell culture media and phosphate buffered saline (PBS) were pre-warmed in a 37°C water bath. The exhausted medium was removed from the culture dishes by pipetting

and the cells were washed twice with PBS. 1 mL 1x Trypsin-EDTA was added to the cells and the plates were placed in the incubator (37°C) for 10 minutes. A 50 mL centrifuge tube was filled with 10 mL culture medium and the detached cells were harvested and transferred from the plate to the tube. The cells were pelleted by centrifugation (Heraeus Labofuge 400R) at 500 x g for 3 minutes. The supernatant was discarded and the cells were resuspended in 1 mL culture medium. New petri dishes were inoculated with the volume corresponding to the respective split ratio and placed in the incubator (37°C, 5% CO_2).

1.3. Cell counting

For subsequent experiments, the cells were counted using a hemocytometer (Neubauer cell counting chamber), which is a graduated counting chamber that can be viewed under a microscope to determine the concentration of cells in a suspension.

The instrument is made of ground glass with a central area that is defined by a set of grooves that form an "H" shape. Two counting areas with ruled grids are separated by the horizontal groove of the H. A glass coverslip is held at 0,1 mm above the surface of the counting areas by ground glass ridges on either side of the vertical grooves of the H shape. Each side (counting area) of a hemocytometer is etched with a grid of 9 square millimeters which is further subdivided into mm^2. Since each mm^2 has a depth of 0,1 mm, the corresponding volume is 0,0001 mL. By multiplying the obtained cell count by the dilution factor and 10^4, the cell number per mL in the original suspension can be determined.

Cell counting was conducted as follows:

The cells were trypsinized and collected as for subcultivation and resuspended in 1 mL culture medium. 10 µL of this suspension were diluted in 990 µL PBS in an eppendorf tube, resulting in a dilution factor of 1:100. In order to distinguish dead cells, 100 µL of this dilution were mixed with 100 µL trypan blue (Sigma) on a separate glass slide. Trypan blue is a live dye which selectively traverses the cell membrane of dead cells only. The counting chamber and glass cover slip were cleaned with 70% ethanol and the slip was placed on the chamber. The diluted cell suspension was pipetted onto the border of the glass cover slip and sucked into the counting chamber by capillary action. Live cells were counted in the four outer 1 mm^2

squares of both counting areas and the result was averaged and multiplied by 2 x 100 x 10^4 = 2 x 10^6 to obtain the cell concentration [cells/mL] of the initial suspension.

1.4. DiI labeling of cells

DiI (1,1'-dioctadecyl-3,3,3'3'-tetramethylindocarbocyanine iodide) is a non-toxic hydrophobic and lipophilic cyanine dye, which is retained in lipid bilayers and diffuses laterally to stain the entire cell. It exhibits an absorption maximum at 549 nm and emission at 565 nm. Its fluorescence is significantly enhanced upon membrane incorporation.

Several different cell types were labeled, the tumor cell lines (H460, H520, Calu-3 and DMS53) before injection into mice as well as lymphatic endothelial cells (LEC), which were used for the assessment of tube formation, as described later.

The staining procedure was conducted as follows:
2 µL of DiI stock solution (Invitrogen) were added to 2 mL of cell suspension in PBS in a 15 mL centrifuge tube and mixed by inverting. The mixture was incubated for 10 min at 37°C, followed by 5 min on ice. The cells were spun down at 500 x g for 3 minutes and washed with 10 mL PBS. This procedure was repeated 3 times to a total of 4 washes. The cells were resuspended in 1 mL culture medium for the tube formation assay or ringer solution for the injection into mice.

2. Xenografts

2.1. Establishment of tumor growth

The mouse is the most common model organism in cancer research. The murine and human genomes have approximately the same size, contain the same number of genes and show extensive synteny (conserved gene order). Most human genes have mouse counterparts and their functions are closely related.

Mice are small, easy to maintain in the laboratory (compared to most mammals) and have a short breeding cycle of about 2 months. Many mutants are available. Human tumor cell lines can give rise to progressively growing, and potentially lethal cancers

in mutant, immune-deficient mice which allows the use of human tumor xenografts for the study of virtually all types of anti-cancer drugs and treatment strategies.

Obvious disadvantages of xenograft models are that the tumor cells and target organ are not from the same species and that the study of initiating events in carcinogenesis is precluded. Nevertheless, these models appear to have considerable utility for the investigation of diverse human cancers.

Male nude mice (Athymic Nude-*nu*) were obtained from a commercial source (Harlan Winkelmann GmbH, Borchen, Germany) and housed under sterile conditions at the Department of Biomedical Research at the Medical University of Vienna. The mice were acclimatized for 2 weeks after arrival. 100 μL of tumor cell suspension in Ringer solution were injected subcutaneously through a 27-gauge needle into the left flank. For the assessment of tumor growth, two randomized groups of 4 animals were established for each of the 4 cell lines to a total of 32 animals. Each group received a different number of cells (5×10^6 or 10×10^6), chosen according to past publications (Table 1). Two animals of each cell-number group were injected with unmodified cells, while the remaining two animals received DiI-labeled cells in order to trace possible tissue invasion and distant metastases formation.

Cell line	Nr. of animals	Cell number
H460	4	5×10^6
	4	10×10^6
H520	4	5×10^6
	4	10×10^6
Calu-3	4	5×10^6
	4	10×10^6
DMS53	4	5×10^6
	4	10×10^6

Table 1: Animal groups for xenograft model establishment

Tumor size was measured with a caliper every 2 to 3 days after implantation of the cells. Caliper measurements were used to calculate tumor volumes using the formula $V = \pi / 6 * (length * width * width)$ and to generate growth curves. As soon as the

tumor size exceeded 2 cm^3, the animals were killed by intra-peritoneal injection of Ketavet (200 mg/kg) and Rompun (10 mg/kg).

The tumors were removed, weighed and halved. One part of the tumor mass was fixed in formalin, the other one was frozen in liquid nitrogen for further analysis. In the case of the DiI-labeled cells, tumors, as well as defined organs (lung, lymph nodes, liver, kidney, and brain) were extracted in a sterile environment, under a tissue culture hood according to the cell isolation procedure described later. The unlabeled tumors were also subjected to cell isolation and prepared for flow cytometric analysis as described later.

2.2. Cell isolation

Surgical instruments were sterilized by autoclaving. 5 mL of PBS were added to 10 cm petri dishes and a sterile 100 μm nylon mesh cell strainer (BD Falcon) was placed in each dish. After sacrification, the mice were placed in a tissue culture hood and their skin was doused with 70% ethanol. Using surgical scissors, an incision of about 2,5 cm in length was made in the abdomen on the left side of each animal (at the tumor site), cutting the skin but not the peritoneal wall. With a fresh pair of surgical scissors, the tumor was extracted, weighed and divided into three parts. One part was placed in the cell strainer for cell isolation, the other two were fixed in formaldehyde or frozen in liquid nitrogen. With another fresh pair of surgical scissors, the peritoneal wall was cut and lung, discernible lymph nodes, liver, kidney and brain were extracted, using new and sterilized forceps and scissors for every organ. The organs were placed into a new cell strainer. The extracted tumors and organs were cut into small pieces with sterilized scissors and meshed through the cell strainer by gently applying force using the Gilson pipettor and the rubber end of a plunger from a 5 mL syringe. The resulting suspension was filtered again through a new cell strainer, transferred into a 50 mL tube and centrifuged at 500 x g for 3 minutes. The pellet was resuspended in 1 mL culture medium and the cells were seeded onto a new 10 cm petri dish, supplied with 15 mL culture medium.

Tumor cells were isolated in this way for every animal, whereas organ cells were only isolated from animals bearing DiI-stained tumors, in order to identify metastatic cells in subsequent cell culture.

When colony formation and extensive growth of cells isolated from an organ was

observed, cells were picked, further subcultivated and their human provenance was checked by PCR.

2.3. Flow cytometric analysis

Flow cytometry is a technology that simultaneously measures and then analyzes multiple physical characteristics of single cells, as they flow in a fluid stream through a beam of light. The properties measured include relative size and relative granularity and they are determined using an optical-to-electronic coupling system that records how the cell scatters incident laser light and emits fluorescence. The cells can be additionally labeled with a range of fluorescent dyes which can be coupled to specific antibodies.

CD31, also named platelet endothelial cell adhesion molecule-1 (PECAM-1), is a molecule present on the surface of all endothelial cells, but also platelets, macrophages, T cells and neutrophils. It plays a role in the successful identification and subsequent degradation of damaged neutrophils by macrophages through the reciprocative binding of CD-31 molecules of both cells. Since it is ubiquitously expressed on all endothelial cells, it can be used in combination with other markers to identify specific endothelial cells, such as LECs.

Lymphatic vessel endothelial hyaluronan receptor (LYVE-1) is a protein involved in the binding of hyaluronic acid by lymphatic endothelial cells. Since it is exclusively expressed on LECs, it can be used as a specific marker.

In order to determine the incidence of murine lymphatic endothelial cells (LECs) in xenografted tumors and thus assess the degree of intra-tumoral lymphangiogenesis, isolated cells were double-stained with two antibodies against the lymph-specific cell-surface proteins CD31 and LYVE-1.

The previously unlabeled LYVE-1 (MBL) antibody was detected by a secondary antibody (Jackson), labeled with fluorescein isothiocyanate (FITC), which shows excitation at 494 nm and emission at 521 nm

The CD31 antibody (BD Pharmingen) was directly labeled with phycoerythrin (PE), which has an absorption peak at 495 and an emission peak at 575 nm.

7-Amino-actinomycin D (7aad) (BD Pharmingen) was used to discriminate dead cells. It has an excitation maximum at 546 and shows emission at 647 nm. 7aad has a strong affinity for DNA but is unable to pass through intact cell membranes, thus staining only dead cells.

The preparation and labeling of isolated cells was conducted as follows:

After extraction and isolation, tumor cells were resuspended in 1 mL erythrocyte lysis buffer and incubated for 8 min at 4°C. 40 mL PBS were added and the tube was centrifuged at 500 x g for 3 minutes. The cells were resuspended in 1 mL PBS and counted. 10^6 cells were transferred to a flow cytometry tube and brought to a volume of 1 mL with PBS, as a control. 2,5 x 10^5 cells were transferred to another flow cytometry tube and brought to a volume of 0,5 mL with PBS. 2,5 µL of unlabeled rat anti-mouse LYVE-1 antibody were added to a dilution of 1:200 and the mixture was incubated for 30 min at 4°C. The cells were spun down at 500 x g for 3 minutes, the supernatant was discarded and the cells were washed in 4 mL PBS, which was removed after another centrifugation. Again, the cells were resuspended in 500 µL PBS and 12,5 µL FITC-conjugated anti-rat antibody was added to a dilution of 1:40. The cells were incubated for 30 min at 4°C, washed and resuspended as previously. 1 µL of PE-conjugated anti-mouse CD31 antibody were added to a dilution of 1:500 and the tube was incubated again for 30 min at 4°C. The cells were washed and resuspended in 500 µL PBS. 2 µL 7aad were added to a final concentration of 4 µg/mL and the measurements were conducted (BD FACScan).

3. Cell culture experiments

3.1. Initial mRNA expression screening

For subsequent mRNA expression analysis, all cell lines (H460, H520, Calu-3, DMS53) were cultured under normal conditions on 10 cm petri dishes. Upon attainment of 70 % confluency, total RNA was isolated according to the procedure described later. The mRNA expression of VEGF-A, VEGF-C, VEGF-D, CSF-1 and ANGPTL4 was assessed.

3.2. Investigation of ANGPTL4 expression under different conditions

For the assessment of ANGPTL4 mRNA expression of cell lines (H460, H520, Calu-3, DMS53) and metastatic cells (C3LuMet, C3LNMet, C3BrMet), isolated from organ tissue of tumor bearing mice, the cells were seeded onto 10 cm petri dishes and supplied with their respective media and incubated at 37°C and 5 % CO_2. Once 70 % confluency was reached, different groups were established. Each cell type was incubated for 24 additional hours under normoxia or under hypoxia, either in medium with 10 % FBS, in medium deprived of FBS, in medium with 10 % FBS and with TGF-β1 added to a concentration of 100 pM, in medium without FBS and with TGF-b1 added. In case of the FBS starved groups, starvation was applied 24 hours prior to TGF-β1 and/or hypoxia addition.

Following the incubation, mRNA was isolated according to the procedure described later.

For the assessment of ANGPTL4 protein secretion, the same cell lines were used and 3 x 10^4 cells were seeded onto two 92 well plates. The groups were established and incubation was conducted as for mRNA expression analysis. The experiment was performed twice in order to verify the result.

Subsequently, the cell culture supernatant was used for the ELISA described later.

3.3. Migration

Due to EMT, many *a priori* epithelial cells change into a mesenchymal-like phenotype during malignant transformation. This goes hand in hand with the acquirement of increased motility, allowing them to invade adjacent tissues and to actively enter or leave vessels, ultimately forming metastases. Eukaryotic cells have a typical diameter of 50-100 µm. If seeded onto a porous membrane with a pore diameter of only 8 µm, it is impossible for them to traverse it, unless they possess active migration capacity. For a defined number of cells seeded onto the membrane, the amount of cells which manage to get to the other side can be used for the relative quantification of migratory capacity between different cell types.
DAPI (4',6-diamidino-2-phenylindole) is a fluorescent dye which strongly binds to DNA. It is excited by fluorescent light and can thus be used to identify migrated cells by staining their nucleus.

Using cells from all cell lines, as well as isolated C3LuMet lung metastatic cells, a trans-well migration assay was performed. The wells of two 24-well plates were supplied with 500 µL medium containing 10 % FBS and a 8 µm permeable support (BD Falcon) was placed on each well. 2 x 10^5 cells of each cell line in 200 µL medium containing 1 % FBS were seeded onto the respective supports. Cells were incubated under normoxia or hypoxia for 24 hours (37°C, 5 % CO_2). Following incubation, the supports were taken out and washed twice with 1 mL ice-cold PBS and 500 µL PBS were added. Cells remaining on the upper side of the membrane were carefully removed with cotton swabs and the membranes were cut out of the supports using a surgical blade. The membranes were then transferred upside down into clean wells containing 1 mL PBS. 1 mL of pre-chilled (-20°C) methanol was added to new wells and the membranes transferred from PBS to methanol. Fixation was performed for 2 min and the membranes were washed in ice-cold PBS. 1 µL of DAPI stock solution (1 mg/mL) was added to new wells containing 1 mL PBS to a final concentration of 1 µg/mL and the membranes were transferred to these wells. Staining was conducted for 10 minutes in the absence of light at room temperature. The membranes were washed twice in PBS, transferred to a glass slide and covered with a cover slip. They were observed through a microscope, 5 representative sectors were counted.

3.4. Tube formation

Endothelial cells exhibit the ability to form three-dimensional capillary-like tubular structures when cultured on a gel of basement membrane extract, mimicking angiogenesis. This can be visualized and quantified relatively.

In order to determine the possible influence of tumor cells on the tube formation ability of LECs, a matrigel tube formation assay was conducted in coculture.
A 96-well tissue culture plate was supplied with 50 µL of growth-factor reduced matrigel (BD Biosciences). 1×10^4 tumor cells in 50 µL culture medium without FBS were added to the wells, as well as 1×10^4 DiI-labeled LEC cells in 50 µL culture medium without FBS. This was done for every tumor cell line (H460, H520, Calu-3 and DMS53) and as a control, LEC cells alone were used. The plates were incubated at 37°C, 5 % CO_2 and tube formation was monitored after 2, 8 and 24 hours. A high pressure mercury lamp was used to induce fluorescence in the labeled cells. Tubes were counted in 5 representative sectors, averaged and compared to the control.

4. mRNA expression

4.1. RNA-isolation

TRIzol®Reagent is a ready-to-use reagent for the isolation of total RNA from cells and tissues. The reagent, which is a mono-phasic solution of phenol and guanidine isothiocyanate, maintains the integrity of the RNA, while disrupting cells and dissolving cell components. Addition of chloroform followed by centrifugation, separates the solution into an aqueous phase and an organic phase. RNA remains exclusively in the aqueous phase. After transfer of the aqueous phase, the RNA is recovered by precipitation with 2-propanol.

Homogenization was the first step in RNA isolation. In the case of tumor tissue, approximately 10 mm³ of cryopreserved material were placed on dry ice and cut into small pieces using a clean razorblade. The pieces were transferred into a 1,5 mL eppendorf tube and 1 mL TRIzol Reagent (Invitrogen) was added. The tissue was

homogenized with a homogenizer (Heidolph Diax 900).

For cells grown in culture, the culture medium was removed and 1mL TRIzol Reagent was directly added to the cells. The cell lysate was passed through a pipette several times and transferred into an 1,5 mL eppendorf tube.

The next steps were identical for tissue and cultured cell RNA isolation.

The homogenized samples were incubated for 5 minutes at room temperature in order to assure complete dissociation of nucleoprotein complexes. 200 µL of chloroform were added, the tubes were vortexed for 20 seconds and incubated at room temperature for another 3 minutes. The samples were centrifuged at 12000 x g for 15 minutes at 4°C. Following centrifugation, the upper aqueous phase was transferred into a new tube and the remaining organic phase was discarded. In order to precipitate the RNA, 500 µL -20°C isopropanol were added and the tubes were inverted several times to mix the solution. After 30 minutes of incubation as -20°C, the samples were centrifuged again at 12000 x g for 30 minutes at 4°C. The isopropanol was decanted off and 1 mL -20°C, 70 % ethanol was added to the pellet. The tubes were centrifuged again at 12000 x g for 8 min at 4°C and as much ethanol as possible was removed by pipetting, without disturbing the pellet. The remaining ethanol was allowed to evaporate for 30 minutes at room temperature and the RNA pellet was finally dissolved in 25 to 50 µL DEPC-treated water, depending on its size. The RNA was stored at -80°C.

4.2. RNA quantification

The RNA concentration can be determined by measuring the absorbance at 260 nm (A_{260}). Quartz cuvettes are used in order to prevent absorbance by plastic or glass.

Due to the partial overlapping of the absorbance of nucleic acids and proteins at 260 nm (because of the aromatic amino acids tyrosine, phenylalanine and tryptophan) and the specific absorbance of proteins at 280 nm, the ratio A_{260}/A_{280} can be used to determine the purity of the RNA. It should be between 1,8 and 2.

The measurements were conducted as follows:

The isolated RNA of tumor samples and cultured cells was incubated for 10 min at 65°C on the heating block in order to separate RNA double strands. 1 µL of the solution was diluted in 999 µL ddH$_2$O in an eppendorf tube and transferred to the

quartz cuvette. The absorption was measured at 260 and 280 nm on a spectrophotometer (Cary 50 Bio). The concentration of total RNA in the stock solution was calculated according to the following equation:

$C \, [\mu g/\mu L] = A_{260}$ x dilution factor x extinction coefficient

4.3. Reverse transcription

Complementary DNA (cDNA) is synthesized from a mature mRNA template in a reaction catalyzed by the enzyme reverse transcriptase. The reaction is a necessary step for subsequent quantitative real-time polymerase chain reaction (qRT-PCR), since DNA polymerase can only act on DNA templates. Because cDNA originates from processed mRNA, it lacks introns.

Reverse transcription was performed as follows:

2 µg of RNA were diluted to 10 µL with DEPC-treated water in an eppendorf tube. 1 µL oligo-dT primer (1 µg/µL, Fermentas) was added and the mixture was incubated for 5 min at 70°C on the heating block. The tubes were transferred to ice, incubated for another 5 min and the condensed liquid was spun down. Reagents were added in the following amount and order:

2,5 µL DEPC-treated water (Fermentas)

4 µL RevertAid^{TM} M-MuLV Reverse Transcriptase buffer (5x, Fermentas)

1 µL dNTP mix (25 pmol, Fermentas)

0,5 µL ribonuclease inhibitor (40 units, Fermentas)

1 µL RevertAid^{TM} M-MuLV Reverse transcriptase (200 units, Fermentas)

For multiple samples, a master mix was made, multiplying the amounts by the number of samples plus 2.

The mixture was incubated for 60 min at 42°C on the heating block and the cDNA was stored at -20°C.

4.4. Real-time PCR

Real-time PCR uses the amplification of specific DNA fragments via polymerase chain reaction combined with a dye which preferentially binds to double stranded DNA (SYBR Green I) and exhibits fluorescence when bound only. A modified, thermo-stable Taq DNA polymerase (FastStart Taq Polymerase) is used. Specific primer pairs consisting of 18-21 bp DNA fragments are chosen to amplify the mRNA of interest. They should span intron-exon boundaries or their sequence should at least be located on two distant exons, in order to prevent the amplification of residual genomic DNA. Also, when working with a mixture of cells from two different organisms as it is the case with xenografted tumors, the primers must be species-specific and their GC-content should be around 50 % to assure specific binding at 50 to 65°C. The reaction itself comprises 45 PCR cycles and is performed in 20 µL capillaries which are placed in an RT-PCR cycler (LightCycler Instrument, Roche). Upon exponential amplification of the mRNA fragment, the amount of bound fluorescent dye increases accordingly. This can be detected by excitation at 488 nm and measurement of fluorescence at 522 nm. The number of cycles required to reach exponential amplification is inversely proportional to the original mRNA concentration of the sample. Primer specificity can be assessed after amplification by a melting curve analysis, which records the fluorescence while increasing the temperature. If the product is uniform, the synthesized DNA-duplexes melt and the fluorescence drops sharply at some point. The respective melting temperature is specific for each amplicon. In addition, the size of the fragment can be checked by agarose gel electrophoresis.

Even though a defined amount of RNA was used initially for the reverse transcription, the efficiency of cDNA synthesis can vary strongly, due to differences in quality of the RNA. Therefore, the resulting data from a qRT-PCR is always compared to a housekeeping gene, which is assumed to be expressed to the same degree in every cell. In this case, the corresponding gene is beta-2-microglobulin (B2M), which is expressed ubiquitously in every nucleated cell as a component of major histocompatibility complex class I (MHC-I) molecules. This allows the relative mRNA quantification between samples.

The used primer sequences are shown in the annex.

The qRT-PCR was conducted as follows:

The cDNA samples were diluted 1:10 in DEPC treated water.

For each sample, one 20 µL capillary was placed in precooled (4°C) centrifuge adapter and a master mix was prepared using components from the LightCycler FastStart Kit (Roche).

Component and stock concentration	Volume for one reaction	Final concentration
H_2O, PCR grade	10,2 µL	
$MgCL_2$ stock solution (25 mM)	1,3 µL	3 mM
LightCycler FastStart DNA Master SYBR Green I	1,5 µL	1x
Forward primer (10 pmol)	0,5 µL	0.33 pmol
Reverse primer (10 pmol)	0,5 µL	0.33 pmol
Total volume	14 µL	

The amount of each reagent was multiplied by the number of samples plus 2. The LightCycler FastStart DNA Master SYBR Green I solution contains the dye, as well as the taq polymerase.

14 µL of the master mix were pipetted into each capillary and 1 µL of diluted cDNA sample was added. The capillaries were sealed with a stopper and the liquid was spun down in a standard benchtop microcentrifuge (Heraeus Biofuge Pico). They were transferred into the LightCycler instrument and the PCR was conducted, comprising the following programs:

First, a preincubation step was performed, heating the samples to 95°C for 10 min.

The second program was repeated automatically 45 times and represents the actual PCR. It implied a fist segment, where primer dimers and double stranded DNA were separated. This was achieved by incubation at 95°C for 10 s. The second segment permitted primer annealing and had a specific temperature for every primer, ranging from 50 to 65 °C for 5 s. The last segment, the synthesis step, was performed at 72°C, which is the optimal temperature for the taq polymerase. Its duration depended on the template length and was calculated by the formula: amplicon length [bp] / 25. After every synthesis cycle, the fluorescence intensity was measured.

Melting, the third program, was performed in order to establish a melting curve and thus identify the corresponding melting temperature for every amplicon. For this purpose, the samples were heated to 95°C in 0,1°C steps per second and the fluorescence was measured constantly.

Data analysis was performed using LightCycler analysis software, which yielded a quantification curve, displaying the fluorescence values for each sample in relation to the cycle number and a melting curve, showing the derivative of the fluorescence value during the melting program in relation to temperature.

4.5. Agarose gel electrophoresis

Due to their phosphate backbone, nucleic acids are negatively charged. If they are added to an agarose gel matrix and an electric field is applied, they migrate towards the anode. Shorter molecules move faster than longer ones, due to the net-like structure of the gel which makes it possible to separate a mixture of nucleic acids according to their length. This method is called agarose gel electrophoresis. A DNA ladder which contains DNA fragments of a defined size can be run simultaneously to allow determination of the length of analyzed DNA.

Ethidium bromide (EtBr) is an intercalating DNA dye, which is excited by ultraviolet light and emits an orange color. If it is added to the gel, it allows visualization of the DNA fragments.

DNA samples must be mixed with a loading buffer, which contains bromphenol blue, which exhibits the same migration characteristics as a DNA fragment of 370 bp and allows monitoring the DNA movement during the experiment. In addition, the loading buffer contains sodium dodecyl sulfate (SDS) which eliminates DNA-protein interactions and the annealing of the ends of DNA molecules. Another component is glycerol, which permits the correct stacking of the sample inside the well.

In addition to melting curve analysis, the amplification of human B2M was verified by agarose gel electrophoresis in a 1,5 % agarose gel. This was done for all primary organ isolates, where moderate or low cell proliferation could be observed, as well as for strongly proliferating, picked and subcultured cells from colonies of isolated organ cells.

Gel preparation and electrophoresis were conducted as follows:

3 g agarose were added to 220 mL 1x TAE buffer in a clean 500 mL bottle. The solution was heated in a microwave, brought to boil and allowed to cool a little bit and brought to boil again. This was repeated until the agarose was fully dissolved. The solution was then allowed to cool to approximately 60 °C and 10 μL EtBr stock solution (10 mg/mL) were added and the gel to a final concentration of 0,5 μg/mL and the solution was poured into a 15 x 15 cm gel rack to obtain a gel of 1 cm thickness. A 30-well comb was inserted at one side and the gel was left to cool and solidify for about 30 min. The gel was removed from the rack and transferred to the electrophoresis apparatus, which was then filled with 1x TAE buffer to cover the gel.

The capillaries from the qRT-PCR were removed from the PCR machine and put upside down into 1,5 mL eppendorf tubes. The tubes were put into a standard benchtop centrifuge and the liquid was transferred from the capillaries into the tubes by bringing the centrifuge to 3000 rpm and stopping it again.

2,5 μL DNA loading dye (6x DNA Loading Dye & SDS Solution, Fermentas) were added to the 15 μL DNA samples and the samples were loaded into the wells of the gel, while sparing the 2 outer wells on each side. 10 μL of DNA ladder mix (GeneRuler DNA Ladder Mix 100-10000 bp, Fermentas) were added to one of the outer wells on both sides of the gel and ultra-low range DNA ladder (GeneRuler Ultra Low Range DNA Ladder 10-300 bp, Fermentas) was added to the other ones.

The gel was run at 80V for 1,5 hours and photographs were taken in a long wave UV-box.

5. Protein expression

The ELISA (Enzyme Linked Immunosorbent Assay) technique is based on the antibody sandwich principle. First, a capture antibody, specific to the analyte of interest is bound to a microtiter plate and a sample or standard is added. If the sample is added, the analyte is retained on the plate by the first antibody and a second antibody is added, which binds another epitope but is also analyte-specific as well as biotinylated. Straptavidin, conjugated to the enzyme horse radish peroxidase (HRP), binds to the biotin of the second antibody. By addition of a substrate (tetramethylbenzidine and H_2O_2), the analyte can be quantified through a color

reaction.

For the assessment of ANGPTL4 protein secretion, the same cell lines were used and the same culture conditions applied as for ANGPTL mRNA expression analysis. 3×10^4 cells were seeded onto two 92 well plates. The experiment was performed twice in order to verify the result. An ELISA duo kit (R&D Systems) was used to assess ANGPTL4 expression.

Plate preparation was conducted as follows:

The capture antibody was reconstituted in 1 mL PBS to a stock concentration of 144 µg/mL. 111,2 µL of capture antibody stock solution were diluted in 20 mL PBS to a working concentration of 0,8 µg/mL. 100 µL of this solution were pipetted into each well of two 96-well plates, the plates were sealed and incubated overnight at room temperature. The next day, the wells were emptied and washed with 400 µL wash buffer (0,05 % Tween 20 in PBS), which was discarded afterwards. This process was repeated twice for a total of three washes. The plates were blocked for one hour at room temperature by adding 300 µL of reagent diluent (1 % BSA in PBS, 0,2 µm filtered) to each well and the washing steps were repeated.

Standards were generated as follows:

Recombinant human ANGPTL4 protein was reconstituted in 0,5 mL reagent diluent, resulting in a stock concentration of 820 ng/mL. 78,04 µL of the protein stock solution were diluted in 721,96 µL reagent diluent to a final concentration of 80 ng/mL, which was used as the high standard. Four two-fold serial dilutions were made in eppendorf tubes, using 200 µL high standard solution every time and transferring 100 µL of this solution to a new eppendorf tube containing 100 µL reagent diluent. The resulting solutions were further diluted in the same way to a total of 7 concentrations (80, 40, 20, 10, 5, 2,5 and 1,25 ng/mL).

The assay was performed as follows:

Of the four standard dilution series, two were pipetted onto each plate. 100 µL of sample or standard were added to the wells, the plates were sealed and incubated for 2 hours at room temperature. The aspiration/wash step was repeated as for plate preparation.

Detection antibody was reconstituted with 1 mL reagent diluent to a stock

concentration of 72 µg/mL. Again, 111,2 µL of the stock solution were diluted in 20 mL reagent diluent to a working concentration of 0,4 µg/mL.

100 µL of detection antibody solution were added to each well, the plates were sealed and incubated for 2 hours at room temperature. The washing step was performed again.

100 µL of Streptavidin-HRP solution were diluted in 20 mL reagent diluent and 100 µL of the resulting solution were added to each well. The plates were incubated protected from light for 20 minutes at room temperature and washed. 100 µL substrate solution (tetramethylbenzidine/peroxide) were added to each well and the plate was again incubated, protected from light, for 20 minutes at room temperature. 50 µL of 2 N H_2SO_4 were added to the wells and the optical density was measured using an ELISA reader at 450 nm. To correct for optical imperfections in the plates, the readings at 570 nm were subtracted. A seven point standard curve was generated with the GraphPad Prism 5.0 software by the four parameter logistic curve-fit method and the ANGPTL4 concentration of samples was calculated by interpolation.

6. Immunohistochemical staining

Immunohistochemistry (IHC) is a method which allows the localization of cell-surface or intracellular proteins through the binding of specific antibodies. The method used involves a primary, unlabeled antibody which is antigen-specific and a secondary antibody, which is biotinylated and binds to the invariable fragment cristallizable region (Fc region) of the primary antibody. Streptavidin, conjugated to HRP can then bind the biotin of the secondary antibody and its location can be visualized by the addition of a substrate (diaminobenzidine and H_2O_2) through a color reaction.

Von Willebrand Factor (vWF) is a glycoprotein, located on the surface of endothelial cells and plays a role in blood coagulation through the permission of thrombocyte-binding. Even though it is also present on megakaryocytes and subendothelial connective tissue, it can be used as a marker for endothelial cells and thus serve to identify peri- and intratumoral blood vessels.

Ki-67 is a nuclear protein, associated with ribosomal RNA (rRNA) transcription. It is most abundant in proliferating cells and can serve as a marker for intra-tumoral cell division.

Paraffin embedded tissue sections of extracted xenograft tumors were stained with rabbit anti mouse vWF (Dako) or mouse anti mouse Ki-67 (Dako) antibodies in order to assess vessel formation and tumor cell proliferation.

Preparation and staining were conducted as follows:

After tumor extraction, one half of the tumor was fixed in a 4 % formaldehyde solution for 1 week at 4°C. Following fixation, the samples were paraffin embedded and slices of 5 µm in thickness were made. The slices were transferred to glass slides and incubated in clean xylol for 15 min in order to deparaffinize them. The xylol was changed and the slices were again incubated for another 5 min. Hereafter, they were transferred to 96 % ethanol and incubated for 5 min. The ethanol was changed, the incubation was repeated and the slides were transferred to 70 % ethanol. After an incubation of 5 min, they were put into PBS. To assure the demasking of antigens, the slides were transferred to a tumbler and covered with citrate buffer (2 g tri-sodium citrate dihydrate in 1000 mL ddH$_2$O, pH 6,5). They were heated in the microwave to 95°C at 350 W for 20 min and allowed to cool for 10 min. Following a 5 min rinsing with tap water, the slides were washed in PBS and the samples were encircled using a delimiting pen (Dako). To avoid interference by any endogenous peroxidase activity, they were incubated in 6 % H$_2$O$_2$ for 20 min and rinsed again in PBS. Blocking solution (1 % BSA and 5 % horse serum in PBS) was added to the samples and they were incubated in a closed wet chamber for 10 minutes. The solution was dripped down. 10 µL primary vWF antibody solution were diluted in 2 mL PBS (1:200) and 27 µL primary Ki-67 antibody solution were diluted in 2 mL PBS (1:75). Either vWF or Ki-67 antibody solution was added to the slides, they were incubated in the wet chamber for 60 min at room temperature and washed 3 times with PBS. 20 µL of the secondary horse biotinylated anti-mouse/anti-rabbit antibody (Vector) stock solution were diluted in 4 mL PBS (1:200) and added to the slides, which were again incubated in the wet chamber for 60 min at room temperature. The slides were washed 3 times in PBS, 4 drops of Streptavidin-HRP solution were added (Dako) and they were incubated for 30 min in the wet chamber. They were rinsed again 3 times

in PBS and 5 drops of DAB/Peroxydase solution (Vector) were added. Incubation took place for 10 min and the slides were washed again in the same way.

For counterstaining, Hematoxylin which colors basophilic structures, such as the nucleus and eosin which colors eosinophilic structures, such as the cytoplasm were used. The slides were washed for 5 min with ddH$_2$O and incubated for 30 s with hematoxylin/eosin solution (Fluka). They were allowed to blue for 10 min under running tap water.

In order to increase the stability of the stained slides, they were dehydrated by subsequent incubation for 5 min in 70 % ethanol, 96 % ethanol and, after drying, xylol. They were mounted by adding a drop of DPX (Fluka).

Results

1. Initial mRNA expression screening

1.1. Primer specificity

Primer specificity was proven for all primers for human cDNA amplification, used in the subsequent experiments. These were huB2M, huVEGF-A, huVEGF-C, huVEGF-D, huCSF-1, huANGPTL4, huTGF-β1 and huTGF-β2. In order to achieve this, qRT-PCR was conducted with cDNA from mRNA isolated from human cells as well as mRNA isolated from murine muscle tissue. Melting curve analysis revealed that the primers permitted the amplification of human cDNA only, which is reflected by a readily discernable peak in the negative derivative of fluorescence intensity at the specific melting temperature (Figure 5). A decrease in fluorescence intensity reflects the melting of double stranded DNA at increasing temperatures. The melting temperature is proportional to the fragment length and thus specific. According to the manufacturer, a drop in fluorescence must be higher than 2 to discern the melting peak from background or artifact fluorescence. Amplification with huTGF-β1 primers also showed a distinct signal in the murine sample. Nevertheless, the lower melting temperature of 85°C and fluorescence intensity drop of 1 suggest a much shorter and less abundant fragment, possibly the result of primer-dimers.

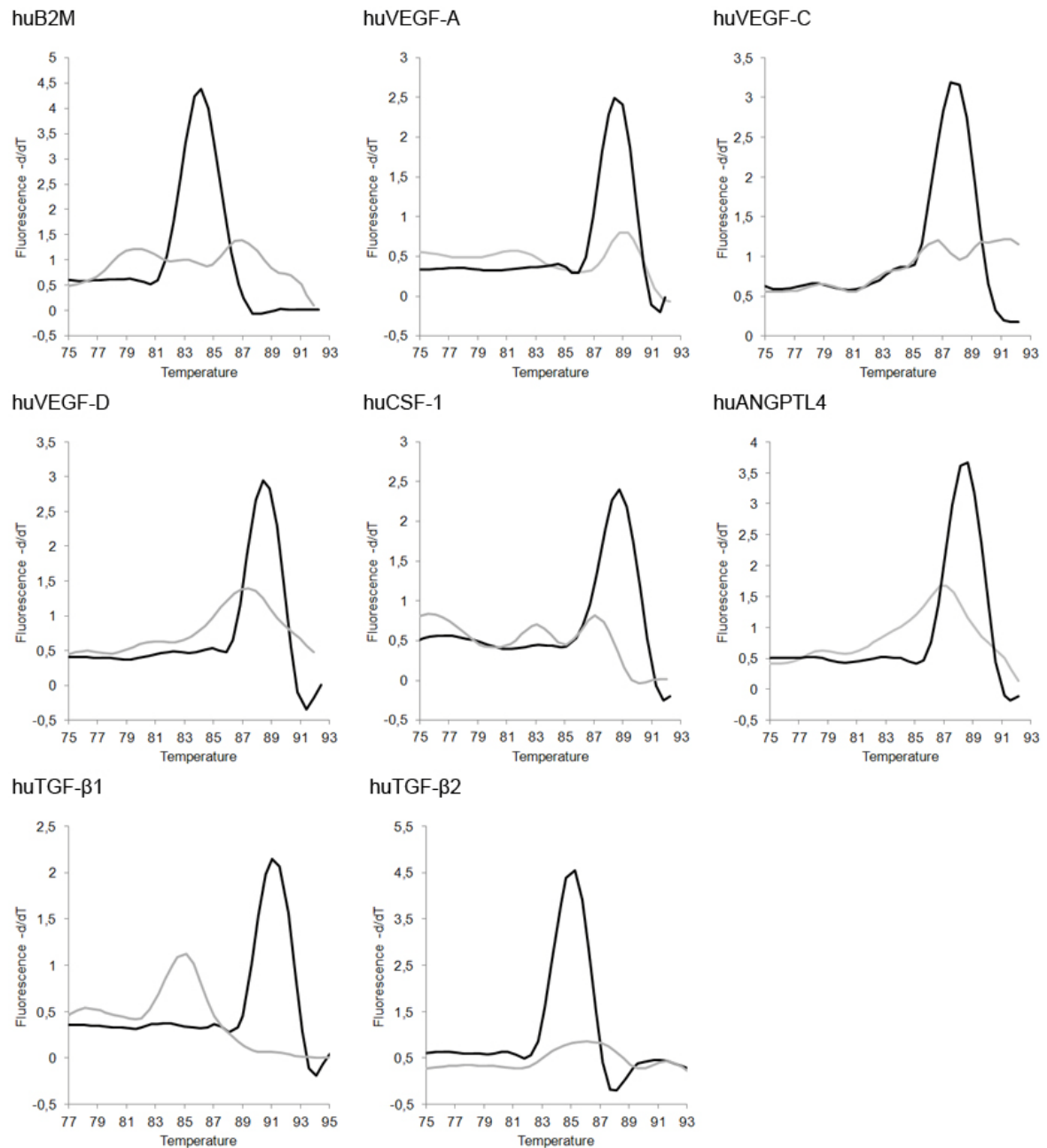**Figure 5: Specificity of primers for human cDNA.**
Melting curves of amplified B2M, VEGF-A, VEGF-C, VEGF-D, CSF-1, ANGPTL4, TGF-β1 and TGF-β2 cDNA fragments. The graphs represent the negative derivative of fluorescence intensity in relation to temperature. Only human cDNA samples (black lines) show a melting peak, whereas samples from murine tissue (grey lines) do not.

49

1.2. *in vitro* mRNA expression of angiogenic and lymphangiogenic factors

RNA was isolated from all NSCLC (H460, H520 and Calu-3) and SCLC (DMS53) cell lines, reverse transcribed to cDNA and the expression of VEGF-A, VEGF-C, VEGF-D and CSF-1 was assessed by qRT-PCR.

The results showed that VEGF-A was most abundantly expressed in Calu-3 cells, and present also in H460 cells. Calu-3 cells expressed VEGF-A approximately 5 times stronger than H460 cells. Other cell lines show no expression at all, suggesting a possible high angiogenic activity in Calu-3 tumors, as well as possible higher metastatic potential (Figure 6A).

Furthermore, VEGF-C expression was present in H460 and Calu-3 only. It was approximately 5 times higher in H460 than in Calu-3 cells, which could indicate a higher lymphangiogenic activity inside or in the periphery of H460 tumors, compared to other cell lines, suggesting possible higher metastases formation to the lymph nodes (Figure 6B).

VEGF-D expression could be observed in all cell lines, most abundantly in Calu-3 and H520 cells. For Calu-3, it was approximately 2,5 times as high as in H460 and 10 times higher than in DMS53 cells. This correlates with a relatively high incidence of lymphatic endothelial cells in Calu-3 derived tumors, as shown later by FACS analysis as well as lymph node metastasis observed *in vivo*.

For H520, VEGF-D expression was twice as high as in H460 cells and 8 times higher than in DMS53 cells. This is in accord with the high amount of tube formation by lymphatic endothelial cells in coculture with H520 cells shown later.

Lastly, CSF-1 expression could only be observed in Calu-3 and H460 cells with Calu-3 expressing approximately twice as much mRNA than H460, which could indicate a higher angiogenic and lymphangiogenic activity in tumors derived from these cells (Figure 6D).

In summary, DMS53 showed the lowest expression of angiogenic and lymphangiogenic factors, whereas Calu-3 exhibits the highest expression for three of the four assessed factors.
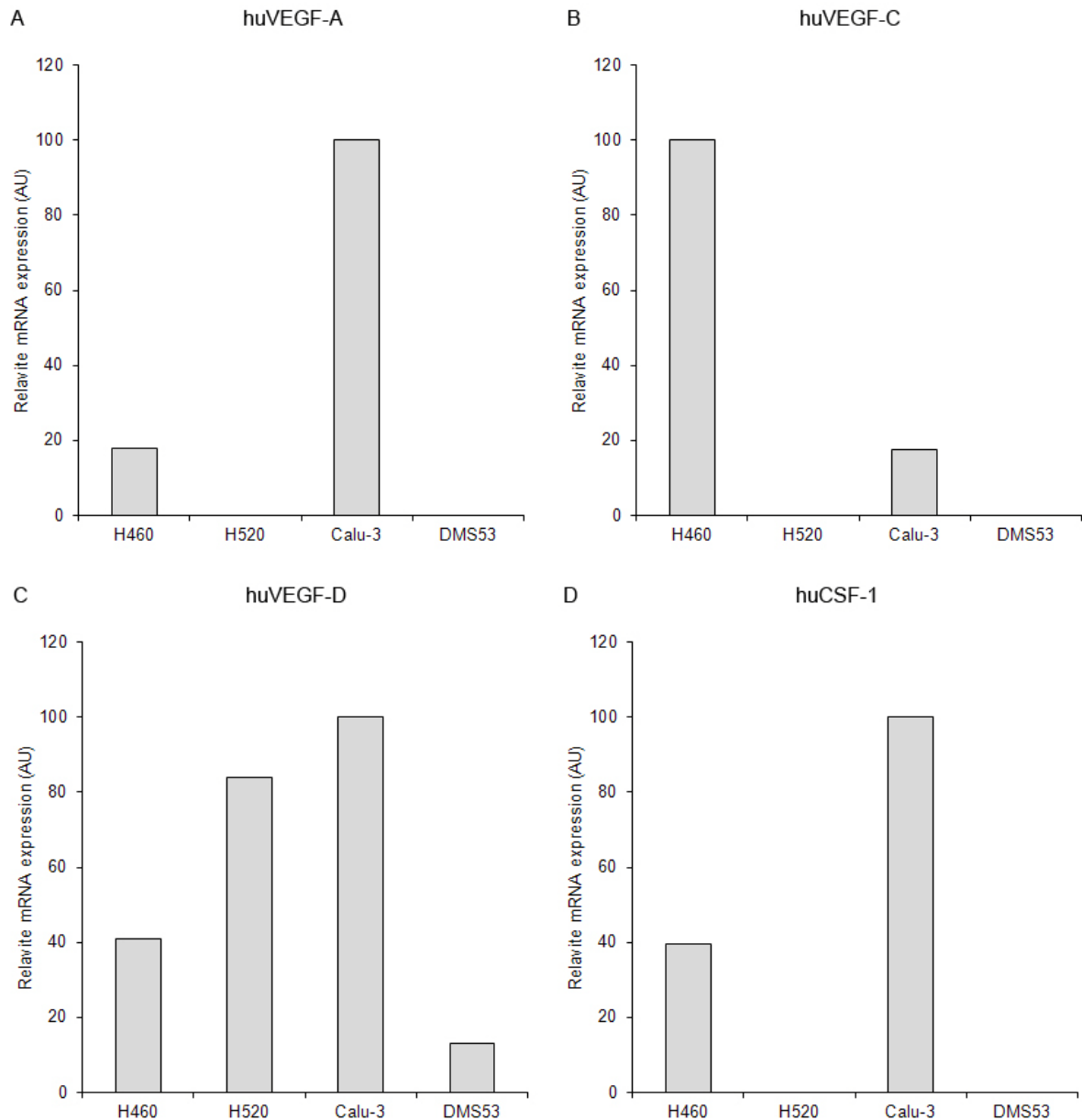
Figure 6: *in vitro* mRNA expression of VEGF-A, VEGF-C, VEGF-D and CSF-1 in NSCLC and SCLC cell lines measured by qRT-PCR

mRNA expression of human VEGF-A (A) with Calu-3 cells showing much higher expression than other cell lines; VEGF-C (B) with H460 cells showing the highest expression; VEGF-D (C) with Calu-3 and H520 showing the highest expression and CSF-1 (D) with Calu-3 showing the highest expression. Data are shown in arbitrary units (AU), normalized to the highest expression value for each assessed factor.

2. Large cell and squamous cell bronchus carcinoma induce LEC tube formation

A matrigel tube formation assay was conducted with all bronchus carcinoma cell lines in coculture with lymphatic endothelial cells (LECs) in order to assess a possible

influence on lymphangiogenic activity. LECs were previously DiI-labeled to discern them from tumor cells. Tube formation was checked every 4 hours for 24 hours and photomicrographs were taken (Figure 7).
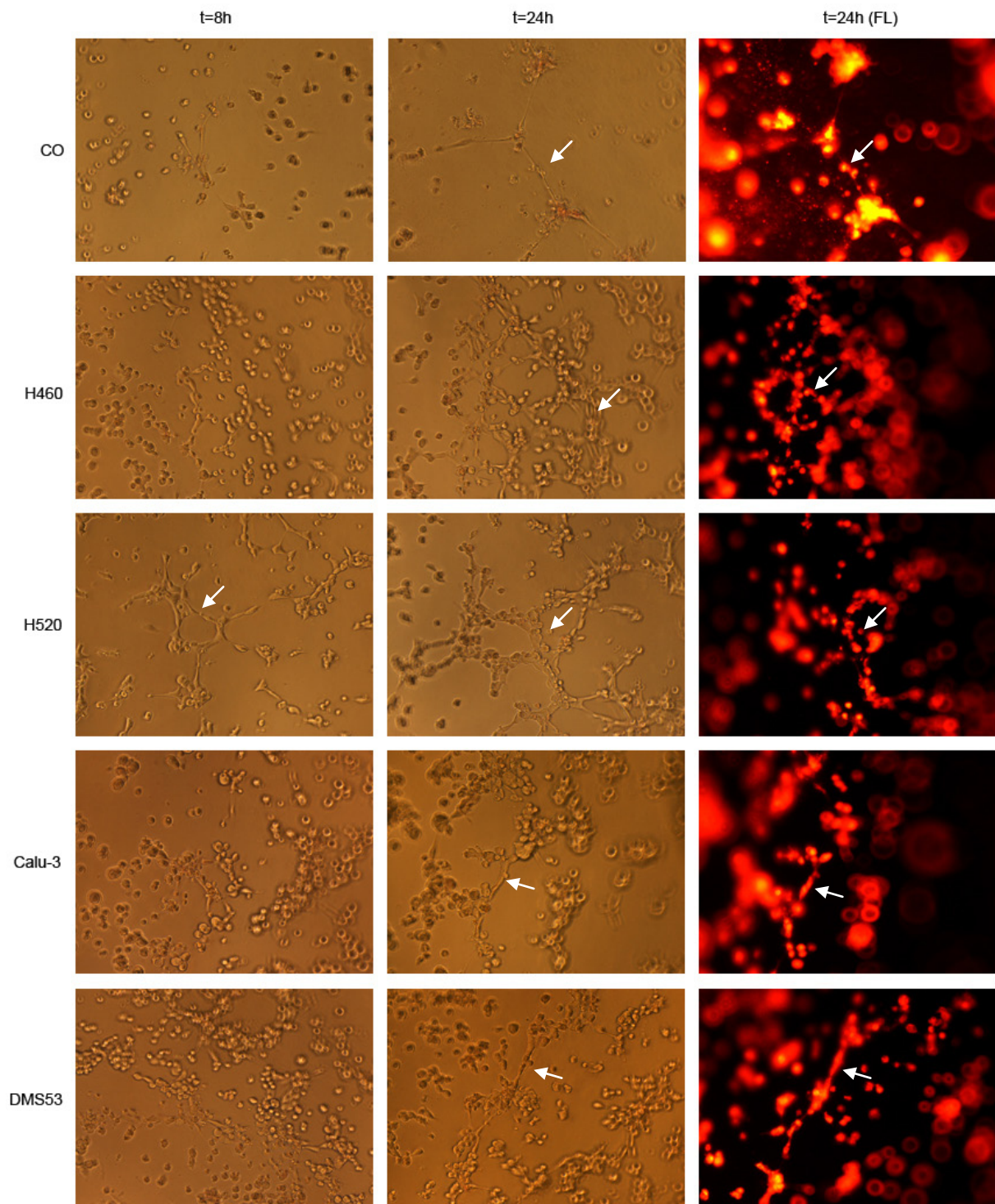
Figure 7: Tube formation by LECs on growth factor reduced matrigel.
Photomicrographs (magnification: 100 x) of tube formation by DiI-labeled LECs in coculture with H460, H520, Calu-3 and DMS53 after 8 and 24 hours. After 8 hours, extensive tube formation compared to control (LECs only) can only be detected in H520 samples. After 24 hours, all samples show tube formation to a certain degree, the highest in H520 and H460 cocultured LECs. Arrows indicate tubes. To discern LECs from tumor cells, fluorescence images were taken, showing only the DiI-labeled LECs (FL)

Tube formation was quantified relative to the control (LECs only) by counting in 5 representative sectors and averaging. LECs in coculture with H460 cells exhibited the fastest and strongest tube formation, 2,5 times higher than the control without tumor cells added at 24 hours incubation. LECs cultured with H520 cells also showed twice as much tube formation capacity as the control at 24 h. Calu-3 and DMS53 did not increase tube formation of LECs, with DMS53 even causing strongly decreased LEC capillary formation (Figure 8).

The fact that H520 and H460 showed the highest tube formation induction in LECs is in accordance with the high VEGF-C expression of H460 and the high VEGF-D expression of H520, determined by qRT-PCR *in vitro*.

Nevertheless, Calu-3 did not increase tube formation, despite its high VEGF-D expression. Hence, a universal correlation between VEGF-C or VEGF-D mRNA expression and LEC tube formation could not be established.

Figure 8: Tube formation

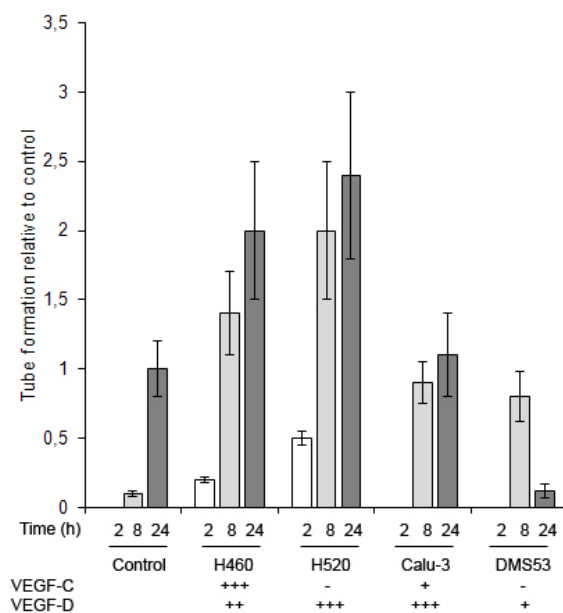Relative quantification of tube formation capacity by LECs in coculture with H460, H520, Calu-3 and DMS53 after 2, 8 and 24 hours. *In vitro* VEGF-C and VEGF-D mRNA expression of each cell line is indicated below. H520 and H460 show the strongest and fastest tube formation induction capacity. Data are expressed as mean ± SD in arbitrary units, normalized to the tube formation value of LECs only (n = 5).

3. Xenografts

3.1. Large cell and squamous cell bronchus carcinoma show the fastest tumor growth

The bronchus carcinoma cell lines used in the *in vitro* experiments (H460 large cell carcinoma, H520 squamous cell carcinoma, Calu-3 adenocarcinoma and DMS53 small cell carcinoma) were injected into the flanks of athymic, nude mice (n = 8 for each cell line) in two different cell numbers (5×10^6 and 10×10^6, n = 4 for each cell number) in order to examine tumor growth. According to our termination criteria, animals were sacrificed as soon as the tumor size reached 2 cm^3.

Almost all injected cell lines exhibited 100 % tumor formation, except for DMS53 with only 2 out of 4 animals with 10×10^6 cells injected developing tumors. There were large discrepancies in growth rate and latency time between different cell lines.

H460 large cell bronchus carcinoma cells showed the fastest growth, compared to the other cell lines, for both 5×10^6 and 10×10^6 cells injected. The 10×10^6 cell group reached a tumor size of 2 cm^3 after 16 days and the animals were terminated accordingly at day 18 post injection (Figure 9A).

H520 squamous cell bronchus carcinoma cells showed a far slower growth overall, with tumors attaining 2 cm^3 for the 10×10^6 group after 32 days. For the 5×10^6 group, tumor formation was almost unnoticeable during the first 30 days of the experiment and after this period, tumor size remained almost unchanged. The animals of the 5×10^6 and 10×10^6 groups were terminated at day 32 and 78 respectively. The results indicate that 10×10^6 is an appropriate cell number for further experiments in order to assess the impact of applied therapies on tumor growth and metastasis (Figure 9B).

Calu-3 bronchus adenocarcinoma cells showed growth rates similar to H520, with the 10×10^6 group attaining 2 cm^3 after 37 days and high growth latency for the 5×10^6 group. Animals were killed at day 42 for the 10×10^6 group and day 49 for the 5×10^6 group. It is important to note that the animals which had received 10×10^6 cells showed very heterogenic tumor growth. Nevertheless, 10×10^6 cells seem to be an appropriate cell number for the future investigation of metastases formation and therapeutic impact (Figure 9C).

DMS53 small cell bronchus carcinoma cells exhibited far less frequent tumor formation with two animals of the 10 x 10^6 cell group not developing tumors at all. The latency was higher than for every other cell line with stagnant tumor sizes up to day 40 post injection. In the case of the 5 x 10^6 cell group, tumor growth remained slow until termination at day 78. The 10 x 10^6 group however showed much faster growth after onset, with tumors reaching 2 cm^3 after 59 days but owing to the long latency time and the fact that two animals did not develop any tumor at all, the cell concentration seems too low for future experiments. The animals were terminated at day 59 (Figure 9D).

In summary, great discrepancies exist between the different bronchus carcinoma subtypes. H460 showed by far the fastest and DMS53 the slowest tumor growth rate. H520 and Calu-3 revealed considerable differences in tumor growth, depending on the cell number injected. The onset of tumor growth also varies greatly, with H460 and H520 showing the earliest and Calu-3 and DMS53 the latest. All tumor cell lines developed spherical subcutaneous tumors comparable in shape, with no observable invasive process into the peritoneum (Figure 9E).
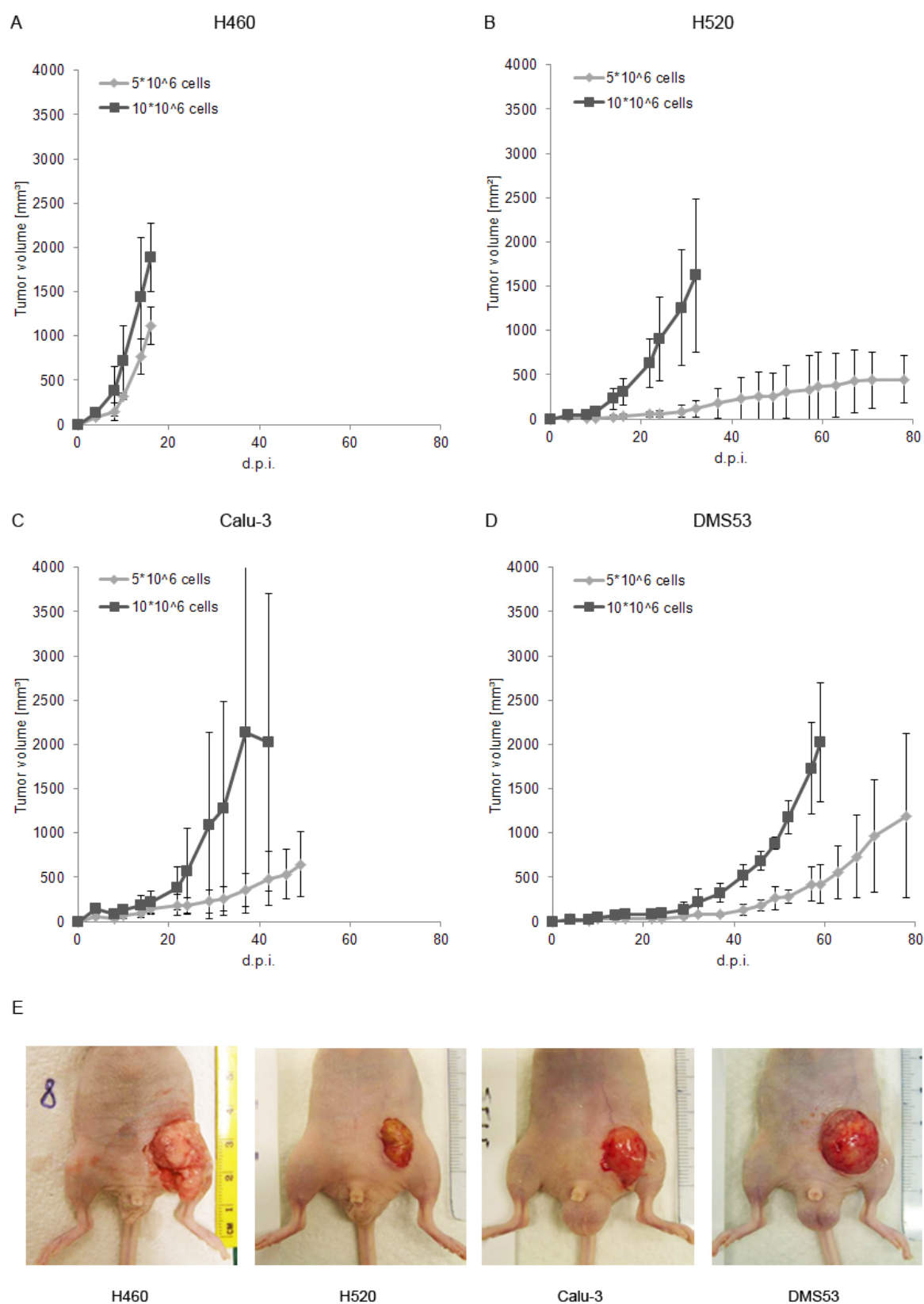
Figure 9: Establishment of lung cancer xenograft models in athymic, nude mice

Tumor growth curves for H460 (A), H520 (B), Calu-3 (C), and DMS53 (D) (n = 4 for each cell line and number) and representative pictures of tumors (E). H460 shows the fastest tumor growth and DMS53 the slowest. All tumors exhibit spherical morphology. Data are expressed as mean ± SD.

3.2. *in vivo* mRNA expression of angiogenic and lymphangiogenic factors

RNA was isolated from all extracted tumor samples, reverse transcribed and qRT-PCR performed for huVEGF-A, huVEGF-C, huVEGF-D and huCSF-1 (n = 8 for each cell line).

All cell types showed VEGF-A mRNA expression with H520 and Calu-3 cells exhibiting the highest.

In contrast to *in vitro* data, VEGF-A mRNA expression in H520 was the highest among all cell lines, 0,8 fold higher than in H460 and 0,6 fold higher than in DMS53 cells. Accordingly, as shown later by immunohistochemical staining, tumors derived from H520 show the second highest overall vessel density.

Expression in Calu-3 remained high as compared to the other cell lines with a 0,6 fold increase compared to H460 and 0,3 fold compared to DMS53.

H460, which had moderate expression *in vitro*, showed an increase in VEGF-A mRNA *in vivo* and DMS53 cells, which did not express VEGF-A *in vitro*, now had mRNA levels comparable to those of H460 cells (Figure 10A). Physiological changes within the tumor, such as hypoxia may have induced VEGF-A expression (Figure 10D).

VEGF-C mRNA expression in tumor samples was present in all cell lines, except for DMS53. Again, H520, which did not express VEGF-C *in vitro* and Calu-3 showed the highest mRNA expression. VEGF-C expression was 0,5 fold higher in H520 as compared to Calu-3 and 1 fold higher as compared to H460 tumors. Calu-3 VEGF-C expression was 0,4 fold higher than in H460 tumors (Figure 10B).

Accordingly, H520 cells exhibited the highest tube formation induction capacity in LECs *in vitro*, even though no lymphatic endothelial cells could be found inside the tumor tissue by FACS analysis, as shown later.

VEGF-D mRNA expression was detected in all tumors, comparable to *in vitro* data. Calu-3 and H520 again showed the highest expression and H460 and DMS53 had comparable but lower expression, further underlining the possibility for lymphangiogenesis to play a role in Calu-3 and H520 tumor progression and increased metastases formation, observed in animals bearing these tumor types, as shown later (Figure 10C).

CSF-1 mRNA could not be detected in any of the samples.

The variability was very high in all groups, indicating a high heterogeneity in gene expression even among tumors of the same type.

		VEGF-A	VEGF-C	VEGF-D	CSF-1
H460	in vitro	+	+++	++	+
	in vivo	++	++	+	-
H520	in vitro	-	-	+++	-
	in vivo	+++	+++	++	-
Calu-3	in vitro	+++	+	+++	+++
	in vivo	+++	++	+++	-
DMS53	in vitro	-	-	+	-
	in vivo	++	-	+	-
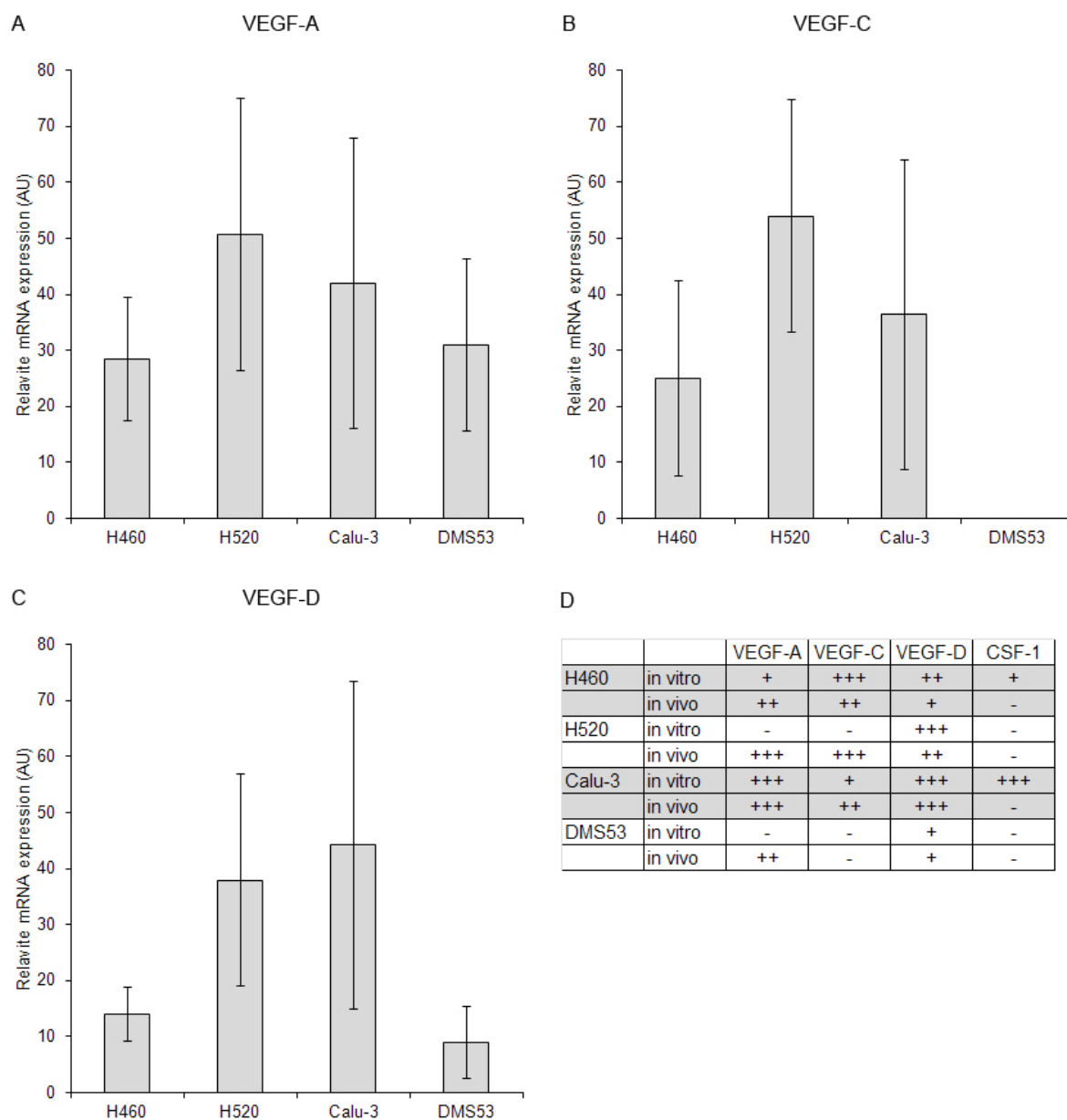
Figure 10: *in vivo* mRNA expression of VEGF-A, VEGF-C, VEGF-D and CSF-1

mRNA expression of huVEGF-A (A) huVEGF-C (B) and huVEGF-D (C) in tumor samples from H460, H520, Calu-3 or DMS53 bearing mice with H520 and Calu-3 having the highest levels in all cases. CSF-1 expression *in vivo* is negative. Comparison of *in vitro* and *in vivo* expression (D) shows major changes in every cell line, except for Calu-3. Data are expressed as mean ± SD in arbitrary units (AU), normalized to the highest expression value of each assessed factor (n = 8 for each cell line).

3.3. Murine lymphatic endothelial cells are present within large cell bronchus carcinoma xenografts

In order to determine the presence of lymphatic endothelial cells within the tumor, cells from unlabeled tumors were isolated and double-stained with antibodies against endothelium-specific CD31 (PE-labeled) and lymph-specific LYVE-1 (FITC-labeled) (n = 4 for each cell line). Dead cells were excluded by 7aad-staining. Following the staining procedure, the cells were subjected to flow cytometric analysis. Side scatter versus front scatter representation revealed a very heterogeneous cell mixture in all tumor isolates, containing cellular debris of very small size, as well as cellular aggregates of very large size, which were excluded by gating (Figure 12).

Also, dead cells exhibiting high 7aad fluorescence, visualized in fluorescence channel 3 (fl3), were removed by gating (Figure 12).

The FITC-fluorescence of LYVE-1 antibodies (fluorescence channel 1, fl1) was then plotted against the PE-fluorescence of CD31 antibodies (fluorescence channel 2, fl2) and single, as well as double positive cells could be identified and quantified by gating (Figure 12). Tumors derived from H460 showed 0,17 % percent CD31/LYVE-1 double positive, intra-tumoral lymphatic endothelial cells, whereas H520 and Calu-3 only showed 0,05 %. This suggests that H460 cells possibly promote lymphangiogenesis *in vivo* and is in accord with their high LEC tube formation induction capacity and their high VEGF-C mRNA expression *in vitro (*Figure 11). There were almost no lymphatic cells present in DMS53 derived tumors, which validated the mRNA expression and tube formation data. Even though H520 and Calu-3 showed high VEGF-D mRNA expression both *in vitro* and *in* vivo and high VEGF-C mRNA expression *in vivo*, tumors derived from these cells showed a much lower percentage of lymphatic endothelial cells (Figure 11). There may be a translational control mechanism involved or a higher density of extra-tumoral lymph vessels, which would not be included in this experiment.

In summary, *in vivo* VEGF-C and VEGF-D mRNA expression did not correlate with LEC incidence within tumor tissue, except for large cell bronchus adenoma xenografts (Figure 11 B).

A

B

		VEGF-C	VEGF-D	LECs in tumor tissue
H460	in vitro	+++	++	
	in vivo	++	+	+
H520	in vitro	-	+++	
	in vivo	+++	++	-
Calu-3	in vitro	+	+++	
	in vivo	++	+++	-
DMS53	in vitro	-	+	
	in vivo	-	+	-
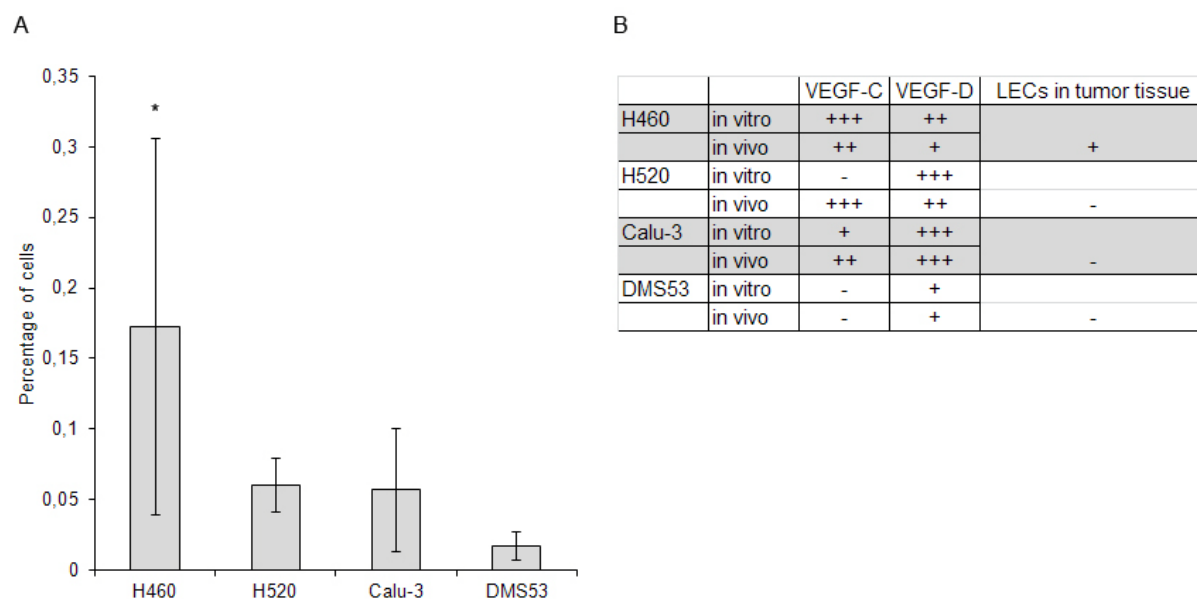
Figure 11: Measurement of murine LECs in tumor tissue

Percentage of CD31/LYVE-1 double positive cells in tumors of H460, H520, Calu-3 and DMS53 cells (A). Data are expressed as mean ± SD (n = 4 for each cell line; * indicates $p < 0,05$; unpaired t-test) The table shows *in vitro* and *in vivo* VEGF-C and VEGF-D expression, as well as murine LEC incidence in tumor tissue (B). H460 is the only tumor subtype, which exhibited a significant number of murine LECs.
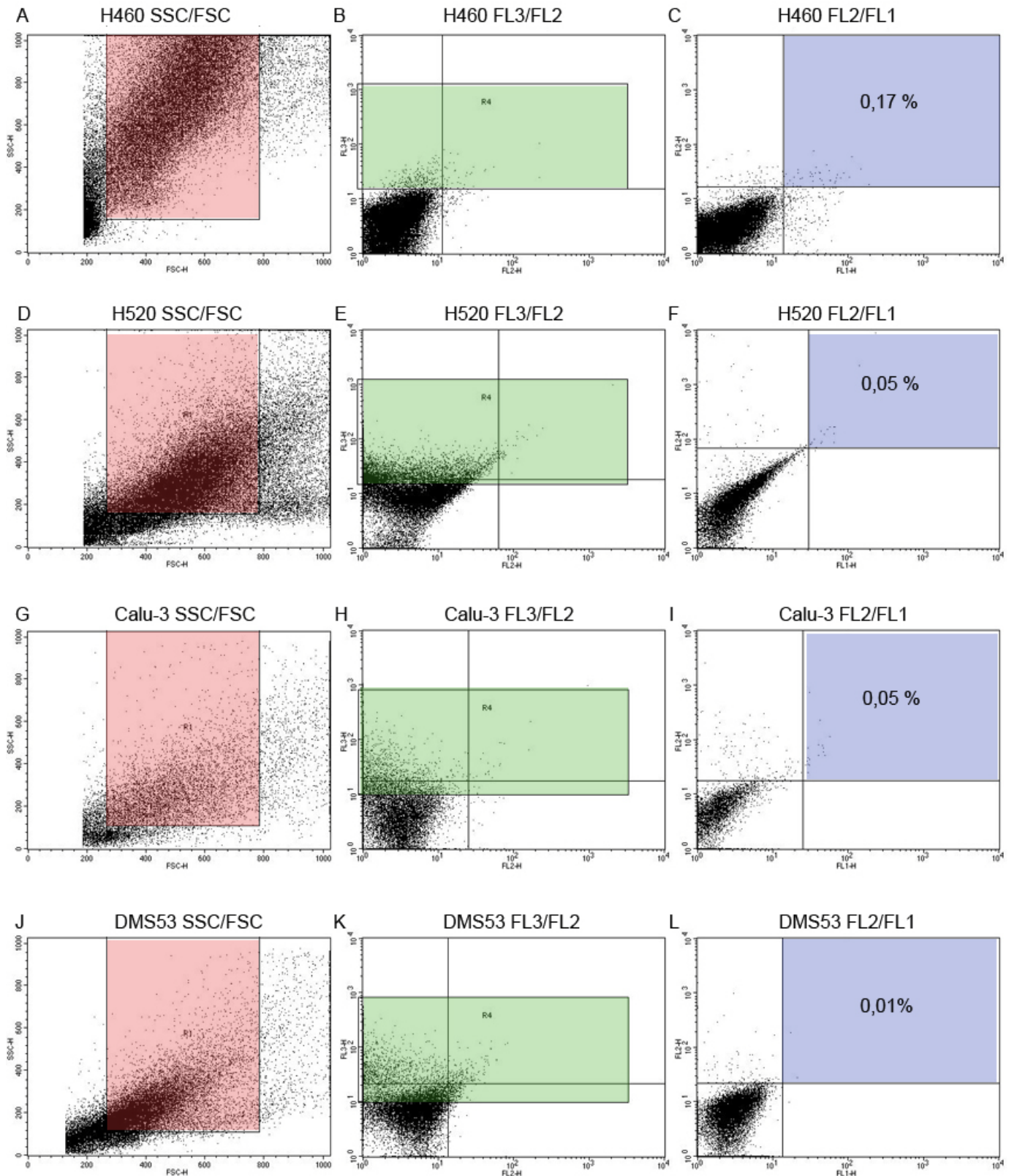
Figure 12: FACS analysis

Representation of flow cytometric data. Front scatter/side scatter representation of H460 (A), H520 (D), Calu-3 (G) and DMS53 (J) isolates. The gate excluding cellular debris and cell aggregates is shown in red. 7aad fluorescence (Fl 3) of H460 (B), H520 (E), Calu-3 (H) and DMS53 (K). Dead cells exhibiting high fluorescence (green) are excluded. FITC (Fl 1) and PE (Fl 2) fluorescence of gated, double stained H460 (C), H520 (F), Calu-3 (I) and DMS53 (L). Double positive murine LECs (blue) and their percentage are shown. H460 large cell carcinomas are the only tumors in which a significant number of LECs could be detected.

3.4. Large cell bronchus carcinoma xenografts show the highest proliferation rate and overall blood vessel density

In order to determine the extent of cell proliferation and angiogenesis inside xenografted tumors, formalin fixed, paraffin-embedded tumor slices were immunohistochemically stained with antibodies against the proliferation-marker Ki67 and the angiogenesis marker vWF. The relative extent of cell proliferation and angiogenesis was determined by the comparison of five representative microscopic fields of tumors from all cell lines.

Ki67 staining revealed the highest proliferation rate for H460, compared to the other cell lines, which is in accord with its fast tumor growth (Figure 13A). vWF staining showed the highest vessel density for H460 as well, which is in contrast to its relatively low VEGF-A mRNA expression *in vivo* (Figure 13B). It has to be noted that this was only valid for peritumoral blood vessels, whereas intratumoral angiogenesis was low, compared to the other cell types (Figure 13C and D, Figure 14).

H520 showed the second highest proliferation rate and vessel density, with abundant peritumoral as well as intratumoral vessel formation (Figure 13, Figure 14). This does reflect its high VEGF-A mRNA expression as well as its high metastatic activity *in vivo*, as shown later.

Calu-3 showed lower proliferation rates than H460 and H520, mostly of glandular cells and the lowest vessel density among all cell types (Figure 13A and B). It did however show the highest number of intratumoral vessels. Furthermore, the observed blood vessels were larger in diameter compared to all other cell lines, which may be accounted for by the high VEGF-A mRNA expression of these tumor cells (Figure 13C and D, Figure 14). Also, Calu-3 exhibited the highest metastasis rate of all tumor types, as shown later.

Lastly, DMS53 had very low proliferation rates, coinciding with its very high tumor growth latency (Figure 13A). The overall vessel density was comparable to Calu-3 but there were slightly more peritumoral vessels present (Figure 13B and 14). Nevertheless, vessel diameter was much lower than for Calu-3.
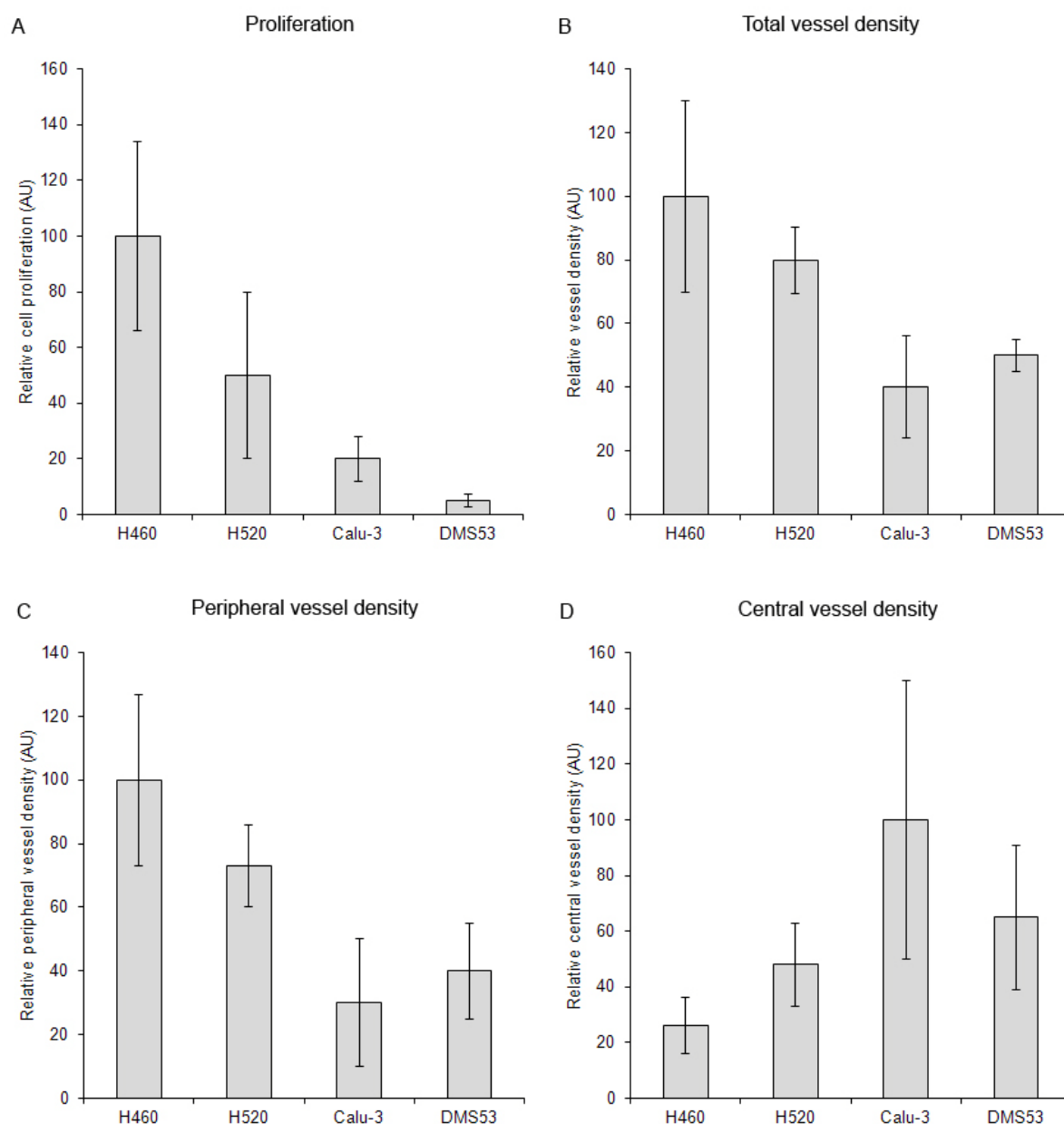
Figure 13: Cell proliferation and vessel density inside xenograft tumors

Relative quantification of cell proliferation (A), overall vessel density (B), peripheral vessel density (C) and central vessel density (D) of extracted tumors from all cell lines. H460 large cell carcinoma shows the highest proliferation and overall vessel density. This is attributable to the high number of peripheral vessels, whereas Calu-3 shows the highest density of central vessels. Data are expressed as mean ± SD in arbitrary units (AU), normalized to the highest value for each assessed feature (n = 5).
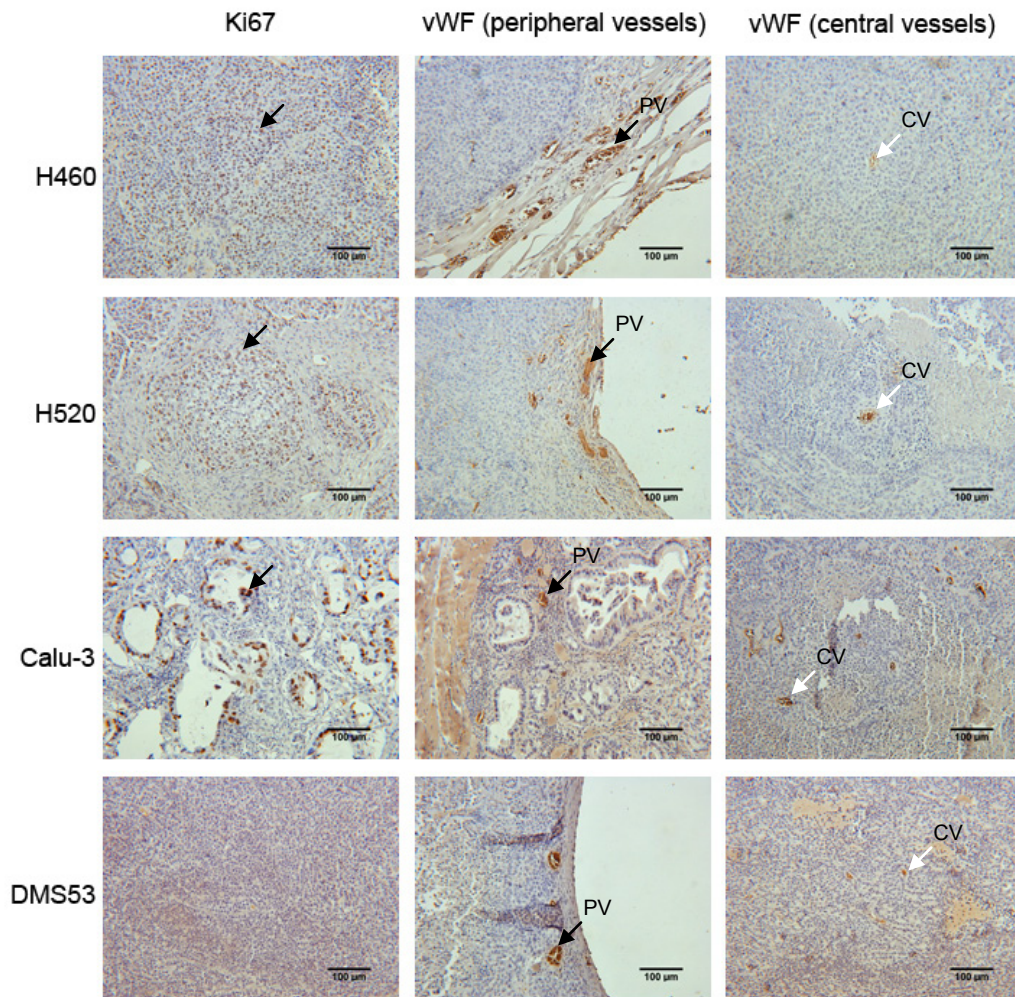
Figure 14: Ki67 and vWF stained tissue sections

Representative pictures of Ki67 and vWF stained slices of extracted tumors from H460, H520, Calu-3 and DMS53 cells. Proliferating, Ki67 positive cells (brown) are indicated by arrows (left). H460 shows by far the most proliferating cells, whereas DMS53 shows the least. Brown, vWF positive cells represent endothelial cells in peripheral tumor sections (center) and central tumor sections (right). H460 exhibits abundant peritumoral vessel (black arrows, PV) formation. Calu-3 and DMS53 show the highest number of central vessels (white arrows, CV) with higher diameter in the case of Calu-3. Note that Calu-3 tumors show glandular morphology only at the periphery.

4. Metastases

4.1. Adenocarcinoma and squamous cell carcinoma exhibit frequent spontaneous metastasis in xenograft animals

Among each tumor cell line and cell number group, two animals had received DiI-labeled cells, which showed high fluorescence prior to injection (n = 2 for each cell concentration and cell line or n = 4 for each cell line). Lung, discernible lymph nodes, kidney and brain of these animals were extracted. Organ cells were isolated, cultured and monitored for fluorescence, which would indicate whether growing cells are of human provenance and thus represent tumor cells which had established distant, metastatic colonies in the respective organ. Presumably due to the nature of DiI as a lipophilic compound which gets diluted by 2 with every cell division, combined with the overall long tumor growth times, DiI fluorescence could not be detected in any of the samples, not even in the tumor itself.

Therefore, another method had to be chosen to assess the human nature of growing cells. The isolates were allowed to grow for 4 weeks and subcultured if necessary as soon as they had reached 70 % confluency, in order to get an enrichment of proliferating cells. RNA was isolated, reverse transcribed to cDNA and specific qRT-PCR was performed for human beta 2 microglobulin (huB2M). The results indicate that metastatic tumor cells were indeed present in various organs. For H460, human cells could be detected in the lung isolates of one animal which had received 10×10^6 cells, which equals to 25 % of examined animals. For H520, they could be detected in the lung isolates of two animals, which had received 10×10^6 cells, representing 50 % of examined animals. For Calu-3, cells of human nature could be detected in one lung isolate of an animal which had received 5×10^6 cells. Among the 10×10^6 animals, human cells could be detected in the organs of both animals. One of them showed human B2M expression in all isolates (lung, lymph node, kidney and brain), while the other one showed expression in lung and lymph node isolates. Overall, this equals to as high as 75 % of all animals. In the case of DMS53, no cells of human provenance at all could be detected in any organ (Figure 15).
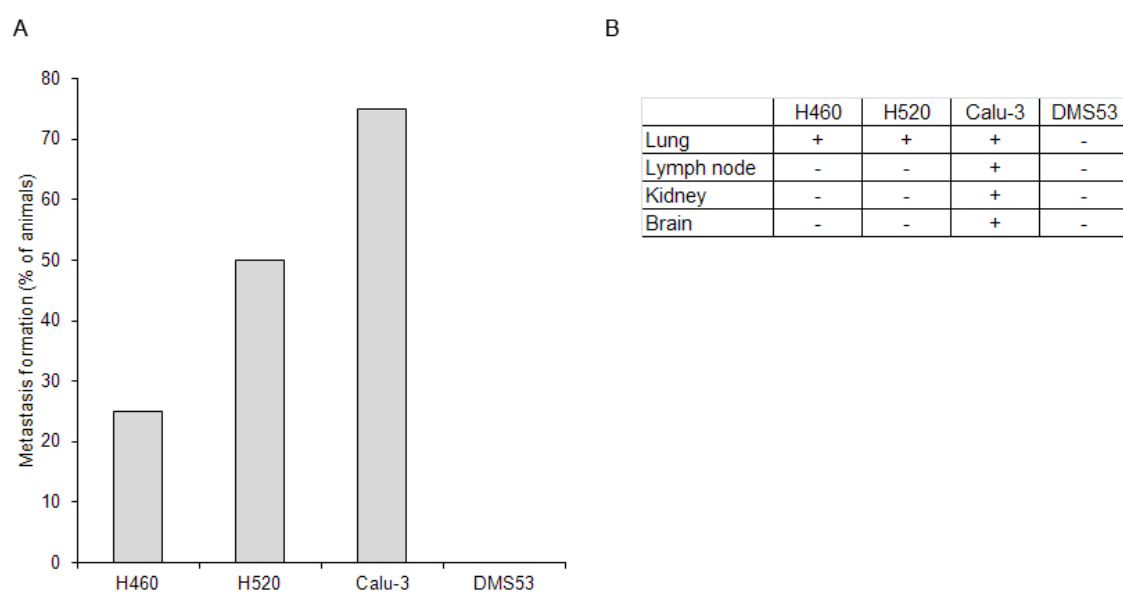
Figure 15: Metastasis in xenograft animals

Overall percentage of the occurrence of metastases in H460, H520, Calu-3 and DMS53 tumor bearing mice, detected by specific qRT-PCR for huB2M (n = 4 for each cell line) (A). Calu-3 adenocarcinoma exhibits the most frequent formation of metastases. Table indicating the site of metastasis for each cell line (B). Calu-3 is the only cell line which develops metastasis in all examined organs.

The correct amplification was checked by agarose gel electrophoresis, which showed that the huB2M fragment was either not present or of the expected length of 114 bp. (Figure 16)
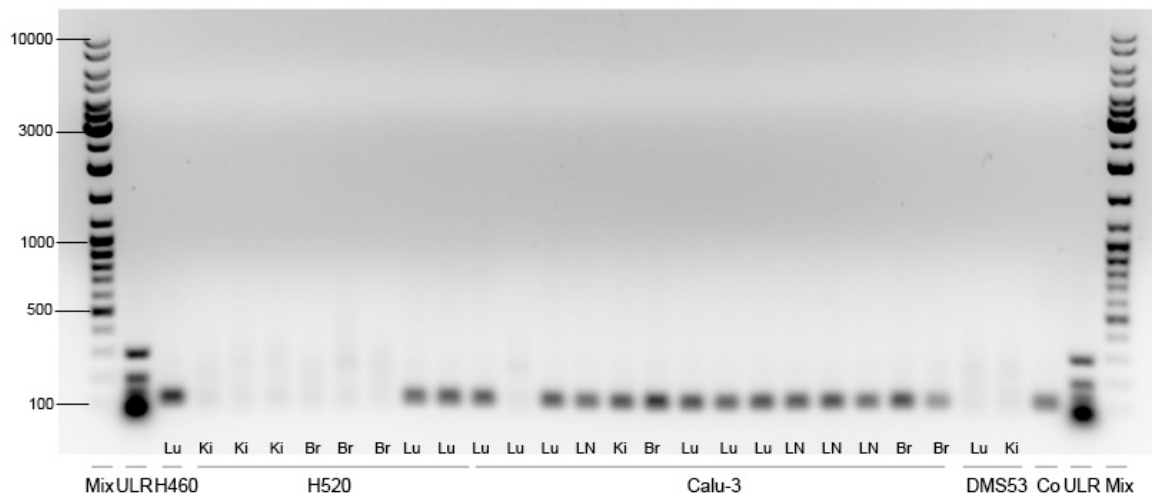
Figure 16: Agarose gel electrophoresis of huB2M PCR-Products

Agarose gel electrophoresis of huB2M PCR-products from organ isolates showing cell growth. Lane 1: DNA Ladder Mix 100-10000 bp (Mix), 2: Ultra low range DNA ladder 10-300 bp (ULR), 3: H460 lung (Lu) isolate from 1 animal, 4-11: H520 brain (Br), kidney (Ki) and lung isolates from 3 animals, 12-25: Calu-3 lung isolates from 2 animals and lung, lymph node (LN), kidney and brain isolates from 1 animal as well as cDNA from picked and subcultured cells from lung, lymph nodes and brain, 26-27: DMS53 lung and kidney isolated from 1 animal, 28: Positive control from cultured H460 cells, 29: Ultra low range DNA ladder 10-300 bp, 30: DNA ladder mix 100-10000 bp. Calu-3 adenocarcinoma shows the most frequent and widespread metastasis.

If extensive cell division and colony formation could be observed, cells were picked, transferred to a new petri dish and further cultivated. This was the case for Calu-3 lung, lymph node and brain isolates of 1 animal, which clearly showed morphological features of tumor cells, such as unlimited cell division, polymorphism, enlarged nuclei and granular chromatin. Photomicrographs were taken (Figure 17).

Figure 17: Metastatic cells

Photomicrographs of proliferating cells, picked from lung, lymph node and brain isolates of one Calu-3 bearing animal. High proliferation, as well as polymorphism and enlarged nuclei suggest a metastatic nature.

RNA was isolated from these cells as well and qRT-PCR for huB2M was conducted. The results showed that these cells really were of human origin and thus represented metastatic cells. They were dubbed C3LuMet for cells isolated from the lung, C3LNMet for cells isolated from the lymph node and C3BrMet for cells isolated from the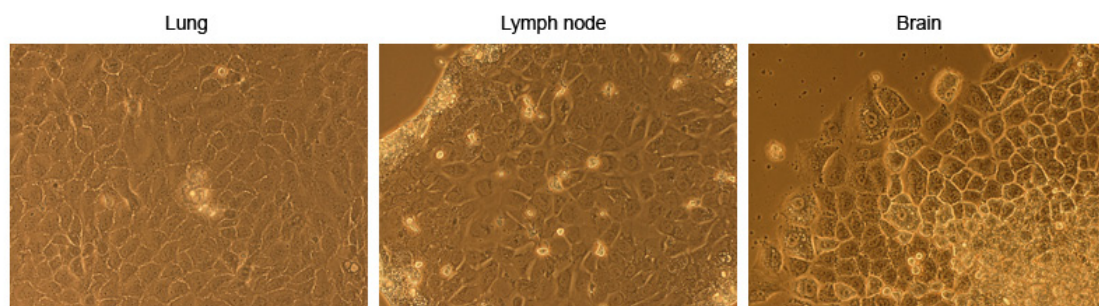 brain (Figure 16). These cells were later used for the assessment of mRNA and protein expression of ANGPTL4 as well as migration.

In summary, metastasis to the lungs was observed in 3 of 4 examined bronchus carcinoma cell lines, namely H460, H520 and Calu-3. Metastases formation in other organs was found in Calu-3 adenocarcinoma bearing mice only. Calu-3 also showed the highest overall metastasis rate.

4.2. Metastatic adenocarcinoma cells show higher migratory capacity than the original cell line

In order to investigate and to compare the migratory capacity of cell lines and isolated metastatic cells, a transwell migration assay was performed under normoxia and hypoxia with H460, H520, Calu-3, DMS53 and C3LuMet cells. After 24 h, the membranes were cut out, fixed, DAPI-stained, photomicrographs were taken and migrated cells in five representative regions were counted (Figure 18A) (n = 5 for each cell line). The results indicate that H460 cells have by far the highest migratory activity, whereas all other cell lines exhibit very low or almost no migration at all (Figure 18A and B). In addition, hypoxia increased cell migration in H460 cells by 129 %, compared to normoxia. Interestingly, Metastatic cells isolated from the lungs of a Calu-3 tumor bearing mouse (C3LuMet) showed vastly increased migration compared to the original Calu-3 cell line (Figure 18C). Hypoxia increased this ability by another 100 % compared to normoxia.

In summary, the migratory capacity of cells showing almost no migration under normoxia (H520, DMS53, Calu-3) was not significantly changed by hypoxia. In contrast, the migration of H460 and C3LuMet cells was strongly increased by the hypoxic environment.
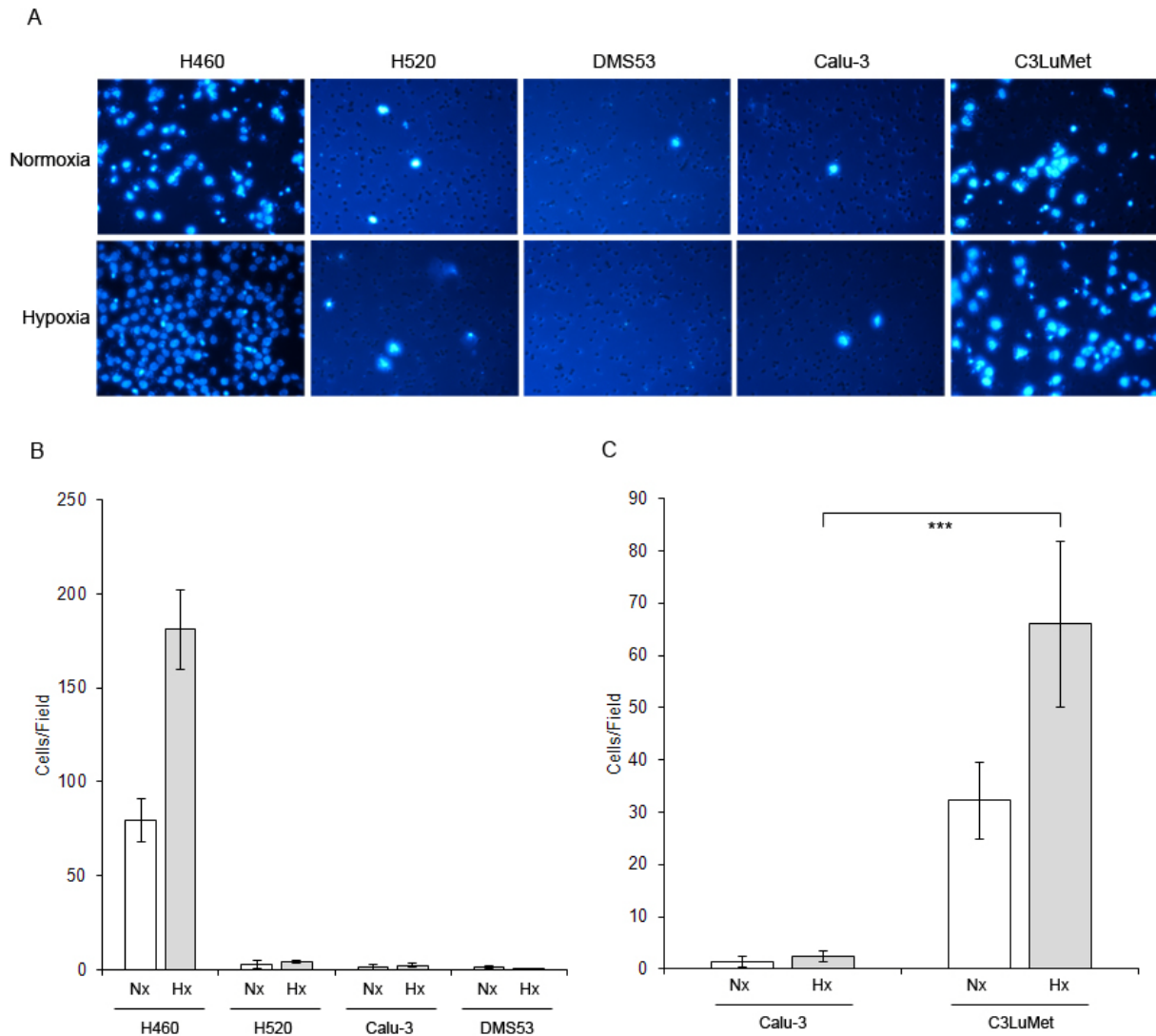
Figure 18: Tumor cell migration

Migration of tumor cells and isolated metastatic cells under normoxia and hypoxia. Representative photomicrographs (A), graphs quantifying the migratory capacity of H460, H520, Calu-3 and DMS53 (B), or Calu-3 cells and isolated C3LuMet cells (C) H460 and C3LuMet showed the highest migratory capacity under normoxia. Hypoxia strongly increased migration for these two cell types. Data are expressed as mean ± SD (n = 5 for each cell line, *** indicates p < 0,001; unpaired t-test).

4.3. Hypoxia strongly induces ANGPTL4 mRNA expression

Tumor cell lines, isolated metastatic cells from Calu-3 tumor bearing mice, as well as cells isolated from the tumor itself (C3Tu) were cultured under serum starvation, hypoxia or both and ANGPTL4 mRNA expression was assessed by qRT-PCR. Serum starvation was chosen as a stress condition since it upregulates many cell

receptors, including TGF-βR, which has been shown to induce ANGPTL4. In addition, hypoxia is also known to increase ANGPTL4 expression[139, 142].

The results showed that starvation and hypoxia had an induction capacity for ANGPTL4 in all cells. However, induction by hypoxia was much stronger than by serum starvation. If both conditions were applied, mRNA expression was even higher than for hypoxia alone. Among the original cell lines, H460 showed the strongest expression under both hypoxia and starvation, 0,5 fold higher than DMS53, 0,9 fold higher than Calu-3 and 2 fold higher than H520 (Figure 19A). Induction of gene expression compared to control by exposition to starvation and hypoxia was also highest in H460 cells, with a 9 fold induction, compared to 7 for DMS53, 4 for H520 and 1,5 for Calu-3.

Calu-3 cells showed the highest expression *a priori*, 2 fold higher than H460, 2,9 fold higher than DMS53 and 3,7 fold higher than H520 (Figure 19A).

This suggests that the high ANGPTL4 mRNA expression may play a role in metastases formation of H460 cells under hypoxia. However, the relatively high expression of ANGPTL4 by Calu-3 cells without any stimulation may also be of importance, possibly allowing quicker metastasis, without the need for extensive physiological stress.

In the case of metastatic Calu-3 cells, ANGPTL4 mRNA expression under normoxia or serum starvation alone was lower than of the original cell line (Figure 19C). Nevertheless, hypoxia or both starvation and hypoxia greatly increased expression, compared to the cell line. If both conditions were applied, brain metastatic cells (C3BrMet) showed 3,8 fold, lymph node metastases (C3LNMet) 2,3 fold, lung metastatic cells (C3LuMet) 1,8 fold and tumor isolates (C3Tu) 1,4 fold higher ANGPTL4 mRNA expression than the original cell line. Expression induction by both starvation and hypoxia was much higher in metastatic cell lines, with a 14,6 fold induction in C3BrMet cells, 14,5 fold in C3LNMet cells, 11 fold in C3LuMet cells and 10,5 fold in C3Tu cells compared to 1,5 fold in Calu-3 cells (Figure 19D).

Summarizing, metastatic cells from Calu-3 bearing mice all showed much higher ANGPTL4 expression under hypoxia and under both hypoxia and starvation than the original cell line. The isolated tumor cells also show higher expression, which indicates a possible selection mechanism during tumor growth already.
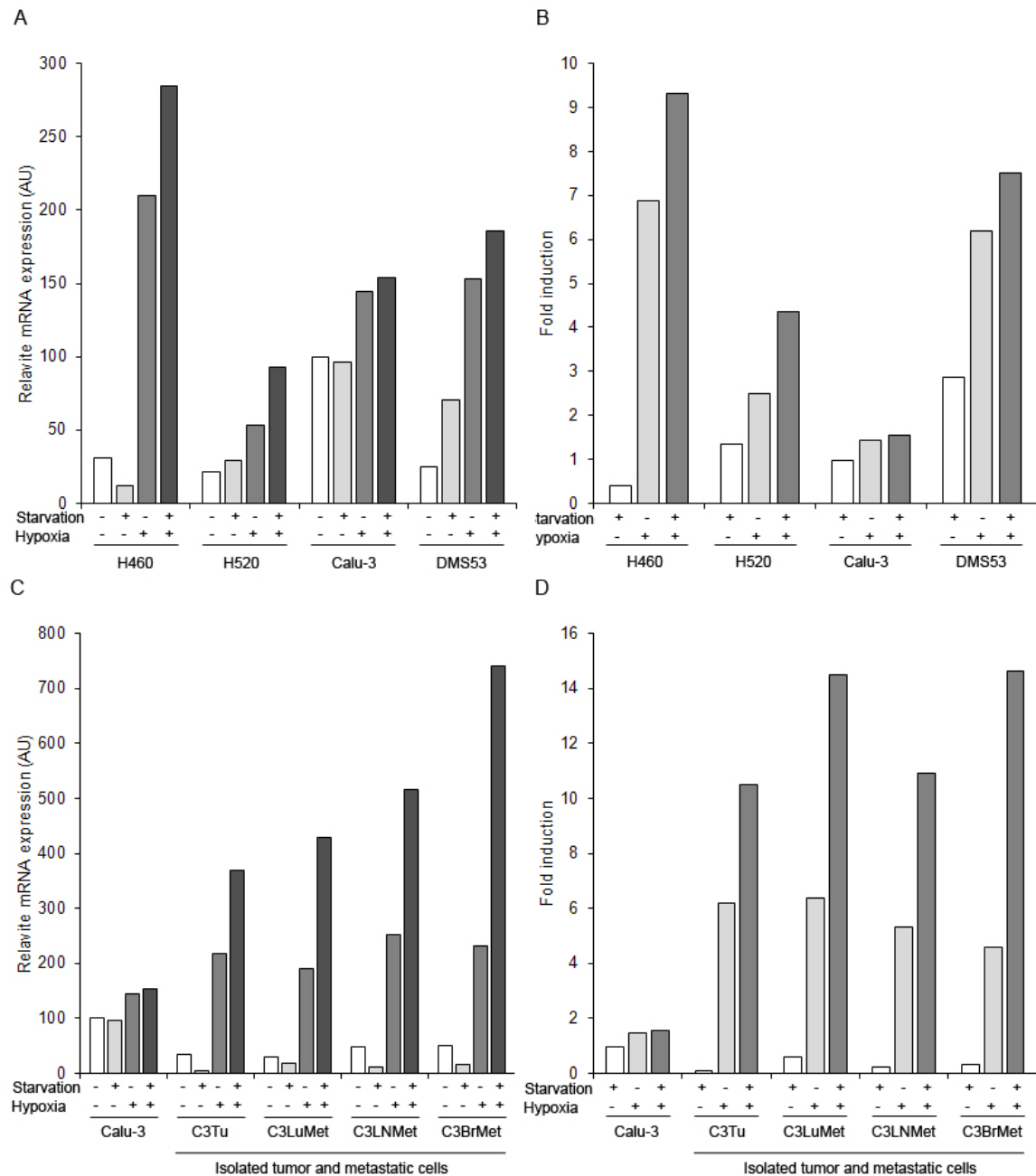
Figure 19: mRNA expression of huANGPTL4

mRNA expression of huANGPTL4 in H460, H520, Calu-3 and DMS53 tumor cell lines under serum starvation (grey bars), hypoxia (dark grey bars) or both (black bars) (A), corresponding fold expression induction compared to control (B). mRNA expression of isolated Calu-3 tumor (C3Tu) and metastatic (C3LuMet, C3LNMet and C3BrMet) cells under serum starvation, hypoxia or both (C), corresponding fold expression induction compared to control (D). Hypoxia and starvation induce huANGPTL4 mRNA expression. Isolated Calu-3 metastatic cells show the highest huANGPTL4 expression of all examined cells if both conditions are applied. mRNA data are expressed in arbitrary units (AU), normalized to the expression value of Calu-3 under normoxic conditions. One representative experiment out of two is shown.

4.4. Metastatic adenocarcinoma cells show the highest ANGPTL4 Protein expression

An ELISA for human ANGPTL4 protein was performed with the same cells and under the same growth conditions as for mRNA expression analysis.

The results showed that among cell lines, that the strongest protein expression occurs under hypoxia, as well as the highest relative induction. In contrast to mRNA expression however, the absolute protein secretion was lower under both starvation and hypoxia than under hypoxia alone (Figure 20A and B). Expression remained highest for H460 cells, even though it was similar to Calu-3 ANGPTL4 expression. Other cell lines showed very little expression or none at all.

As compared to the low level of hypoxia-induced ANGPTL4 mRNA expression in Calu-3 cells, protein secretion was relatively high, possibly due to a post-transcriptional control mechanism, which increases or stabilizes ANGPTL4 protein expression of Calu-3 cells.

Absolute protein secretion of isolated metastatic cells was higher than of the original cell line, validating the results obtained by PCR. It was however highest under hypoxia and lower if both starvation and hypoxia were applied. Under hypoxia, all metastatic cells showed almost identical, high protein concentration of approximately 25 ng/mL, whereas C3Tu showed 12,1 and the original cell line 15,5 ng/mL, compared to 3 ng/mL for the original cell line under normoxia (Figure 20C). This validates the mRNA data and proves that metastatic bronchus adenocarcinoma cells under hypoxia do indeed express more ANGPTL4 than the original cell line, increasing the possibility for ANGPTL4 to play a role in metastases formation. It should be noted that inducibility of ANGPTL4 was lower for metastatic cells than for Calu-3 cells (Figure 20D). This can be explained by the fact that metastatic cells already had high ANGPTL4 baseline protein levels under normal conditions, compared to the original cell line (Figure 20C). For example, the protein expression of 13,1 ng/mL by C3BrMet cells under normal conditions is almost as high as the protein expression of original Calu-3 cells under hypoxia (15,5 ng/mL). This suggests that ANGPTL4 could play a role in metastasis of bronchus adenocarcinoma, even without the need for physiological stress.

Summarized, in contrast to serum starvation, exposure to hypoxia had a significant inducing effect on ANGPTL4 protein secretion. Isolated Calu-3 metastatic cells

showed much higher ANGPTL4 levels than the original cell line, even under normal growth conditions. This discrepancy was even more pronounced under hypoxia.
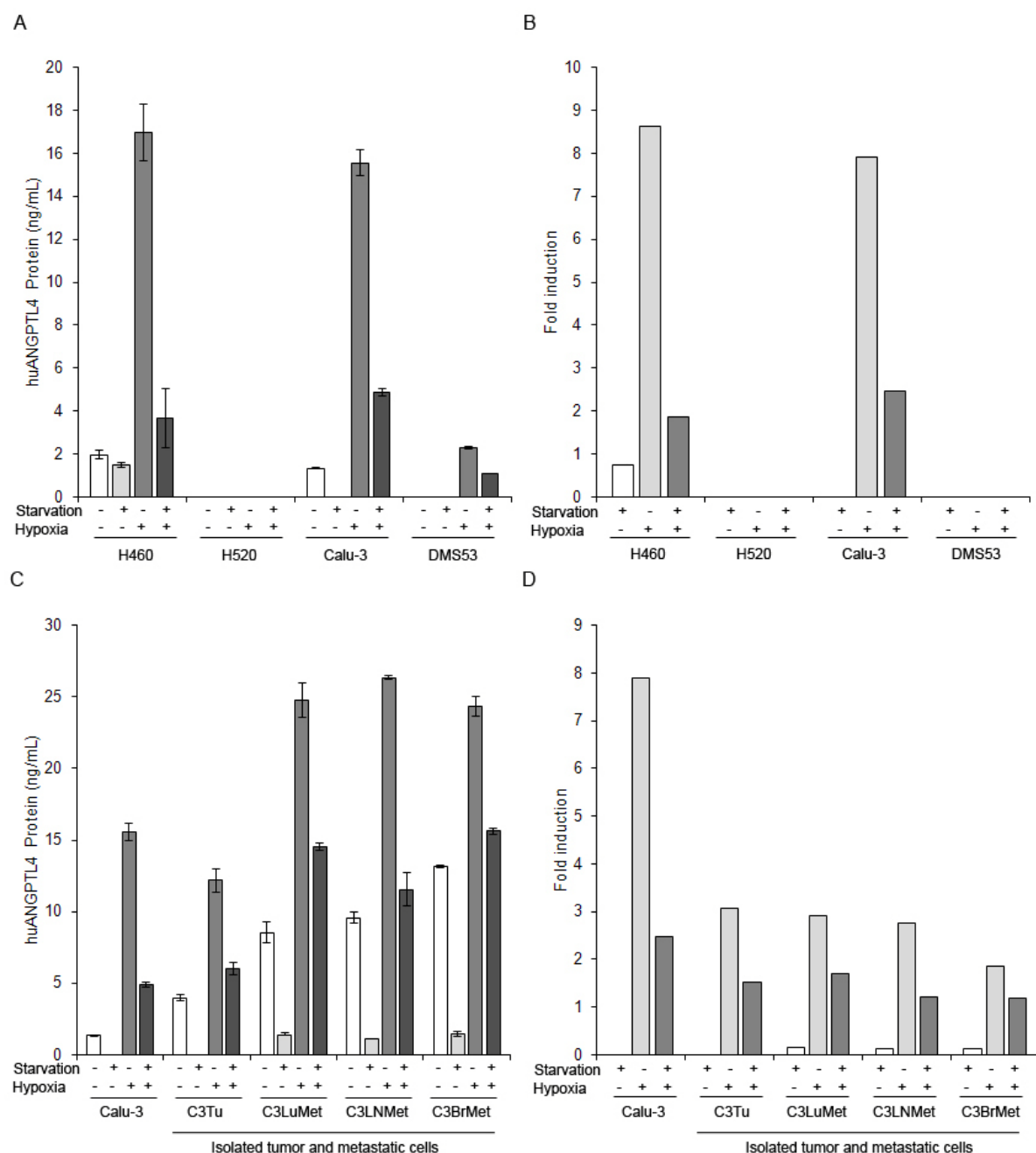
Figure 20: huANGPTL4 protein expression

Protein expression of huANGPTL4 from two independent experiments in tumor cell lines H460, H520, Calu-3 and DMS53 under serum starvation (grey bars), hypoxia (dark grey bars) or both (black bars) (A), corresponding fold expression induction compared to control (white bars) (B). Protein expression of isolated Calu-3 metastatic cells under serum starvation, hypoxia or both (C), corresponding fold expression induction as compared to control (D). Hypoxia strongly induced huANGPTL4 protein expression. Under hypoxia, isolated Calu-3 metastatic cells show the highest absolute and baseline expression of all examined cells. Data are expressed as mean ± SD.

4.5. TGF-β1 is a poor inducer for ANGPTL4 compared to hypoxia

Since it has been shown that ANGPTL4 can be induced by TGF-β1, its effect on mRNA and protein expression of isolated metastatic cells was investigated. Metastatic cells were incubated under normoxia, serum starvation, hypoxia or both starvation and hypoxia in the presence or absence of human recombinant TGF-β1. huANGPTL4 mRNA and protein expression were assessed by qRT-PCR and ELISA respectively. mRNA results showed that TGF-β has the ability to further induce ANGPTL4 in the original cell line under hypoxia, increasing it 1,33 fold. If starvation and hypoxia were applied, the induction capacity sunk to 0,4 fold. C3Tu cells isolated from the tumor of Calu-3 bearing mice showed a similar result with 1,4 fold expression increase under hypoxia alone and 0,6 fold increase under both conditions. For metastatic cells, induction capacity under hypoxia was comparable to the original cell line. In the case of C3LuMet cells, with both conditions applied, TGF-β caused a 1,5 fold increase in ANGPTL4 expression with the highest value among all samples. Interestingly, TGF-β was unable to increase ANGPTL4 expression in C3LNMet cells and C3BrMet cells if both conditions were true, suggesting that for these cells, induction by hypoxia was much more significant. Under normoxia or starvation alone, TGF-β hat no significant effect on ANGPTL4 mRNA expression, compared to hypoxia, which had a much higher impact. Overall, induction by hypoxia or both starvation and hypoxia is much more pronounced than by TGF-β, except for C3LuMet cells (Figure 21A).

Protein data underlined the predominant effect of hypoxia on ANGPTL4 expression, compared to TGF-β addition. Among metastatic cells, if hypoxia or both starvation and hypoxia were applied, TGF-β further increased ANGPTL4 expression only between 0,04 (for C3Tu under hypoxia) and 0,4 fold (for C3BrMet under starvation and hypoxia). Nevertheless, TGF-β did increase ANGPTL4 protein expression strongly under normoxic conditions, between 2 (for C3BrMet) and 5 fold (for Calu-3) (Figure 21B). Starvation did not change inducibility by TGF-β, which was consistent with mRNA data.

In summary, TGF-β did increase huANGPTL4 mRNA and protein expression in all isolated metastatic cells. However, the inducing effect of hypoxia was much more

pronounced.

A

B
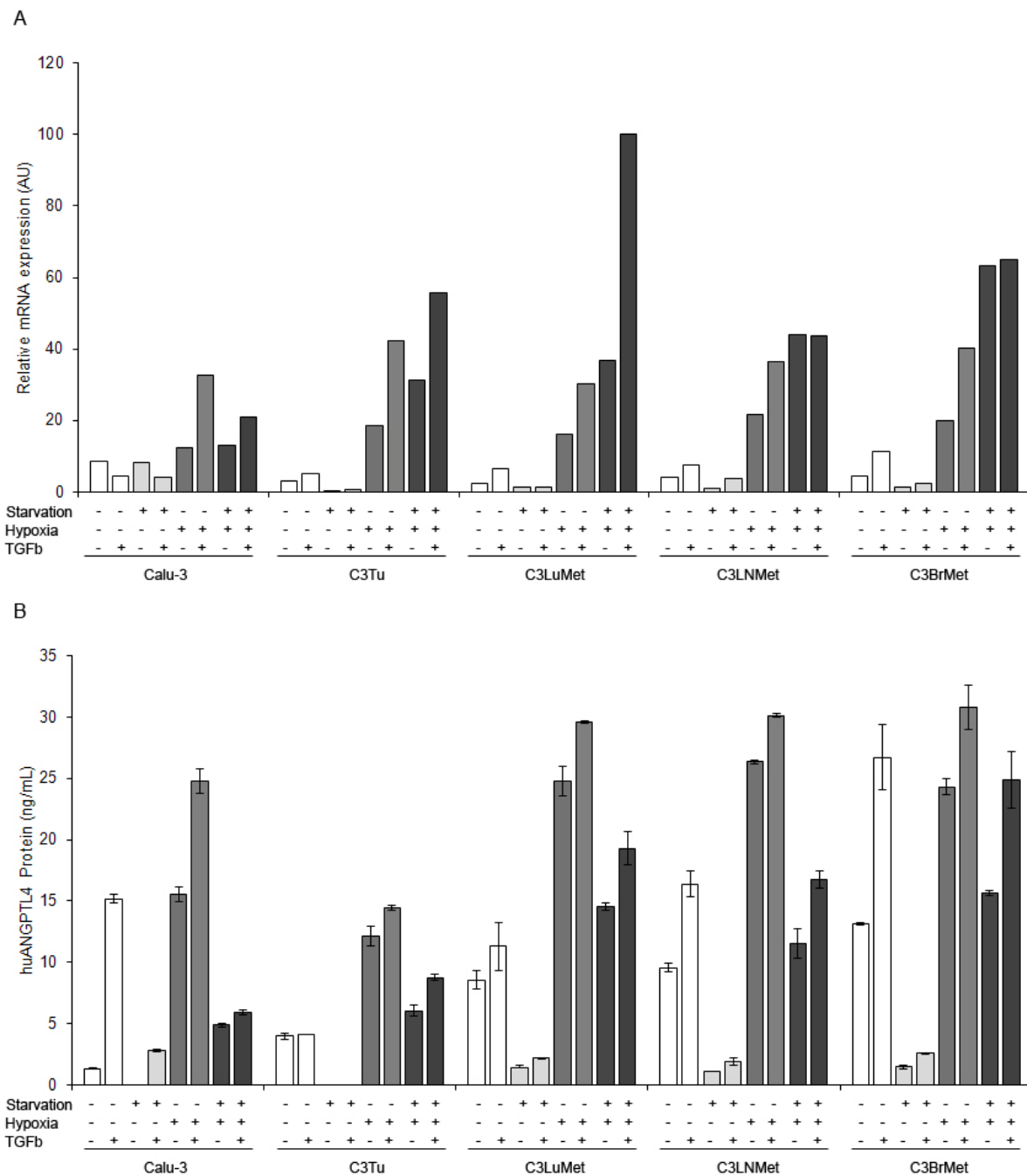
Figure 21: Effects of TGF-β1 on huANGPTL4 mRNA and protein expression

Induction of huANGPTL4 by TGF-β1 in Calu-3, tumor isolates and metastatic (C3Tu, C3LuMet, C3LNMet and C3BrMet) cells under serum starvation (grey bars), hypoxia (dark grey bars) or both (black bars). mRNA data (A), protein data from two independent experiments (B). TGF-β1 induces ANGPTL4 in almost all cells. However, hypoxia had a much more pronounced effect on huANGPTL4 mRNA and protein expression. mRNA data are expressed in arbitrary units (AU), normalized to the highest ANGPTL4 expression value. One representative experiment out of two is shown. Protein data are expressed as mean ± SD.

4.6. TGF-β1 and TGF-β2 mRNA expression does not correlate with ANGPTL4 levels

To assess whether high ANGPTL4-expression under hypoxia was a result of increased TGF-β1 or TGF-β2 expression by metastatic cells, their mRNA expression levels were measured by qRT-PCR. The results showed that neither TGF-β1, nor TGF-β2 mRNA expression was increased by hypoxia in any cell line (Figure 22A and B). Concerning TGF-β1, hypoxia even decreased expression to non-detectable levels. The relative upregulation of ANGPTL4 protein under normal conditions in metastatic cells as compared to Calu-3, shown by ELISA (Figure 20B) does not correlate with TGF-β expression either, since mRNA levels are lower in all metastatic cells than in the original cell line (except for TGF-β1 in C3LNMet) (Figure 22A).
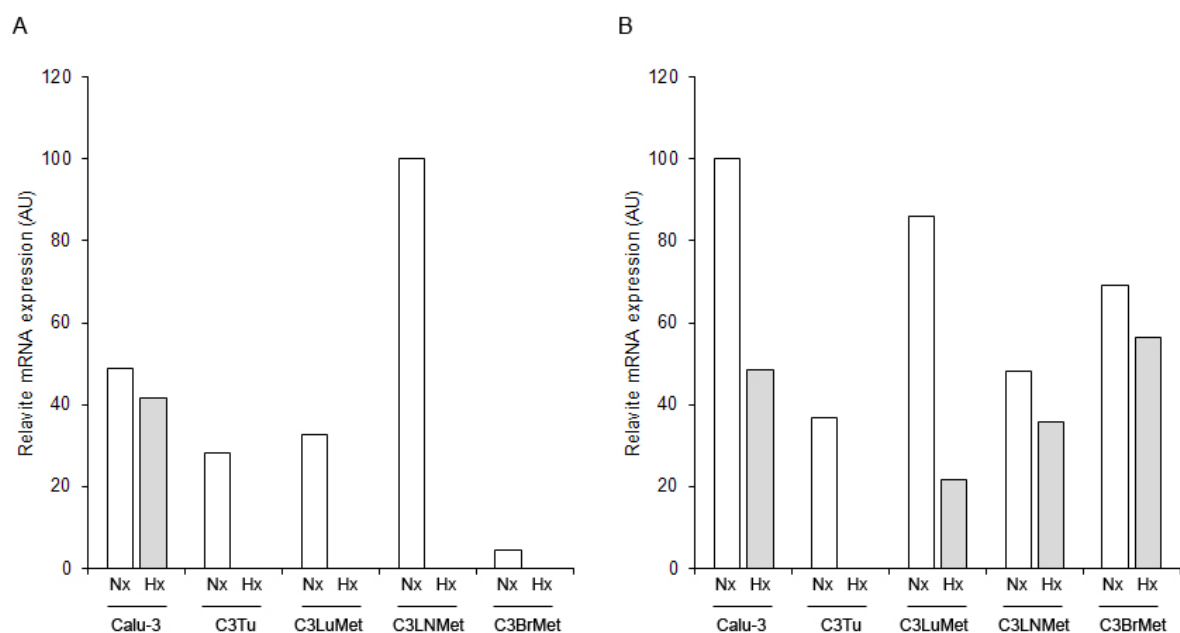
Figure 22: TGF-β1 and TGF-β2 mRNA expression

TGF-β1 (A) and TGF-β2 (B) mRNA expression of Calu-3, isolated tumor (C3Tu) and metastatic cells (C3LuMet, C3LNMet, C3BrMet) under normoxia (Nx, white bars) and hypoxia (Hx, grey bars). TGF-β1 and TGF-β2 mRNA levels of metastatic cells are lower or equivalent to Calu-3. Hypoxia did not increase TGF-β mRNA expression. mRNA data are expressed in arbitrary units (AU), normalized to the highest expression value of each assessed factor.

Discussion

1. Angiogenesis and lymphangiogenesis

Neoangiogenesis has been shown to be implicated in the process of metastasis for many cancers, including bronchus carcinoma. Not only can new blood vessels provide the necessary resources for further tumor growth, allowing the tumor to grow in size and subsequently permitting local invasion, but also do they represent a gateway into the whole body. The correlation between VEGF-A secretion, angiogenic activity in the tumor environment and metastatic activity has also been proven multiple times[75, 78].

The consequences of lymphangiogenesis in tumor progression are not as well understood as for blood vessels. There are indications that increased expression of the lymphangiogenic factors VEGF-C and VEGF-D correlates with higher incidence of metastasis to the lymph nodes as well as decreased survival in adenocarcinoma, as well as NSCLC patients[90, 101]. However, no functional intratumoral lymph vessels have been found so far[102]. Still, VEGF-C and VEGF-D expression definitely coincides with lymphangiogenesis in the adult organism for a number of other diseases[100].

The established xenograft model allowed the assessment of *in vivo* neoangiogenic and lymphangiogenic activity among all major subtypes of bronchus carcinoma. These phenotypic features could be compared to the expression of VEGF-A in the case of angiogenesis and VEGF-C and VEGF-D for lymphangiogenesis.

For H460 large cell bronchus carcinoma cells, VEGF-A expression can be found *in vivo*, but lower than for the other cell lines. Still, a high number of peritumoral blood vessels can be detected and despite the short growth time, compared to the other tumors, 25 % of the animals show metastases. This is in accordance with clinical data, showing a high incidence of metastasis for this tumor type[140]. Given the low VEGF-A mRNA level, other angiogenic factors or stroma derived VEGF-A (e.g. by TAMs) may have contributed to increased angiogenesis in this case of large cell bronchus carcinoma[82].

H460 cells show higher migration than any other cell line, further underlining its metastatic potential.

Concerning lymphatics, H460 shows strong VEGF-C expression *in vitro*, compared to moderate levels of VEGF-C and VEGF-D *in vivo*. Accordingly, H460 shows high tube formation induction in LECs and it is the only cell line for which intratumoral LECs can be found by flow cytometry in relevant numbers.

Since metastasis is an inefficient process, the high cell number injected and subsequent fast growth may have led to termination of H460 bearing animals prior to metastases formation. This is a drawback, limiting a comparison to the other cell lines. Further experiments, involving a lower injected cell number could be useful to investigate the role of angiogenesis and lymphangiogenesis in metastasis formation of H460 tumors.

For H520 squamous cell bronchus carcinoma cells, no VEGF-A expression is detected *in vitro*. Nevertheless, high *in vivo* expression and corresponding vessel formation may have contibuted to the high metastasis rate of 50 %. Thus, neoangiogenesis, induced by tumor-secreted VEGF-A is likely to play a role in the metastatic progression of H520 tumors, validating past publications underlining the importance of VEGF-A mediated angiogenesis and subsequent metastasis[141].

The low migratory capacity of this cell line is contradictory to this but as for Calu-3, low initial migration rates do not necessarily predict a low metastatic potential. A clonal selection mechanism may subsequently increase the migration of H520 tumor cells.

Despite the facts that H520 shows the highest tube formation induction capacity *in vitro*, the highest VEGF-C expression *in vivo*, as well as high VEGF-D expression both *in vitro* and *in vivo*, no LECs can be found by flow cytometry. This may be due to the fact that extratumoral lymphatics were not taken into account by the method. Nevertheless, lymphangiogenesis may still play a role in metastases formation of H520 tumors, given the evidence provided by this work.

DMS53 shows no *in vitro* VEGF-A expression and *in vivo* expression is lower than for most of the other cell lines. Low *in vivo* expression is in accord with its low vessel density, vessel diameter, as well as the fact that no metastases could be identified in this small bronchus carcinoma xenograft model. Possibly, additional anti-angiogenic mechanisms are at work here. In this respect, a more thorough assessment of the expression of other angiogenic factors, such as angiopoietins would be reasonable.

Concerning the expression of lymphangiogenic factors, DMS53 exhibits low expression of VEGF-C and VEGF-D both *in vivo* and *in vitro* or even none at all. This is in conformity with its low ability to induce tube formation in LECs as well as the fact that no intratumoral lymphatic vessels could be identified.

Calu-3 shows high VEGF-A expression both *in vitro* and *in vivo*, as well as a high density of intratumoral blood vessels and 75 % metastasis rate. This may indicate that in this case of lung adenocarcinoma, neoangiogenesis, induced by tumor-secreted VEGF-A contributes to a high rate of intravasated tumor cells, leading to extensive metastasis formation. This is in concordance with previous publications, demonstrating the correlation between adenocarcinoma VEGF-A expression, vascularization and metastasis[78].

Calu-3 exhibits high VEGF-D expression both *in vitro* and *in vivo,* as well as high VEGF-C expression *in vivo*. Accordingly, it exhibits metastasis to the lymphnodes in this xenograft model, validating past publications[90]. Still, Calu-3 neither shows the ability to induce LEC tube formation, nor can murine LECs be found inside the tumor tissue. Again, peritumoral lymphatics could play a role in this respect, adding to the effect of angiogenesis on metastasis formation. Further investigation, comprising the assessment of peritumoral lymphangiogenesis could elucidate these findings.

The high migration rate of isolated metastatic cells compared to the original cell line provides evidence that clonal selection may have taken place and that a subpopulation of Calu-3 cells may have acquired increased migratory capacity in the course of tumor progression.

In summary, VEGF-A mRNA expression does correlate with vessel formation and metastasis rate in the investigated squamous cell bronchus carcinoma and adenocarcinoma tumors but not the large cell bronchus carcinoma, which shows only moderate levels. CSF-1 is undetectable *in vivo* in all cases and thus does not seem to contribute to VEGF-A expression, even though adenocarcinoma cells exhibit high *in vitro* levels. Our further investigations will focus on the influence of stromal VEGF-A and its impact on tumor angiogenesis. VEGF-C and VEGF-D mRNA expression does not generally reflect the degree of LEC tube formation induction *in vitro* and a significant number of invading murine LECs could only be found in large cell bronchus carcinoma xenografts. We will assess the role of peritumoral lymphatics

thoroughly in the future. Metastasis does occur in all three examined NSCLC subtypes, with the highest incidence in adenocarcinoma bearing animals. The isolated metastatic adenocarcinoma cells will be extensively studied by our laboratory, concerning the mRNA and protein expression of multiple angiogenic and lymphangiogenic factors, compared to the original cell line. This may provide further insight into the molecular mechanisms of metastasis in bronchus adenocarcinoma. Future xenograft experiments with these cells will subsequently enable us to evaluate the effectiveness of anti-metastatic therapies.

2. ANGPTL4

The role of ANGPTL4 in cancer progression is poorly studied, possibly because it is outshined by the impact of ANGPTL4 on triglyceride metabolism, which also has many implications concerning health. Nevertheless, ANGPTL4 has been shown to be involved in endothelial cell-cell adhesion as well as in tumor metastasis, although reports concerning the latter are ambiguous[138, 139].

Also, recent publications suggest its upregulation by fasting, hypoxia as well as TGF-β[139]. The upregulation by hypoxia is attributed to the activation of HIF-1α.

According to this work, hypoxia increases ANGPTL4 mRNA as well as protein expression in general, validating past publications[138, 139]. Serum starvation shows an inhibitory effect on ANGPTL4 expression. Furthermore, even though the combination of starvation and hypoxia leads to increased ANGPTL4 mRNA expression levels, compared to hypoxia alone, this is not reflected by protein data. Still, since tumor environments definitely show hypoxic regions, it can be hypothesized that ANGPTL4 is upregulated under *in vivo* conditions in all bronchus carcinoma types investigated here, although to a different degree.

The influence of TGF-β addition on ANGPTL4 expression is detectable but minor, compared to hypoxia. Also, hypoxia does not increase TGF-β mRNA expression in tumor cells. Serum starvation does not significantly increase ANGPTL4 protein expression in response to TGF-β addition in this particular case, although past publications infer that TGF-β receptor expression is upregulated by this condition[142].

Thus a different regulatory mechanism, such as the HIF-1α pathway, may be driving ANGPTL4 expression in bronchus carcinoma progression.

H460 shows the highest expression level of ANGPTL4 protein and mRNA under hypoxia, compared to the other primary cell lines. Despite the fact that no metastatic cells could be isolated, metastasis did occur, as shown by qRT-PCR. Thus, the high ANGPTL4 expression may contribute to the early formation of metastases by H460 tumor cells. Again, further experiments, decreasing the injected cell dose would most likely be helpful to further investigate this effect.

According to expression data in the cell line, the role of ANGPTL4 in the formation of metastases by H520 does not seem to be as important as for other bronchus carcinoma subtypes, since no observable protein expression occurred and mRNA levels were lower than for the other cell lines. Nevertheless, this may be due to the harsh culture conditions and may not reflect the actual *in vivo* environment. Furthermore, no metastatic cells could be isolated from extracted organs in this case either, leaving the possibility that H520 metastases may still express higher amounts of ANGPTL4. Further experiments are necessary, involving stably (e.g. GFP) labeled tumor cells, which can be identified and isolated more easily from organ tissue.

For DMS53, as for H520, small amounts of ANGPTL4 protein are secreted under hypoxia, while none at all are detectable under normal growth conditions. mRNA levels do however rise. Again, this suggests a less pronounced importance of ANGPTL4 in the formation of metastases in small cell bronchus carcinoma but since expression induction is measurable on the mRNA level, the growth conditions are to be reevaluated. Nevertheless, DMS53 does not form any metastases at all, which may be partly attributable to its low ANGPTL4 expression.

The original Calu-3 cell line shows high ANGPTL4 protein expression under hypoxia, compared to the other cell lines and in the case of isolated metastatic cells, this effect is even more pronounced. Also, all metastatic cells show strongly increased protein expression under normal growth conditions compared to the original cell line. Together these data suggest that a selection mechanism during tumor progression has favored the survival of ANGPTL4 protein expressing cells, even without the

influence of hypoxia. It can be suspected that a mutation may have subverted existing regulatory mechanisms, leading to constitutively expressed ANGPTL4 protein. Since mRNA levels in metastatic cells under normal growth conditions are not increased, this control mechanism may be located at the post-transcriptional level. Further experiments, involving the inhibition of ANGPTL4 expression and its effect on metastasis, as well as ANGPTL4 overexpression in metastatic cells could provide more evidence for the importance of this protein in the formation of metastases. Still, it is probable that ANGPTL4 may enhance the metastatic potential of human lung adenocarcinoma cells, establishing the possibility of future therapeutic options.

In summary, except for the squamous cell bronchus carcinoma, ANGPTL4 expression does correlate with metastases formation in all examined NSCLC and SCLC subtypes. This correlation is especially pronounced in the case of adenocarcinoma xenografts for which metastatic cells exhibit significantly stronger ANGPTL4 protein expression than the original cell line. The established murine model will allow us to further investigate the effect of ANGPTL4 on bronchus carcinoma progression in order to elucidate the possible causal relation between increased protein secretion and metastasis. This relation may include the previously studied endothelium disruptive effect of ANGPTL4, which may facilitate intra- or extravasation of motile tumor cells[138, 139].

References

[1] Heron M, Hoyert DL, Murphy SL, Xu J, Kochanek KD, Tejada-Vera B. Deaths: final data for 2006. *Natl Vital Stat Rep.* 2009 Apr 17;57(14):1-134.

[2] Jemal A, Siegel R, Ward E, Hao Y, Xu J, Murray T, Thun MJ.Cancer statistics, 2008.*CA Cancer J Clin.* 2008 Mar-Apr;58(2):71-96.

[3] Nowell P.C.The clonal evolution of tumor cell populations.*Science.*1976 194:23-28.

[4] Cahill DP, Kinzler KW, Vogelstein B, Lengauer C. Genetic instability and darwinian selection in tumours. *Trends Cell Biol.* 1999 Dec;9(12):M57-60.

[5] Peltomaki P, de la Chapelle A. Mutations predisposing to hereditary nonpolyposis colorectal cancer. *Adv. Cancer Res.* 1997 71:93-119

[6] Eshleman JR, Lang EZ, Bowerfind GK, Parsons R, Vogelstein B, Willson JK, Veigl ML, Sedwick WD, Markowitz SD. Increased mutation rate at the hprt locus accompanies microsatellite instability in colon cancer. *Oncogene.* 1995 Jan 5;10(1):33-7.

[7] Livingstone LR, White A, Sprouse J, Livanos E, Jacks T, Tlsty TD. Altered cell cycle arrest and gene amplification potential accompany loss of wild-type p53. *Cell.* 1992 Sep 18;70(6):923-35.

[8] Duesberg P, Rausch C, Rasnick D, Hehlmann R. Genetic instability of cancer cells is proportional to their degree of aneuploidy. *ProcNatlAcadSci U S A.* 1998 Nov 10;95(23):13692-7.

[9] Hanahan D, Weinberg RA. The hallmarks of cancer.*Cell.* 2000 Jan 7;100(1):57-70.

[10] Hartwell LH, Kastan MB.Cell cycle control and cancer.*Science.* 1994 Dec 16;266(5192):1821-8.

[11] Fedi P, Tronick SR and Aaronson SA.Growth factors.*Cancer Medicine.* 1997 41-64

[12] Hayflick L. Mortality and immortality at the cellular level.A review.*Biochemistry (Mosc).* 1997 Nov;62(11):1180-90.

[13] Shay JW, Bacchetti S. A survey of telomerase activity in human cancer.*Eur J Cancer*. 1997 Apr;33(5):787-91.

[14] Bouck N, Stellmach V, Hsu SC. How tumors become angiogenic. *Adv Cancer Res.* 1996;69:135-74.

[15] Ferlay J, Autier P, Boniol M, Heanue M, Colombet M, Boyle P.Estimates of the cancer incidence and mortality in Europe in 2006.*Ann Oncol.* 2007 Mar;18(3):581-92. Epub 2007 Feb 7.

[16] Molina JR, Yang P, Cassivi SD, Schild SE, Adjei AA.Non-small cell lung cancer: epidemiology, risk factors, treatment, and survivorship.*Mayo Clin Proc.* 2008 May;83(5):584-94.

[17] Smith W, Khuri FR.The care of the lung cancer patient in the 21st century: a new age.*SeminOncol.* 2004 Apr;31(2 Suppl 4):11-5.

[18] Travis WD.Pathology of lung cancer.*Clin Chest Med.* 2002;23:65-81

[19] Brambilla E, Travis WD, Colby TV, Corrin B, Shimosato Y.The new World Health Organization classification of lung tumours.*EurRespir J.* 2001 Dec;18(6):1059-68.

[20] Travis, WD; Travis LB, Devesa SS. Lung cancer.*Cancer.* 1995;75(Suppl. 1):191–202.

[21] Rosti G, Bevilacqua G, Bidoli P, Portalone L, Santo A, Genestreti G.Small cell lung cancer.*Ann Oncol.* 2006 Mar;17Suppl 2:ii5-10.

[22] Sporn MB.The war on cancer.*Lancet.* 1996 May 18;347(9012):1377-81.

[23] Liotta LA, Tryggvason K, Garbisa S, Hart I, Foltz CM, Shafie S.Metastatic potential correlates with enzymatic degradation of basement membrane collagen.*Nature.* 1980 Mar 6;284(5751):67-8.

[24] Coussens LM, Werb Z. Matrix metalloproteinases and the development of cancer.*Chem Biol.* 1996 Nov;3(11):895-904.

[25] Pollard JW.Tumour-educated macrophages promote tumour progression and metastasis.*Nat Rev Cancer*. 2004 Jan;4(1):71-8.

[26] Thiery JP, Sleeman JP. Complex networks orchestrate epithelial-mesenchymal transitions. *Nat Rev Mol Cell Biol.* 2006 Feb;7(2):131-42.

[27] Potter RF, Groom AC.Capillary diameter and geometry in cardiac and skeletal muscle studied by means of corrosion casts.*Microvasc Res.* 1983 Jan;25(1):68-84.

[28] Chambers AF, Groom AC, MacDonald IC.Dissemination and growth of cancer cells in metastatic sites.*Nat Rev Cancer.* 2002 Aug;2(8):563-72.

[29] Orr FW, Wang HH.Tumor cell interactions with the microvasculature: a rate-limiting step in metastasis.*SurgOncolClin N Am.* 2001 Apr;10(2):357-81, ix-x.

[30] Chambers AF, Groom AC, MacDonald IC.Dissemination and growth of cancer cells in metastatic sites.*Nat Rev Cancer*. 2002 Aug;2(8):563-72.

[31] Nguyen DX, Bos PD, Massagué J.Metastasis: from dissemination to organ-specific colonization.*Nat Rev Cancer*. 2009 Apr;9(4):274-84.

[32] Coultas L, Chawengsaksophak K, Rossant J.Endothelial cells and VEGF in vascular development.*Nature.* 2005 Dec 15;438(7070):937-45.

[33] Carmeliet P, Jain RK.Angiogenesis in cancer and other diseases.*Nature.* 2000 Sep 14;407(6801):249-57.

[34] Carmeliet P.Angiogenesis in health and disease.*Nat Med.* 2003 Jun;9(6):653-60.

[35] Greenblatt M, Shubi P.Tumor angiogenesis: transfilter diffusion studies in the hamster by the transparent chamber technique.*J Natl Cancer Inst.* 1968 Jul;41(1):111-24.

[36] Kerbel RS.Tumor angiogenesis: past, present and the near future.*Carcinogenesis.* 2000 Mar;21(3):505-15.

[37] Carmeliet P.Developmental biology.Controlling the cellular brakes.*Nature.* 1999 Oct 14;401(6754):657-8.

[38] Carmeliet P.Mechanisms of angiogenesis and arteriogenesis.*Nat Med.* 2000 Apr;6(4):389-95.

[39] Roitt I, Brostoff J, Male D. *Immunology.* 1998

[40] Jussila L, Alitalo K. Vascular growth factors and lymphangiogenesis. *Physiol Rev.* 2002 Jul;82(3):673-700.

[41] Saharinen P, Tammela T, Karkkainen MJ, Alitalo K. Lymphatic vasculature: development, molecular regulation and role in tumor metastasis and inflammation. *Trends Immunol.* 2004 Jul;25(7):387-95.

[42] Wick N, Saharinen P, Saharinen J, Gurnhofer E, Steiner CW, Raab I, Stokic D, Giovanoli P, Buchsbaum S, Burchard A, Thurner S, Alitalo K, Kerjaschki D. Transcriptomal comparison of human dermal lymphatic endothelial cells ex vivo and in vitro. *Physiol Genomics*. 2007 Jan 17;28(2):179-92.

[43] Skobe M, Detmar M. Structure, function, and molecular control of the skin lymphatic system. *J Investig Dermatol Symp Proc.* 2000 Dec;5(1):14-9.

[44] Tammela T, Enholm B, Alitalo K, Paavonen K. The biology of vascular endothelial growth factors. *Cardiovasc Res*. 2005 Feb 15;65(3):550-63.

[45] Alitalo K, Tammela T, Petrova TV. Lymphangiogenesis in development and human disease. *Nature*. 2005 Dec 15;438(7070):946-53.

[46] Kajiya K, Detmar M. An important role of lymphatic vessels in the control of UVB-induced edema formation and inflammation. *J Invest Dermatol*. 2006 Apr;126(4):919-21.

[47] Kunstfeld R, Hirakawa S, Hong YK, Schacht V, Lange-Asschenfeldt B, Velasco P, Lin C, Fiebiger E, Wei X, Wu Y, Hicklin D, Bohlen P, Detmar M. Induction of cutaneous delayed-type hypersensitivity reactions in VEGF-A transgenic mice results

in chronic skin inflammation associated with persistent lymphatic hyperplasia. *Blood*. 2004 Aug 15;104(4):1048-57.

[48] Warren AG, Brorson H, Borud LJ, Slavin SA. Lymphedema: a comprehensive review. Ann Plast Surg. 2007 Oct;59(4):464-72.

[49] Machnik A, Neuhofer W, Jantsch J, Dahlmann A, Tammela T, Machura K, Park JK, Beck FX, Müller DN, Derer W, Goss J, Ziomber A, Dietsch P, Wagner H, van Rooijen N, Kurtz A, Hilgers KF, Alitalo K, Eckardt KU, Luft FC, Kerjaschki D, Titze J. Macrophages regulate salt-dependent volume and blood pressure by a vascular endothelial growth factor-C-dependent buffering mechanism. *Nat Med*. 2009 May;15(5):545-52.

[50] Achen MG, McColl BK, Stacker SA. Focus on lymphangiogenesis in tumor metastasis. *Cancer Cell.* 2005 Feb;7(2):121-7.

[51] Karpanen T, Alitalo K. Molecular biology and pathology of lymphangiogenesis. *Annu Rev Pathol.* 2008;3:367-97.

[52] Joyce JA, Pollard JW. Microenvironmental regulation of metastasis. *Nat Rev Cancer.* 2009 Apr;9(4):239-52.

[53] Sleeman JP, Thiele W. Tumor metastasis and the lymphatic vasculature. *Int J Cancer.* 2009 Dec 15;125(12):2747-56.

[54] Tammela T, Alitalo K. Lymphangiogenesis: Molecular mechanisms and future promise. *Cell.* 2010 Feb 19;140(4):460-76.

[55] Weryńska B, Dziegiel P, Jankowska R. Role of lymphangiogenesis in lung cancer. *Folia Histochem Cytobiol.* 2009 Jan;47(3):333-42.

[56] Breen EC.VEGF in biological control.*J Cell Biochem.* 2007 Dec 15;102(6):1358-67.

[57] Ferrara N, Gerber HP, LeCouter J.The biology of VEGF and its receptors.*Nat Med.* 2003 Jun;9(6):669-76.

[58] Houck KA, Ferrara N, Winer J, Cachianes G, Li B, Leung DW.The vascular endothelial growth factor family: identification of a fourth molecular species and characterization of alternative splicing of RNA.*MolEndocrinol*. 1991 Dec;5(12):1806-14.

[59] Suto K, Yamazaki Y, Morita T, Mizuno H.Crystal structures of novel vascular endothelial growth factors (VEGF) from snake venoms: insight into selective VEGF binding to kinase insert domain-containing receptor but not to fms-like tyrosine kinase-1*. J Biol Chem*. 2005 Jan 21;280(3):2126-31. Epub 2004 Nov 12.

[60] Yamazaki Y, Morita T.Molecular and functional diversity of vascular endothelial growth factors.*Mol Divers.* 2006 Nov;10(4):515-27.

[61] Senger DR, Galli SJ, Dvorak AM, Perruzzi CA, Harvey VS, Dvorak HF.Tumor cells secrete a vascular permeability factor that promotes accumulation of ascites fluid.*Science.* 1983 Feb 25;219(4587):983-5.

[62] Leung DW, Cachianes G, Kuang WJ, Goeddel DV, Ferrara N.Vascular endothelial growth factor is a secreted angiogenic mitogen.*Science.* 1989 Dec 8;246(4935):1306-9.

[63] Harper SJ, Bates DO. VEGF-A splicing: the key to anti-angiogenic therapeutics? *Nat Rev Cancer.* 2008 Nov;8(11):880-7. Epub 2008 Oct 16.

[64] Otrock ZK, Makarem JA, Shamseddine AI.Vascular endothelial growth factor family of ligands and receptors: review.*Blood Cells Mol Dis.* 2007 May-Jun;38(3):258-68. Epub 2007 Mar 6.

[65] Breier G, Albrecht U, Sterrer S, Risau W. Expression of vascular endothelial growth factor during embryonic angiogenesis and endothelial cell differentiation.*Development.* 1992 Feb;114(2):521-32.

[66] Dumont DJ, Fong GH, Puri MC, Gradwohl G, Alitalo K, Breitman ML.Vascularization of the mouse embryo: a study of flk-1, tek, tie, and vascular endothelial growth factor expression during development. *DevDyn* 1995;203:80-92.

[67] Carmeliet P, Ferreira V, Breier G, et al. Abnormal blood vessel development and lethality in embryos lacking a single VEGF allele.*Nature* 1996;380:435-9.

[68] Risau W. Differentiation of endothelium.*FASEB J*, 1995;9:926-33.

[69] Simon M, Grone HJ, Johren O, et al. Expression of vascular endothelial growth factor and its receptors in human renal ontogenesis and in adult kidney. *Am J Physiol* 1995;268(2 Pt 2):F240-50.

[70] Hatva E, Kaipainen A, Mentula P, et al. Expression of endothelial cell-specific receptor tyrosine kinases and growth factors in human brain tumors. *Am J Pathol* 1995;146:368-78.

[71] Shweiki D, Itin A, Neufeld G, Gitay-Goren H, Keshet E. Patterns of expression of vascular endothelial growth factor (VEGF) and VEGF receptors in mice suggest a role in hormonally regulated angiogenesis. *J Clin Invest* 1993;91:2235-43.

[72] Berse B, Brown LF, Van de Water L, Dvorak HF, Senger DR. Vascular permeability factor (vascular endothelial growth factor) gene is expressed

differentially in normal tissues, macrophages, and tumors. *MolBiol Cell* 1992;3:211-20.

[73] Flamme I, von Reutern M, Drexler HC, Syed-Ali S, Risau W. Overexpression of vascular endothelial growth factor in the avian embryo induces hypervascularization and increased vascular permeability without alterations of embryonic pattern formation. *DevBiol* 1995;171:399-414.

[74] Rossiter H, Barresi C, Pammer J, Rendl M, Haigh J, Wagner EF, Tschachler E. Loss of vascular endothelial growth factor a activity in murine epidermal keratinocytes delays wound healing and inhibits tumor formation. *Cancer Res*. 2004 May 15;64(10):3508-16.

[75] Sheen IS, Jeng KS, Shih SC, Kao CR, Chang WH, Wang HY, Wang PC, Wang TE, Shyung LR, Chen CZ.Clinical significance of the expression of isoform 165 vascular endothelial growth factor mRNA in noncancerous liver remnants of patients with hepatocellular carcinoma.*World J Gastroenterol*. 2005 Jan 14;11(2):187-92.

[76] Bacic M, Edwards NA, Merrill MJ.Differential expression of vascular endothelial growth factor (vascular permeability factor) forms in rat tissues. *Growth Factors*. 1995;12(1):11-5.

[77] Storkebaum E, Lambrechts D, Carmeliet P. VEGF: once regarded as a specific angiogenic factor, now implicated in neuroprotection. *Bioessays*. 2004 Sep;26(9):943-54.

[78] Nishi M, Abe Y, Tomii Y, Tsukamoto H, Kijima H, Yamazaki H, Ohnishi Y, Iwasaki M, Inoue H, Ueyama Y, Nakamura M.Cell binding isoforms of vascular endothelial growth factor-A (VEGF189) contribute to blood flow-distant metastasis of pulmonary adenocarcinoma. *Int J Oncol*. 2005 Jun;26(6):1517-24.

[79] Ladoux, A, Frelin C. Hypoxia is a strong inducer of vascular endothelial growth factor mRNA expression in the heart. *BiochemBiophys Res Commun* 1993;195:1005-10.

[80] Vacca A, Ribatti D, Iurlaro M, Albini A, Minischetti M, Bussolino F, Pellegrino A, Ria R, Rusnati M, Presta M, Vincenti V, Persico MG, Dammacco F.Human lymphoblastoid cells produce extracellular matrix-degrading enzymes and induce endothelial cell proliferation, migration, morphogenesis, and angiogenesis. *Int J Clin Lab Res*. 1998;28(1):55-68.

[81] Norrby K.Mast cells and angiogenesis.*APMIS*. 2002 May;110(5):355-71.

[82] Sica A, Saccani A, Mantovani A.Tumor-associated macrophages: a molecular perspective.IntImmunopharmacol. 2002 Jul;2(8):1045-54.

[83] Melder RJ, Koenig GC, Witwer BP, Safabakhsh N, Munn LL, Jain RK.During angiogenesis, vascular endothelial growth factor and basic fibroblast growth factor regulate natural killer cell adhesion to tumor endothelium. *Nat Med*. 1996 Sep;2(9):992-7.

[84] Ohm JE, Carbone DP.Immune dysfunction in cancer patients.*Oncology (Williston Park)*. 2002 Jan;16(1 Suppl 1):11-8.

[85] Takahashi H, Shibuya M. The vascular endothelial growth factor (VEGF)/VEGF receptor system and its role under physiological and pathological conditions. *Clin Sci (Lond).* 2005 Sep;109(3):227-41.

[86] Joukov V, Pajusola K, Kaipainen A, Chilov D, Lahtinen I, Kukk E, Saksela O, Kalkkinen N, Alitalo K. A novel vascular endothelial growth factor, VEGF-C, is a ligand for the Flt4 (VEGFR-3) and KDR (VEGFR-2) receptor tyrosine kinases. *EMBO J.* 1996 Apr 1;15(7):1751.

[87] Joukov V, Sorsa T, Kumar V, Jeltsch M, Claesson-Welsh L, Cao Y, Saksela O, Kalkkinen N, Alitalo K. Proteolytic processing regulates receptor specificity and activity of VEGF-C. *EMBO J.* 1997 Jul 1;16(13):3898-911.

[88] Siegfried G, Basak A, Cromlish JA, Benjannet S, Marcinkiewicz J, Chrétien M, Seidah NG, Khatib AM. The secretory proprotein convertases furin, PC5, and PC7 activate VEGF-C to induce tumorigenesis. *J Clin Invest*. 2003 Jun;111(11):1723-32.

[89] Tammela T, Enholm B, Alitalo K, Paavonen K. The biology of vascular endothelial growth factors. *Cardiovasc Res*. 2005 Feb 15;65(3):550-63.

[90] Duff SE, Jayson GC. Vascular Endothelial Growth Factor C and Vascular Endothelial Growth Factor D: Biology, Functions and Role in Cancer. *VEGF and Cancer.* 2004

[91] Kaipainen A, Korhonen J, Mustonen T, van Hinsbergh VW, Fang GH, Dumont D, Breitman M, Alitalo K. Expression of the fms-like tyrosine kinase 4 gene becomes restricted to lymphatic endothelium during development. *Proc Natl Acad Sci U S A.* 1995 Apr 11;92(8):3566-70.

[92] Kukk E, Lymboussaki A, Taira S, Kaipainen A, Jeltsch M, Joukov V, Alitalo K. VEGF-C receptor binding and pattern of expression with VEGFR-3 suggests a role in lymphatic vascular development. *Development*. 1996 Dec;122(12):3829-37.

[93] Yuan L, Moyon D, Pardanaud L, Bréant C, Karkkainen MJ, Alitalo K, Eichmann A. Abnormal lymphatic vessel development in neuropilin 2 mutant mice. *Development*. 2002 Oct;129(20):4797-806.

[94] Karkkainen MJ, Haiko P, Sainio K, Partanen J, Taipale J, Petrova TV, Jeltsch M, Jackson DG, Talikka M, Rauvala H, Betsholtz C, Alitalo K. Vascular endothelial growth factor C is required for sprouting of the first lymphatic vessels from embryonic veins. *Nat Immunol*. 2004 Jan;5(1):74-80. Epub 2003 Nov 23.

[95] Küchler AM, Gjini E, Peterson-Maduro J, Cancilla B, Wolburg H, Schulte-Merker S. Development of the zebrafish lymphatic system requires VEGFC signaling. *Curr Biol*. 2006 Jun 20;16(12):1244-8.

[96] Yaniv K, Isogai S, Castranova D, Dye L, Hitomi J, Weinstein BM. Live imaging of lymphatic development in the zebrafish. *Nat Med*. 2006 Jun;12(6):711-6. Epub 2006 May 28.

[97] Cursiefen C, Chen L, Borges LP, Jackson D, Cao J, Radziejewski C, D'Amore PA, Dana MR, Wiegand SJ, Streilein JW. VEGF-A stimulates lymphangiogenesis and hemangiogenesis in inflammatory neovascularization via macrophage recruitment. *J Clin Invest*. 2004 Apr;113(7):1040-50.

[98] Ristimäki A, Narko K, Enholm B, Joukov V, Alitalo K. Proinflammatory cytokines regulate expression of the lymphatic endothelial mitogen vascular endothelial growth factor-C. *J Biol Chem.* 1998 Apr 3;273(14):8413-8.

[99] Kerjaschki D, Regele HM, Moosberger I, Nagy-Bojarski K, Watschinger B, Soleiman A, Birner P, Krieger S, Hovorka A, Silberhumer G, Laakkonen P, Petrova T, Langer B, Raab I. Lymphatic neoangiogenesis in human kidney transplants is associated with immunologically active lymphocytic infiltrates. *J Am Soc Nephrol*. 2004 Mar;15(3):603-12.

[100] Paavonen K, Mandelin J, Partanen T, Jussila L, Li TF, Ristimaki A, Alitalo K, Konttinen YT. Vascular endothelial growth factors C and D and their VEGFR-2 and 3 receptors in blood and lymphatic vessels in healthy and arthritic synovium. *J Rheumatol.* 2002 Jan;29(1):39-45.

[101] Su JL, Shih JY, Yen ML, Jeng YM, Chang CC, Hsieh CY, Wei LH, Yang PC, Kuo ML. Cyclooxygenase-2 induces EP1- and HER-2/Neu-dependent vascular endothelial growth factor-C up-regulation: a novel mechanism of lymphangiogenesis in lung adenocarcinoma. *Cancer Res.* 2004 Jan 15;64(2):554-64.

[102] Reis-Filho JS, Schmitt FC. Lymphangiogenesis in tumors: what do we know? *Microsc Res Tech.* 2003 Feb 1;60(2):171-80.

[103] Tang Y, Zhang D, Fallavollita L, Brodt P. Vascular endothelial growth factor C expression and lymph node metastasis are regulated by the type I insulin-like growth factor receptor. *Cancer Res.* 2003 Mar 15;63(6):1166-71.

[104] Kubo H, Cao R, Brakenhielm E, Mäkinen T, Cao Y, Alitalo K. Blockade of vascular endothelial growth factor receptor-3 signaling inhibits fibroblast growth factor-2-induced lymphangiogenesis in mouse cornea. *Proc Natl Acad Sci U S A.* 2002 Jun 25;99(13):8868-73. Epub 2002 Jun 17.

[105] Orlandini M, Marconcini L, Ferruzzi R, Oliviero S. Identification of a c-fos-induced gene that is related to the platelet-derived growth factor/vascular endothelial growth factor family. *Proc Natl Acad Sci U S A.* 1996 Oct 15;93(21):11675-80.

[106] Achen MG, Jeltsch M, Kukk E, Mäkinen T, Vitali A, Wilks AF, Alitalo K, Stacker SA. Vascular endothelial growth factor D (VEGF-D) is a ligand for the tyrosine kinases VEGF receptor 2 (Flk1) and VEGF receptor 3 (Flt4). *Proc Natl Acad Sci U S A.* 1998 Jan 20;95(2):548-53.

[107] McColl BK, Paavonen K, Karnezis T, Harris NC, Davydova N, Rothacker J, Nice EC, Harder KW, Roufail S, Hibbs ML, Rogers PA, Alitalo K, Stacker SA, Achen MG. Proprotein convertases promote processing of VEGF-D, a critical step for binding the angiogenic receptor VEGFR-2. *FASEB J.* 2007 Apr;21(4):1088-98. Epub 2007 Jan 22.

[108] Baldwin ME, Catimel B, Nice EC, Roufail S, Hall NE, Stenvers KL, Karkkainen MJ, Alitalo K, Stacker SA, Achen MG. The specificity of receptor binding by vascular endothelial growth factor-d is different in mouse and man. *J Biol Chem.* 2001 Jun 1;276(22):19166-71. Epub 2001 Feb 20.

[109] Farnebo F, Piehl F, Lagercrantz J. Restricted expression pattern of vegf-d in the adult and fetal mouse: high expression in the embryonic lung. *Biochem Biophys Res Commun.* 1999 Apr 21;257(3):891-4.

[110] Baldwin ME, Halford MM, Roufail S, Williams RA, Hibbs ML, Grail D, Kubo H, Stacker SA, Achen MG. Vascular endothelial growth factor D is dispensable for development of the lymphatic system. *Mol Cell Biol.* 2005 Mar;25(6):2441-9.

[111] Stacker SA, Caesar C, Baldwin ME, Thornton GE, Williams RA, Prevo R, Jackson DG, Nishikawa S, Kubo H, Achen MG. VEGF-D promotes the metastatic spread of tumor cells via the lymphatics. *Nat Med.* 2001 Feb;7(2):186-91.

[112] Achen MG, Williams RA, Minekus MP, Thornton GE, Stenvers K, Rogers PA, Lederman F, Roufail S, Stacker SA. Localization of vascular endothelial growth factor-D in malignant melanoma suggests a role in tumour angiogenesis. *J Pathol*. 2001 Feb;193(2):147-54.

[113] Ishii H, Yazawa T, Sato H, Suzuki T, Ikeda M, Hayashi Y, Takanashi Y, Kitamura H. Enhancement of pleural dissemination and lymph node metastasis of intrathoracic lung cancer cells by vascular endothelial growth factors (VEGFs). *Lung Cancer*. 2004 Sep;45(3):325-37.

[114] He Y, Karpanen T, Alitalo K. Role of lymphangiogeni
c factors in tumor metastasis. *Biochim Biophys Acta*. 2004 Mar 4;1654(1):3-12.

[115] Teng X, Li D, Johns RA. Hypoxia up-regulates mouse vascular endothelial growth factor D promoter activity in rat pulmonary microvascular smooth-muscle cells. *Chest*. 2002 Mar;121(3 Suppl):82S-83S.

[116] Orlandini M, Marconcini L, Ferruzzi R, Oliviero S. Identification of a c-fos-induced gene that is related to the platelet-derived growth factor/vascular endothelial growth factor family. *Proc Natl Acad Sci U S A*. 1996 Oct 15;93(21):11675-80.

[117] Orlandini M, Oliviero S. In fibroblasts Vegf-D expression is induced by cell-cell contact mediated by cadherin-11. *J Biol Chem*. 2001 Mar 2;276(9):6576-81. Epub 2000 Dec 6.

[118] Balkwill F, Mantovani A. Inflammation and cancer: back to Virchow? *Lancet*. 2001 Feb 17;357(9255):539-45.

[119] Pollard JW. Tumour-educated macrophages promote tumour progression and metastasis. *Nat Rev Cancer*. 2004 Jan;4(1):71-8.

[120] Gorelik L, Flavell RA. Immune-mediated eradication of tumors through the blockade of transforming growth factor-beta signaling in T cells. *Nat Med*. 2001 Oct;7(10):1118-22.

[121] Lucas T, Abraham D, Aharinejad S. Modulation of tumor associated macrophages in solid tumors. *Front Biosci*. 2008 May 1;13:5580-8.

[122] Kawasaki ES, Ladner MB, Wang AM, Van Arsdell J, Warren MK, Coyne MY, Schweickart VL, Lee MT, Wilson KJ, Boosman A, et al. Molecular cloning of a complementary DNA encoding human macrophage-specific colony-stimulating factor (CSF-1). *Science*. 1985 Oct 18;230(4723):291-6.

[123] Stanley ER, Berg KL, Einstein DB, Lee PS, Pixley FJ, Wang Y, Yeung YG. Biology and action of colony-stimulating factor-1. *Mol Reprod Dev*. 1997 Jan;46(1):4-10.

[124] Lin EY, Gouon-Evans V, Nguyen AV, Pollard JW. The macrophage growth factor CSF-1 in mammary gland development and tumor progression. *J Mammary Gland Biol Neoplasia.* 2002 Apr;7(2):147-62.

[125] Smith HO, Anderson PS, Kuo DY, Goldberg GL, DeVictoria CL, Boocock CA, Jones JG, Runowicz CD, Stanley ER, Pollard JW. The role of colony-stimulating factor 1 and its receptor in the etiopathogenesis of endometrial adenocarcinoma. *Clin Cancer Res.* 1995 Mar;1(3):313-25.

[126] Kacinski BM. CSF-1 and its receptor in breast carcinomas and neoplasms of the female reproductive tract. *Mol Reprod Dev*. 1997 Jan;46(1):71-4.

[127] Scholl SM, Pallud C, Beuvon F, Hacene K, Stanley ER, Rohrschneider L, Tang R, Pouillart P, Lidereau R. Anti-colony-stimulating factor-1 antibody staining in primary breast adenocarcinomas correlates with marked inflammatory cell infiltrates and prognosis. *J Natl Cancer Inst*. 1994 Jan 19;86(2):120-6.

[128] Kim I, Kim HG, Kim H, Kim HH, Park SK, Uhm CS, Lee ZH, Koh GY. Hepatic expression, synthesis and secretion of a novel fibrinogen/angiopoietin-related protein that prevents endothelial-cell apoptosis. *Biochem J*. 2000 Mar 15;346 Pt 3:603-10.

[129] Kersten S, Mandard S, Tan NS, Escher P, Metzger D, Chambon P, Gonzalez FJ, Desvergne B, Wahli W. Characterization of the fasting-induced adipose factor FIAF, a novel peroxisome proliferator-activated receptor target gene. *J Biol Chem.* 2000 Sep 15;275(37):28488-93.

[130] Yoon JC, Chickering TW, Rosen ED, Dussault B, Qin Y, Soukas A, Friedman JM, Holmes WE, Spiegelman BM. Peroxisome proliferator-activated receptor gamma target gene encoding a novel angiopoietin-related protein associated with adipose differentiation. *Mol Cell Biol*. 2000 Jul;20(14):5343-9.

[131] Ge H, Yang G, Huang L, Motola DL, Pourbahrami T, Li C. Oligomerization and regulated proteolytic processing of angiopoietin-like protein 4. *J Biol Chem*. 2004 Jan 16;279(3):2038-45. Epub 2003 Oct 21.

[132] Sukonina V, Lookene A, Olivecrona T, Olivecrona G. Angiopoietin-like protein 4 converts lipoprotein lipase to inactive monomers and modulates lipase activity in adipose tissue. *Proc Natl Acad Sci U S A*. 2006 Nov 14;103(46):17450-5. Epub 2006 Nov 6.

[133] Murata M, Yudo K, Nakamura H, Chiba J, Okamoto K, Suematsu N, Nishioka K, Beppu M, Inoue K, Kato T, Masuko K. Hypoxia upregulates the expression of angiopoietin-like-4 in human articular chondrocytes: role of angiopoietin-like-4 in the expression of matrix metalloproteinases and cartilage degradation. *J Orthop Res.* 2009 Jan;27(1):50-7.

[134] Li C. Genetics and regulation of angiopoietin-like proteins 3 and 4. *Curr Opin Lipidol.* 2006 Apr;17(2):152-6.

[135] Belanger AJ, Lu H, Date T, Liu LX, Vincent KA, Akita GY, Cheng SH, Gregory RJ, Jiang C. Hypoxia up-regulates expression of peroxisome proliferator-activated receptor gamma angiopoietin-related gene (PGAR) in cardiomyocytes: role of hypoxia inducible factor 1alpha. *J Mol Cell Cardiol.* 2002 Jul;34(7):765-74.

[136] Ito Y, Oike Y, Yasunaga K, Hamada K, Miyata K, Matsumoto S, Sugano S, Tanihara H, Masuho Y, Suda T. Inhibition of angiogenesis and vascular leakiness by angiopoietin-related protein 4. *Cancer Res*. 2003 Oct 15;63(20):6651-7.

[137] Cazes A, Galaup A, Chomel C, Bignon M, Bréchot N, Le Jan S, Weber H, Corvol P, Muller L, Germain S, Monnot C. Extracellular matrix-bound angiopoietin-like 4 inhibits endothelial cell adhesion, migration, and sprouting and alters actin cytoskeleton. *Circ Res.* 2006 Nov 24;99(11):1207-15. Epub 2006 Oct 26.

[138] Galaup A, Cazes A, Le Jan S, Philippe J, Connault E, Le Coz E, Mekid H, Mir LM, Opolon P, Corvol P, Monnot C, Germain S. Angiopoietin-like 4 prevents metastasis through inhibition of vascular permeability and tumor cell motility and invasiveness. *Proc Natl*
Acad Sci U S A. 2006 Dec 5;103(49):18721-6. Epub 2006 Nov 27.

[139] Padua D, Zhang XH, Wang Q, Nadal C, Gerald WL, Gomis RR, Massagué J. TGFbeta primes breast tumors for lung metastasis seeding through angiopoietin-like 4. *Cell*. 2008 Apr 4;133(1):66-77.

[140] Davor Tomas, Mario Ledinsky, Mladen Belicza, Bo•o Krušlin. Multiple metastases to the small bowel from large cell bronchial carcinomas. *World J Gastroenterol* 2005;11(9):1399-1402

[141] Yasuhiko Ohta, MDa, Yoshiharu Tomita, MDa, Makoto Oda, MDa, Shunichi Watanabe, MDa, Shinya Murakami, MDa, Yoh Watanabe, MDa. Tumor angiogenesis and recurrence in stage I non-small cell lung cancer. *Ann Thorac Surg* 1999;68:1034-1038

[142] Kleeff J, Korc M. Up-regulation of transforming growth factor (TGF)-beta receptors by TGF-beta1 in COLO-357 cells. *J Biol Chem*. 1998 Mar 27;273(13):7495-500.

Ich habe mich bemüht, sämtliche Inhaber der Bildrechte ausfindig zu machen und ihre Zustimmung zur Verwendung der Bilder in dieser Arbeit eingeholt. Sollte dennoch eine Urheberrechtsverletzung bekannt werden, ersuche ich um Meldung bei mir.

Appendix

Media, Buffers and Solutions

Cell culture media

Components [mg/L]	RPMI	MEM	Waymouth's
Inorganic Salts			
Calcium Nitrate • 4H2O	100		
Calcium Chloride anhydrous		200	90,6
Potassium Chloride	400	400	150
Magnesium Chloride			112,56
Magnesium Sulphate	48,8	97,7	97,67
Sodium Chloride	6000	6800	6000
Di-Sodium Hydrogen Phosphate (anh.)	800	140	300
Sodium Hydrogen Carbonate	2000	2200	2240
Amino Acids			
L-Alanyl-L-Glutamine	445,9	434	
L-Arginine • HCl	241,86	126	75
L-Asparagine • H2O	50		
L-Aspartic Acid	20		60
Cysteine HCl • H2O			100,29
L-Cystine	50	24	20
L-Glutamic Acid	20		150
L-Glutamine	300	292	350
Glycine	10		50
L-Histidine Base	15		
L-Histidine • HCl • H2O		42	164,1
L-Hydroxyproline	20		
L-Isoleucine	50	52	25
L-Leucine	50	52	50
L-Lysine • HCl	40	72,5	240
L-Methionine	15	15	50
L-Phenylalanine	15	32	50
L-Proline	20		50
L-Serine	30		
L-Threonine	20	48	75
L-Tryptophan	5	10	40
L-Tyrosine	20		57,66
L-Valine	20	46	65
Vitamins			
P-Aminobenzoic Acid	1		
Ascorbic Acid			17,5
D(+)-Biotin	0,2		0,02
D-Calcium Pantothenate	0,25	1	1
Cholin Chloride	3	1	250
Folic Acid	1	1	0,4
Myo-Inositol	35	2	1
Nicotinamide	1	1	1
Pyridoxine • HCl	1	1	1
Riboflavin	0,2	0,1	1
Thiamine • HCl	1	1	10
Vitamin B12	0,005		0,2
Other Components			
D-Glucose anhydrous	2000	1000	5000
Glutathione (red.)	1		15
Hypoxanthine			29
Phenol Red	5	11	10,2

Buffers and Solutions

Name	Formulation
PBS	KCl (0,2 g/L), KH2PO4 (0,2 g/L), NaCl (8 g/L), Na2HPO4anh. (1,15 g/L)
Erythrocyte lysis buffer	NH4Cl (8,26 g/L), KHCO3 (1 g/L), EDTA (0,037 g/L)
RevertAid M-MuLV Reverse Transcriptase Buffer (5x)	Tris-HCl (250 mM), KCl (250 mM), MgCl2 (20mM), DTT (50 mM), pH 8,3
TAE buffer (1x)	Tris-acetate (40 mM), EDTA (0,1 mM)
Citrate buffer	Tri-sodium citrate dihydrate (10 mM), pH 6,5
DAB solution	Buffer stock solution (2 drops), DAB stock solution (4 drops), 30 % H2O2 (120 µL) ad 5 mL with ddH2O

Primer Sequences

Primer	Accession nr.	Forward Primer (5'-3')	Reverse Primer (5'-3')	Product length (nt)
huβ2M	NM_004048	GATGAGTATGCCTGCCGTGTG	CAATCCAAATGCGGCATCT	114
huVEGF-A	all isoforms	AGAAGGAGGAGGGCAGAATC	GCATTCACATTTGTTGTGCTG	300
huVEGF-C	X94216	CCCCAAACCAGTAACAATC	CACAGGCACATTTTCCAG	497
huVEGF-D	D89630	GCGGCAACTTTCTATGAC	GGCAACTTTAACAGGCAC	285
huCSF-1	M37435	GCTGTTGTTGGTCTGTCTC	CATGCTCTTCATAATCCTTG	335
huANGPTL4	NM_139314.1	CACAGCCTGCAGACACAACTC	GGAGGCCAAACTGGCTTTGC	133
huTGF-β1	NM_000660.4	TGGCGATACCTCAGCAAC	CTCGTGGATCCACTTCCAG	405
huTGF-β2	NM_001135599.1	ATCCCGCCCACTTTCTACAGAC	CATCCAAAGCACGCTTCTTCCG	565

Abbreviations

°C	Degree celsius
µg	Microgram
µL	Microliter
µm	Micrometer
µM	Micromolar
7aad	7-Amino-Actinomycin D
A	Absorption
ANG	Angiopoietin
ANGPTL4	Angiopoietin like-4
AU	Arbitrary unit
B2M	Beta-2-microglobulin
bFGF	Basic fibroblast growth factor
bp	Base pairs
cDNA	Complementary DNA
CSF-1	Colony stimulating factor-1
CSF-1R	CSF-1 receptor
C-terminal	Carboxy-terminal
DAB	Diaminobenzidine
DAPI	4',6-diamidino-2-phenylindole
ddH2O	Double distilled water
DiI	1,1'-dioctadecyl-3,3,3',3'-tetramethylindocarbocyanine iodide
DNA	Desoxyribonucleic acid
dNTP	Desoxyribonucleotidetriphosphate
dpi	Days post injection
DSS	Distal splice site
EC	Endothelial cell
EDTA	Ethylenediaminetetraacetic acid
EGF	Epidermal growth factor
ELISA	Enzyme-linked immunosorbent assay
EMT	Epithelial to mesenchymal transition
EtBr	Ethidium bromide
FBS	Fetal bovine serum
Fc region	Fragment cristallizable region
FITC	Fluorescein isothiocyanate
G	Gravitational constant
h	Hour
HIF-1α	Hypoxia inducible factor-1α
HRP	Horse raddish peroxydase
IGF-1	Insulin-like growth factor-1
IHC	Immunohistochemistry
LEC	Lymphatic endothelial cell

LYVE-1	Lymphatic vessel hyaluronan receptor-1
MHC-1	Major histocompatibility complex-1
min	Minute
mL	Milliliter
mm	Millimeter
mM	Millimolar
mRNA	Messenger RNA
NEAA	Non-essential amino acids
ng	Nanogram
nm	Nanometer
NSCLC	Non-small cell lung cancer
N-terminal	Amino-terminal
PBS	Phosphate buffered saline
PC	Proprotein convertase
PCR	Polymerase chain reaction
PDGF	Platelet-derived growth factor
PE	Phycoerythrin
PECAM-1	Platelet endothelial cell adhesion molecule-1
PIGF	Placental growth factor
PSS	Proximal splice site
qRT-PCR	Quantitative real-time PCR
RNA	Ribonucleic acid
rRNA	Ribosomal RNA
s	Second
SCLC	Small cell lung cancer
SDS	Sodium dodecyl sulfate
TAE	Tris, acetic acid, EDTA
TAM	Tumor associated macrophage
Taq	Thermus aquaticus
TGF-β	Transforming growth factor-beta
TNF-α	Tumor necrosis factor-α
VEGF	Vascular endothelial growth factor
VEGF-R	VEGF receptor
vWF	Van Willebrand factor
W	Watt

Abstract

Neoangiogenesis is the formation of new blood vessels in the adult organism and a prerequisite for the establishment of distant colonies by many cancers, including bronchus carcinoma. Lymphangiogenesis represents the formation of new lymphatic vessels and has recently been implicated in the seeding of metastases.

The aim of this thesis was to develop murine xenograft models for representative cell lines of all major bronchus carcinoma subtypes. Using H460 large bronchus carcinoma cells, H520 squamous cell bronchus carcinoma cells, Calu-3 adenocarcinoma cells and DMS53 small cell bronchus carcinoma cells, differences in tumor growth, neoangiogenesis, lymphangiogenesis, metastasis and the presence of invading lymphatic endothelial cells (LECs) were evaluated. In addition, the question was addressed whether these phenotypic differences correlate with mRNA or protein expression of candidate angiogenic and lymphangiogenic factors, such as members of the vascular endothelial growth factor (VEGF) family, colony stimulating factor-1 and angiopoietin-related molecule angiopoietin like-4 (ANGPTL4).

Neoangiogenesis was observed in all tumor samples examined. Overall vessel density was highest in H460 derived tumors, whereas Calu-3 xenografts showed the highest number of large intra-tumoral vessels. VEGF-A mRNA expression *in vivo* correlated with blood vessel development in most tumor types, except for H460, where only moderate expression was observed. Lymphatic vessel formation was not observed in any of the tumors despite VEGF-C and VEGF-D mRNA expression. With the exception of DMS53, all tumors showed metastasis formation and a correlation with intra-tumoral vascularization was established. Calu-3 xenografts exhibited the highest frequency of metastasis and metastatic cells could be isolated from the organs of Calu-3 bearing animals. Calu-3 cells also showed high ANGPTL4 protein expression *in vitro* and hypoxia vastly increased protein secretion from this cell line. Importantly, isolated metastatic Calu-3 cells exhibited much higher ANGPTL4 protein levels than the original cell line under normoxia, as well as hypoxia, indicating a possible role of ANGPTL4 in the metastatic spread of bronchus adenocarcinoma.

The results provided by this thesis underline the importance of VEGF-A induced neoangiogenesis in the metastatic spread of bronchus carcinoma, while the role of VEGF-C and VEGF-D remains unclear. Furthermore, they indicate a possible influence of ANGPTL4 in this context.

Zusammenfassung

Neoangiogenese, die Ausbildung neuer Blutgefäße im adulten Organismus, ist eine notwendige Voraussetzung für die Metastasenbildung vieler Krebsarten, so auch des Bronchuskarzinoms. Lymphangiogenese, die Ausbildung neuer Lymphgefäße, ist erst seit kurzem Gegenstand der Forschung, scheint aber eine ähnliche Rolle in Bezug auf die Metastasenbildung zu spielen.

Ziel dieser Diplomarbeit war die Etablierung muriner Xenograft-Modelle mit repräsentativen Zelllinien aller Bronchuskarzinom-Hauptsubtypen. Zellen des großzelligen Bronchuskarzinoms (H460), des Plattenepithelkarzinoms (H520), des Adenokarzinoms (Calu-3), sowie des kleinzelligen Bronchuskarzinoms (DMS53) wurden verwendet um Unterschiede in Wachstum, Neoangiogenese, Lymphangiogenese, Metastasierung sowie die Anwesenheit von murinen lymphatischen Endothelzellen (LECs) zu untersuchen. Zudem wurde der Frage auf den Grund gegangen, ob diese phänotypischen Unterschiede mit der mRNA bzw. Protein-Expression bekannter angiogener und lymphangiogener Faktoren korellieren, wie beispielsweise den Mitgliedern der vascular endothelial growth factor Familie (VEGF), dem colony stimulating factor-1, sowie dem vor kurzem entdeckten Molekül angiopoietin like-4 (ANGPTL4).

Neoangiogenese konnte in allen untersuchten Tumorproben nachgewiesen werden. Tumore aus H460 Zellen zeigten die höchste insgesamte Blutgefäßdichte, obwohl die intratumorale Gefäßdichte bei Calu-3 höher war. Die *in vivo* VEGF-A mRNA Expression korellierte mit der Blufgefäßdichte in den meisten Tumorsubtypen, jedoch nicht beim großzelligen Bronchuskarzinom. Die Ausbildung neuer Lymphgefäße konnte in keiner der Tumorproben nachgewiesen werden, trotz vorhandener VEGF-C und VEGF-D mRNA Expression. Alle Tumorsubtypen zeigten Metastasenbildung, mit Ausnahme von DMS53. Eine Zusammenhang mit der intra-tumoralen Vaskularisierung konnte festgestellt werden. Calu-3 zeigte die höchste Metastasierungsrate und metastatische Zellen konnten aus den Organen Calu-3 tragender Tiere isoliert werden. Calu-3 Zellen zeigten hohe ANGPTL4 Proteinexpression *in vitro*, welche durch Hypoxie stark gesteigert wurde. Die isolierten, metastatischen Calu-3 Zellen zeigten noch höhere ANGPTL4 Proteinwerte, als die ursprüngliche Zelllinie, sowohl unter Normoxie, wie auch unter Hypoxie. Dies weist auf eine mögliche Rolle von ANGPTL4 bei der Metastasenbildung des Adenokarzinoms hin.

Die Ergebnisse dieser Diplomarbeit unterstreichen die Wichtigkeit von VEGF-A induzierter Neoangiogenese bei der metastatischen Verbreitung des Bronchuskarzinoms, wohingegen die die Rolle von VEGF-C und VEGF-D unklar bleibt. Des weiteren deuten sie auf einen möglichen Einfluss des ANGPTL4-Proteins hin.

Curriculum vitae

<u>Personal details</u>

Name	Patrick Reichl
Date of birth	26.09.1985
Place of birth	Vienna
Citizenship	Austrian
Address	Work:
	Centre of Anatomy and Cell Biology
	Waehringerstrasse 13
	Vienna, A-1090, Austria
	Home:
	Hannbaumstrasse 2
	Vienna, A-1140, Austria
Telephone	+43-(0)650-2609985
E-mail	p.reichl@tele2.at
Languages	German, French, English

<u>Education</u>

School	Lycée Français de Vienne (1991-2003)
1991-1996	Ecole primaire (primary school)
1996-2000	Collège (secondary school I)
2000	Diplôme National du Brevet (GCSE)
2000-2003	Lycée, série S, spécialité: sciences de la vie et de la terre (secondary school II, scientific stream)
2001	First Certificate in English (University of Cambridge ESOL)
2003	Diplôme du Baccalauréat Général, série S and Österreichische Reifeprüfung (GCE Advanced Level)

University	University of Vienna (2003-2011)
Discipline	Genetics and microbiology
Elective subjects	Developmental genetics, molecular genetics
Special practical courses	Confocal microscopy, DNA sequencing, reproductive biotechnology, *Oryzias latipes* developmental genetics
MSc thesis	Establishment and analysis of bronchus carcinoma xenografts in mice

<u>Scientific Work</u>

2007-2010	Medical University of Vienna, Laboratory for Cardiovascular Research
	Molecular biology (RNAi, real-time RT-PCR, cloning, western blot, ELISA), immunohistochemistry, murine models, analytical chemistry (HPLC), biochemistry (protein purification), cell biology, IT (sequence analysis, phylogenetic trees, *in silico* plasmid design)